

Winter 2006

# Investigation of a submerged four-bay mooring system for aquaculture

Glen Rice

*University of New Hampshire, Durham*

Follow this and additional works at: <https://scholars.unh.edu/thesis>

---

## Recommended Citation

Rice, Glen, "Investigation of a submerged four-bay mooring system for aquaculture" (2006). *Master's Theses and Capstones*. 241.  
<https://scholars.unh.edu/thesis/241>

This Thesis is brought to you for free and open access by the Student Scholarship at University of New Hampshire Scholars' Repository. It has been accepted for inclusion in Master's Theses and Capstones by an authorized administrator of University of New Hampshire Scholars' Repository. For more information, please contact [nicole.hentz@unh.edu](mailto:nicole.hentz@unh.edu).

**INVESTIGATION OF A SUBMERGED FOUR-BAY MOORING SYSTEM  
FOR AQUACULTURE**

**BY**

**GLEN RICE**

**Bachelor of Science, University of New Hampshire, 1999**

**THESIS**

**Submitted to the University of New Hampshire**

**in Partial Fulfillment of**

**the Requirements for the Degree of**

**Master of Science**

**in**

**Ocean Engineering**

**December, 2006**

UMI Number: 1439286

### INFORMATION TO USERS

The quality of this reproduction is dependent upon the quality of the copy submitted. Broken or indistinct print, colored or poor quality illustrations and photographs, print bleed-through, substandard margins, and improper alignment can adversely affect reproduction.

In the unlikely event that the author did not send a complete manuscript and there are missing pages, these will be noted. Also, if unauthorized copyright material had to be removed, a note will indicate the deletion.

**UMI**<sup>®</sup>

---

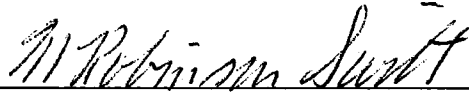
UMI Microform 1439286

Copyright 2007 by ProQuest Information and Learning Company.

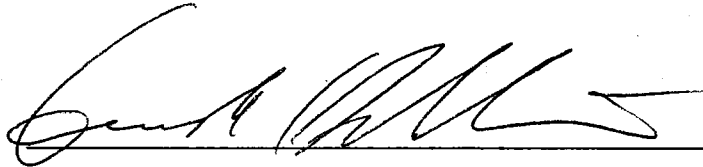
All rights reserved. This microform edition is protected against unauthorized copying under Title 17, United States Code.

ProQuest Information and Learning Company  
300 North Zeeb Road  
P.O. Box 1346  
Ann Arbor, MI 48106-1346

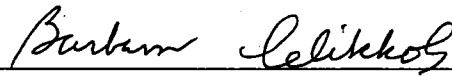
This thesis has been examined and approved.



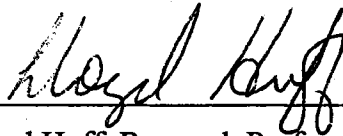
Thesis Director, M. Robinson Swift  
Professor of Mechanical and Ocean Engineering



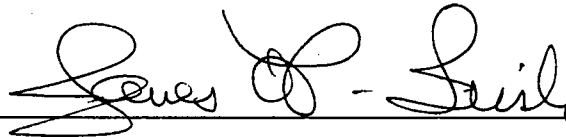
Kenneth C. Baldwin, Professor of Mechanical and Ocean Engineering



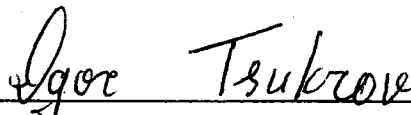
Barbaros Celikkol, Professor of Mechanical Engineering



Lloyd Huff, Research Professor of Ocean Engineering



James D. Irish, Research Professor of Ocean Engineering



Igor I. Tsukrov, Associate Professor of Mechanical Engineering

11/22/06

Date

## DEDICATION

To Margaret for helping me get here

and

To Eliza for helping me get through this chapter of my life.

To OOA:

“It was a hair-raising exploit and, as the salvage arbitrator in London later wrote, ‘it was accomplished by a display of courage that only escaped foolhardiness by virtue of the skill with which it was performed.’”

Farley Mowat, *The Grey Seas Under*.

## ACKNOWLEDGEMENTS

This work is not the culmination of the last six years of my life, but a small excerpt of my education from my time here. There have been many whom I have learned lessons from, ranging from academic to life-long. As a result I would like to thank, in no particular order, the professors: Rob Swift, Barbaros Celikkol, Igor Tsukrov, Jim Irish, Lloyd Huff, Hunt Howell, and Dave Fredriksson, and the Ocean Engineering graduate students: Chad Turmelle, Jud DeCew, Glenn McGillicuddy, John Ahern, Brett Fullerton, Oystein Patursson, Gopal Krishna, and Mashkoor Malik, and those in the field: Matt Stommel, Dave Koorits, Caleb Thibeault, Liz Kintzing, Michael Chambers, Paul Lavioe, and Paul Pelletier.

In addition I thank the National Oceanographic and Atmospheric Administration for their support of Open Ocean Aquaculture at UNH.

## TABLE OF CONTENTS

DEDICATION .....	iii
ACKNOWLEDGEMENTS .....	iv
LIST OF TABLES .....	vii
LIST OF FIGURES.....	viii
ABSTRACT.....	xiii
CHAPTER I .....	1
INTRODUCTION.....	1
Background .....	1
Mooring Design .....	2
The Four-bay Grid.....	5
Objectives.....	6
CHAPTER II .....	8
GRID DEPLOYMENT .....	8
Preparation .....	8
Deployment .....	12
Initial Deployment Assessment.....	15
CHAPTER III.....	18
GRID TENSION SENSITIVITY MODELING .....	18
Background .....	18
Modeling Approach .....	19

Model Results.....	22
Discussion of Model Results.....	27
CHAPTER IV .....	30
MOBILE TENSION METER.....	30
Impetus .....	30
Concept Development.....	31
Preliminary Testing.....	33
Preliminary Trial Data.....	34
Full-scale Design.....	37
Calibration.....	41
Field Measurements .....	45
CHAPTER V.....	51
CONCLUSIONS.....	51
Deployment Success .....	51
Future Work .....	54
LIST OF REFERENCES .....	56
APPENDICES.....	58
APPENDIX A .....	59
APPENDIX B .....	68
APPENDIX C .....	73
APPENDIX D .....	87



## LIST OF TABLES

Table III-1 The properties used for the grid model.....	21
Table IV-1 The parts and their weights as measured as well as predicted by Pro/E. ....	40
Table D-1 The anchor positions used to model the deployed grid. Easting and Northing positions are for the UTM Northern Hemisphere zone 19, (WGS84) convention.	89

## LIST OF FIGURES

Figure I-1 An isometric drawing of the submerged single grid mooring with a Sea Station™ cage in surface mode.....	3
Figure I-2. An isometric view of the submerged four-bay grid system is shown with part labels. ....	4
Figure I-3 A cross-section of the grid along one of the sides. A cross section through the center would show the location of the steel and composite flotation reversed, and the anchor chain is 27m.....	5
Figure II-1 The submerged four-bay grid system. Major parts are labeled. ....	8
Figure II-2 The load cell pendant arrangement for later deployment of the load cells to a grid line. ....	9
Figure II-3 The order in which the anchors were planned to be tensioned. Each number corresponds to the closest anchor and the steps outlined for deployment. ....	11
Figure II-4 The dependency of anchor and grid line tensions on the corner ball buoyancy and the angle of anchor line.....	15
Figure II-5 The designed anchor locations (black diamonds) relative to the deployed positions (pink diamonds). Numbers indicate the distance between these positions. Grid corner positions are shown as pink triangles. ....	16
Figure III-1. The grid system with the modified anchor locations. Mooring system lines are labeled for reference. The a <sub>4</sub> anchor line led to an anchor located at one of the 25 position mesh intersection points shown.....	19

Figure III-2 The pattern for anchor placement modification. Position thirteen is the designed location of the anchor.....	20
Figure III-3 The mesh used in AquaFE simulations of the grid system. ....	21
Figure III-4 The tension in line $f_1$ as the grid settles to equilibrium. ....	22
Figure III-5 The tensions in line $a_4$ as a function of anchor displacement. ....	23
Figure III-6 Northeast grid corner vertical displacement as a function of the horizontal displacement of the northeast anchor. ....	24
Figure III-7 The tension in line $e_1$ as a function of anchor displacement. ....	25
Figure III-8 $e_1$ line tension as a function of the $a_4$ anchor movement from positions 11 to 15. The discontinuous section is where the grid was built at a different depth. ....	26
Figure III-9 Tensions of the individual lines in cross section A as anchor is moved east/west. ....	26
Figure III-10 Anchor line tensions as a function of anchor displacement east/west.....	27
Figure IV-1 A conceptual drawing of rope deflection. Theta is the angle of deflection.	31
Figure IV-2 The relationship between line tension( $T$ ) and the force to displace it orthogonally( $L$ ). ....	32
Figure IV-3 The half-scale tension meter trail setup. ....	33
Figure IV-4 Measured ram load cell force during a half-scale trial.....	35
Figure IV-5 The results of the averaged half-scale data. Black 'x' is the average from each test with the error bars representing the one standard deviation for each trial. The green line is a linear regression.....	36
Figure IV-6 A Pro/Engineer solid model of the assembled tension meter. ....	38

Figure IV-7 The Results from Pro/Mechanica for stress on the frame for the maximum designed load.....39

Figure IV-8 The calibration setup. ....41

Figure IV-9 The calibration time series from the second test. Blue is the load measured in the in-line load cell, while red is the load measured in tension meter (ram) load cell.....43

Figure IV-10 The (a) calibration with a linear fit and (b) the difference between measured force and the linear fit. Data from the separate calibration tests are displayed with different symbols. The “best fit” formula is given on graph (a). Bounds denote one standard deviation of  $\pm 0.8\text{kN}$ . ....44

Figure IV-11 The (a) calibration with a second order fit, and (b) the difference between measured force and the linear fit. Data from the separate calibration tests are displayed with different symbols. The “best fit” formula is given on graph (a). Bounds denote one standard deviation of  $\pm 0.5\text{kN}$ . ....45

Figure IV-12 The mobile tension meter fully assembled pre-deployment. ....46

Figure IV-13 The mobile tension meter during deployment. ....47

Figure IV-14 The current profile as measured from a bottom mounted ADCP at the UNH OOA site.....48

Figure IV-15 A schematic of the grid with the measured tensions next to the lines where they were measured. For reference, grid segment design tensions were 11kN while design anchor line tensions were 14kN. Error is considered to be  $\pm 0.8\text{kN}$ . ....49

Figure IV-16 The tensions in the deployed grid as model in *AquaFE*.....50

Figure V-1 The relationship between the anchor line tension and the crown line angle needed to pick up the anchor. $T_A$ is the anchor line tension, and $W_A$ is the weight of the anchor.....	53
Figure A-1 Cross-section A tensions by line as a function of the northern east anchor displacement.....	60
Figure A-2 Cross-section B tensions by line as a function of the northern east anchor displacement.....	60
Figure A-3 Cross-section C tensions by line as a function of the northern east anchor displacement.....	61
Figure A-4 Cross-section D tensions by line as a function of the northern east anchor displacement.....	61
Figure A-5 Cross-section E tensions by line as a function of the northern east anchor displacement.....	62
Figure A-6 Cross-section F tensions by line as a function of the northern east anchor displacement.....	62
Figure A-7 Grid corner displacement as a function of the northern east anchor displacement.....	63
Figure A-8 Grid corner displacement as a function of the northern east anchor displacement.....	64
Figure A-9 The tensions for cross-section A.....	65
Figure A-10 The tensions for cross-section B.....	65
Figure A-11 The tensions for cross-section C.....	66
Figure A-12 The tensions for cross-section D.....	66

Figure A-13 The tensions for cross-section E.....	67
Figure A-14 The tensions for cross-section F. ....	67
Figure B-1 The tension meter frame. ....	68
Figure B-2 The axel assembly for the wheels. ....	69
Figure B-3 The marithane wheels. ....	69
Figure B-4 The bottle jack. ....	70
Figure B-5 The bottle jack to load cell adaptor.....	70
Figure B-6 The pancake style load cell. ....	71
Figure B-7 The fairlead for the rope over the load cell.....	71
Figure B-8 The pipe chock used for holding the load cell at the correct displacement. .72	
Figure B-9 The load cell recorder. ....	72
Figure D-1 The backscatter data from the 2004 survey of the OOA site. The dark lines are thought to reflect anchor chain and anchor positions. The labeled locations are deployed anchor locations as measured from the surface. WNA is the western north anchor. NNA is the northern center anchor. ENA is the eastern north anchor. .....	88
Figure D-2 (a)The linear regression to find the value for the Young’s Modulus from tension meter calibration data. (b) Data to linear fit difference. Bounds denote one standard deviation. ....	90
Figure D-3 The tensions in the deployed grid as model in <i>AquaFE</i> . ....	92
Figure D-4 The deployed grid depths as modeled by <i>AquaFE</i> . The depth relative to the designed locations and the measured depths at the site are also given. ....	93

## ABSTRACT

### INVESTIGATION OF A SUBMERGED FOUR-BAY MOORING SYSTEM FOR AQUACULTURE

by

Glen Rice

University of New Hampshire, December, 2006

The August 2003 deployment of a second generation mooring system for fish cages at the University of New Hampshire (UNH) open ocean aquaculture site, south of the Isles of Shoals, NH, is described and evaluated. The new system, a submerged four-bay grid similar to those used in inshore aquaculture, uses submerged flotation to maintain its depth and tension. The system's depth and line tensions are sensitive to the deployed anchor locations. Anchors that are not positioned correctly can have reduced holding power or result in problem snap loads.

The mooring system deployment process and its resulting geometry was examined through numerical modeling and field measurements using custom instrumentation, revealing the deployed tension and how it is distributed throughout the grid system. Though discrepancies between measured and designed tensions exist, the differences do not compromise the functionality or safety of the system. Suggestions for improved deployment methods result from these findings.

# CHAPTER I

## INTRODUCTION

### Background

Since ancient times, aquaculture has been employed to provide food for human consumption (Ling (1977)). Small ponds and protected bays have been used to grow various species of algae, shellfish and finfish. Historically, successful aquaculture has been dependent on providing a suitable habitat in which the species can develop for harvest. In the modern world additional factors, such as competing user groups and discharge restrictions coupled with animal health, have created the need for aquaculture to move into more exposed locations in the open ocean. While moving aquaculture operations to the open ocean is inconvenient, difficult and costly, the demand for supplemental sources of edible wild marine species makes Open Ocean Aquaculture (OOA) a future possibility. Among the many components needed to support aquaculture, the move to the open ocean necessitates adaptations in fish containment systems to compensate for environmental conditions. Fundamental to containment systems are the mooring systems and, as such, so is the understanding of mooring systems for the open ocean.

In 1999, the University of New Hampshire (UNH) deployed its first finfish cages and moorings at a 30 acre test site 10 km from the coast of NH in 52 meters of water (Fredriksson *et al.* (1999)). To create a suitable habitat for finfish species,



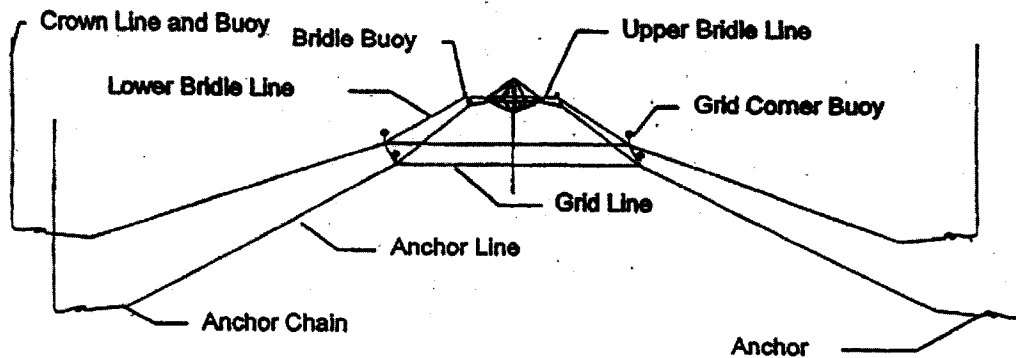
containment cages and feed buoys were secured to two separate single-bay mooring systems. In 2003 the original mooring systems were removed, and at the site a new mooring was deployed which was capable of maintaining four cages. The intention in deploying the new mooring was to provide a platform to which cages and small feed buoys could be readily attached or removed as part of cage evaluation studies, without having to re-deploy large anchors with every change. The mooring, deployed in 2003, was a submerged four-bay grid with underwater flotation and twelve anchors.

### Mooring Design

As the initial UNH Open Ocean Aquaculture mooring system was being developed, environmental conditions were assessed. For design purposes a storm condition was selected by evaluating past oceanographic data and determining the statistical wave characteristics of a fifty year storm event (Fredriksson (2001)). The data included for this determination was not inclusive of an anomalous event, such as a large hurricane. The storm condition consists of a nine meter wave with an 8.8 second period. In addition a collinear 1m/s current is applied uniformly with depth.

With environmental conditions and the particular cage characteristics of the Sea Station™ predetermined, a submerged four-bay grid mooring was designed and tested using a numerical model developed at UNH called *AquaFE* (Tsukrov et al. (2000)). *AquaFE* was developed as a tool to determine mooring loads given particular objects and geometries in a user-defined wave and current field. *AquaFE* was used to determine the mooring equipment sizes as a result of the loads modeled.

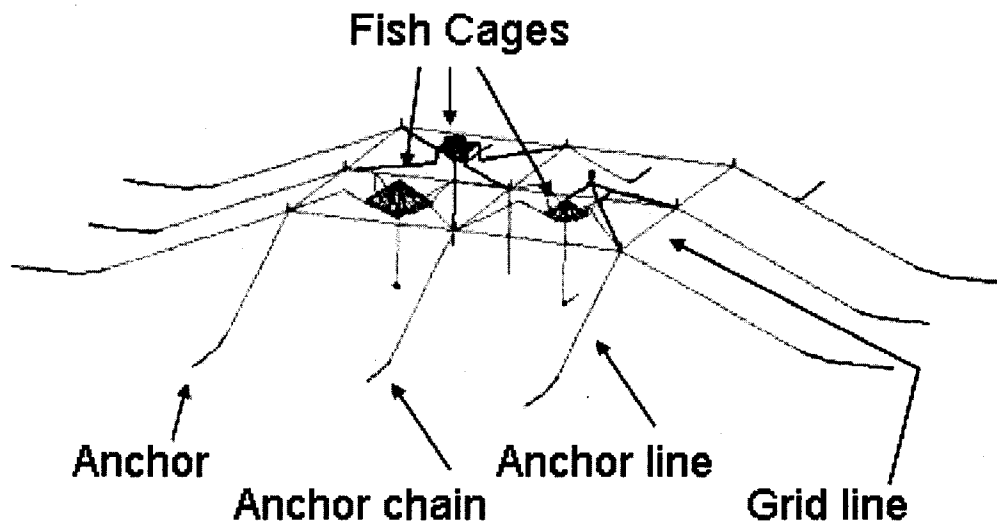
The two single-bay grid systems deployed in 1999 at the UNH OOA site could each hold a single surface or submerged cage, as shown in Figure I-1.



**Figure I-1 An isometric drawing of the submerged single grid mooring with a Sea Station™ cage in surface mode.**

Each single-bay grid had four anchors, one attached diagonally at each corner, and could hold a 600m<sup>3</sup> Sea Station™ cage. Each grid corner was supported by a buoy providing 3.33 kN of buoyancy. This design was robust and successfully moored cages through several winter ‘northeaster’ storms. Each single grid, however, used 15 acres of space, which was very inefficient given the cage volume of 600m<sup>3</sup>. Also, biofouling on the grid and anchor lines over the course of a year added too much weight for the grid flotation to support. As a result, the grid would sink deeper than desired and pull down on the cages and surface buoys.

Much of the equipment and knowledge used in the first grid systems were also used in 2003 in the updated four-bay grid mooring. The carried-over equipment and knowledge included the use of Sea Station™ cages, the anchor system, the deployment techniques, and the design environmental conditions. To increase efficiency, a four grid system was designed (Fredriksson *et al.* (2004)) to provide for twice as many cages to fit in the same amount of site acreage with a similar anchor line scope (Figure I-2).



**Figure I-2. An isometric view of the submerged four-bay grid system is shown with part labels. In addition more flotation was added to the grid so that it could support more biofouling.**

Based on *AquaFe* modeling, the updated grid consisted of twelve one-ton anchors with 57mm chain capable of holding two 600m<sup>3</sup> Sea Stations™ and two 3000m<sup>3</sup> Sea Stations™ during a fifty year storm condition. Gael Force rope rings were used in the corners in conjunction with 1m diameter steel flotation balls and 1.4m diameter composite urethane foam balls for flotation. Forty-eight mm, eight plait polysteel lines were used throughout the grid, anchor and bridle lines. The designed line lengths remained the same as those in the original grid with each side of a grid being 65m and an anchor line being 78m long. Figure I-3 shows a cross section of the grid with these lengths.

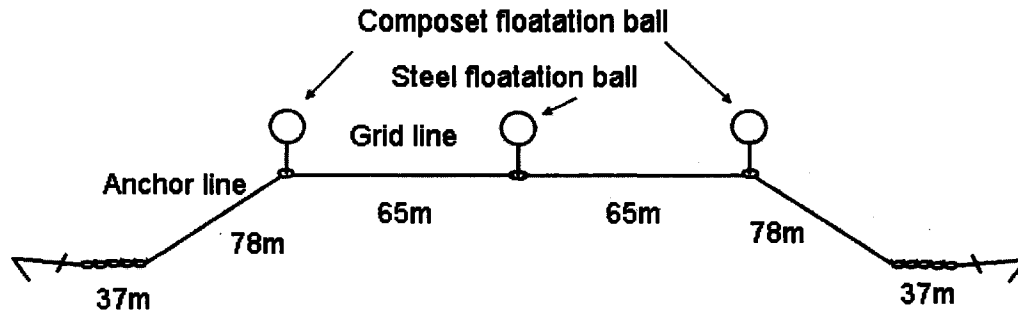


Figure I-3 A cross-section of the grid along one of the sides. A cross section through the center would show the location of the steel and composite floatation reversed, and the anchor chain is 27m.

### The Four-bay Grid

During July of 2003 the original two single-bay grids were removed, and the four-bay grid system was deployed. The original two 600 m<sup>3</sup> Sea Station™ cages were installed in the new mooring system immediately, and a 3000m<sup>3</sup> Sea Station™ cage was added a month later. Several cages and feed buoys have been added and removed from the grid since it was deployed, but the system has not been used to its full capacity with four cages in the grid at one time. Future plans to add larger capacity surface cages to the grid could push the grid to, and possibly beyond, its designed limits. Each proposed change to the grid loading will be analyzed using *AquaFe* to predict whether anchor and line capabilities would be exceeded during storm conditions. The *AquaFe* analysis, however, critically depends on the anchors being exactly in their designed positions.

Deviations from the designed geometry in the actual deployment of the system can significantly affect the grid's capacity for holding fish cages in place. Anchors deployed closer to the grid than designed can result in slack lines that cause excessive

system wear and snap loading. Anchors deployed further from the grid than their designed locations can over-tension the grid. Anchors that are under a much larger static tension will be more likely to drag once storm loads are reached, upsetting the deployed geometry. Once the geometry is altered, the anchors would need to be reset, at great cost operationally, to sink the grid back to the preferred depth. Since the mooring gear was deployed from a surface vessel in 52m of water using only indicator floats, lines from the grid corners to surface buoys, as position aids, some error in placement was inevitable. Given the implications of anchor misplacement, it is important to know how well the grid was originally deployed.

## Objectives

The objectives of this study were to:

- 1) Calculate the sensitivity of the grid to changes in anchor positioning,
- 2) Measure actual grid tensions,
- 3) Compare measured grid tensions with calculated tensions based on ideal geometry in order to evaluate the accuracy of model inputs,
- 4) Estimate possible errors in anchor deployment location.

The deployment process is detailed in Chapter Two, including use of the Global Positioning System (GPS) and marker buoys to optimize deployment for a mooring system such as this. Chapter Three investigates the sensitivity of a submerged four bay grid mooring to the repositioning of a single anchor in order to assess what changes in grid tensions will result for a given position discrepancy. The sensitivity of grid

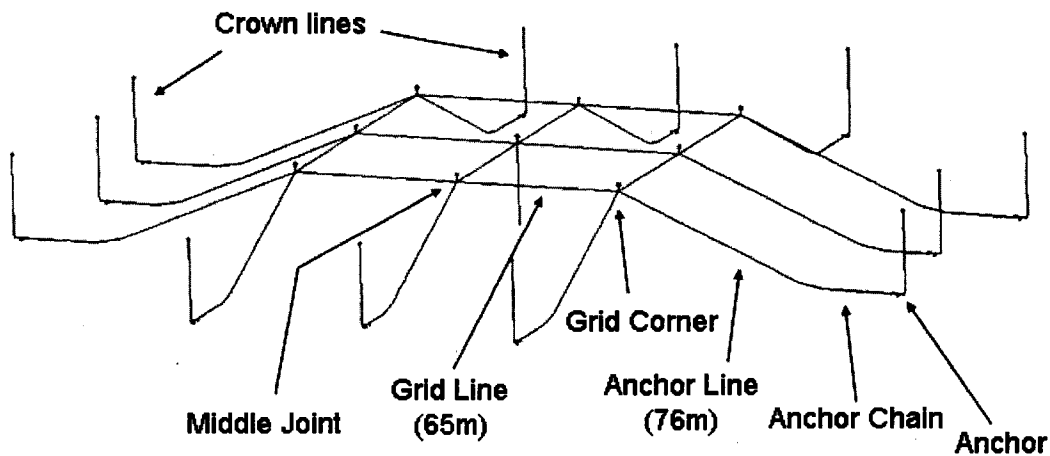
component tensions is calculated using *AquaFe*. In Chapter Four efforts to measure grid tensions three years after deployment are detailed. A final chapter includes an assessment of the present grid system, expected limitations on installation of similar moorings and recommendations for improvement.

## CHAPTER II

### GRID DEPLOYMENT

#### Preparation

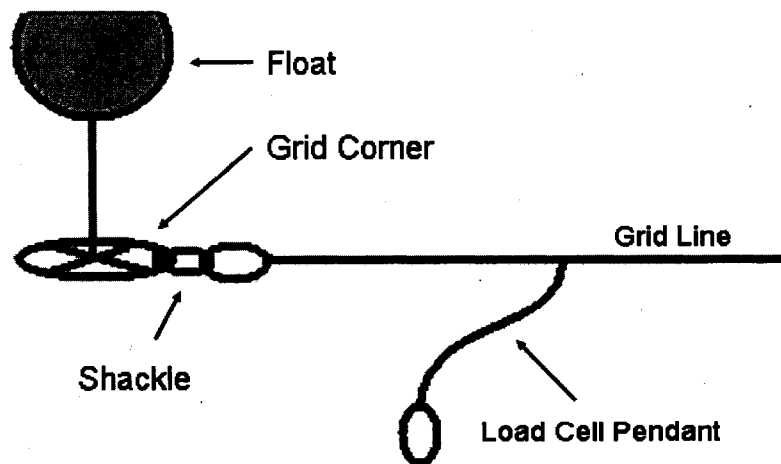
Mooring gear. In anticipation of a need for expanded cage space at the UNH OOA site, a submerged four bay grid mooring system was designed during the early spring of 2003 (see Figure II-1).



**Figure II-1** The submerged four-bay grid system. Major parts are labeled. Details of this design can be found in Fredriksson et al. (2004). Shortly thereafter, in preparation for deploying the new mooring system, rope, rope rings, shackles, anchors and chain were ordered from Gael Force Marine, Inverness Scotland, and delivered to facilities at the Woods Hole Oceanographic Institution (WHOI), Woods Hole, MA. Steel and Syntactic foam balls were ordered from Buoy Tech and Flotation Technologies respectively.

Upon arrival at Woods Hole, MA, all mooring gear was removed from its shipping container and inventoried. All parts were labeled to allow for proper storage during transport to the OOA site, as well as to allow for an organized deployment. Preparatory work for grid deployment included splicing additional lines, measuring and labeling all lines, and preparing a deployment plan. The pendant line for maintaining the depth of the center of the grid was spliced onto its weight. Although the main lines had been measured, cut and spliced by Gael Force Marine, they were re-measured. It was discovered that they were two meters shorter than their designed length. It was speculated that each line had been cut to length but the splicing process had shortened the line. All local mooring parts were loaded onto the F/V Nobska for transport and deployment.

In order to allow in-line load cells to measure anchor and grid line tensions, additional one-meter lines with eye thimbles and shackles were spliced into the grid and anchor lines attached to the northeast corner of the grid, as shown in Figure II-2.



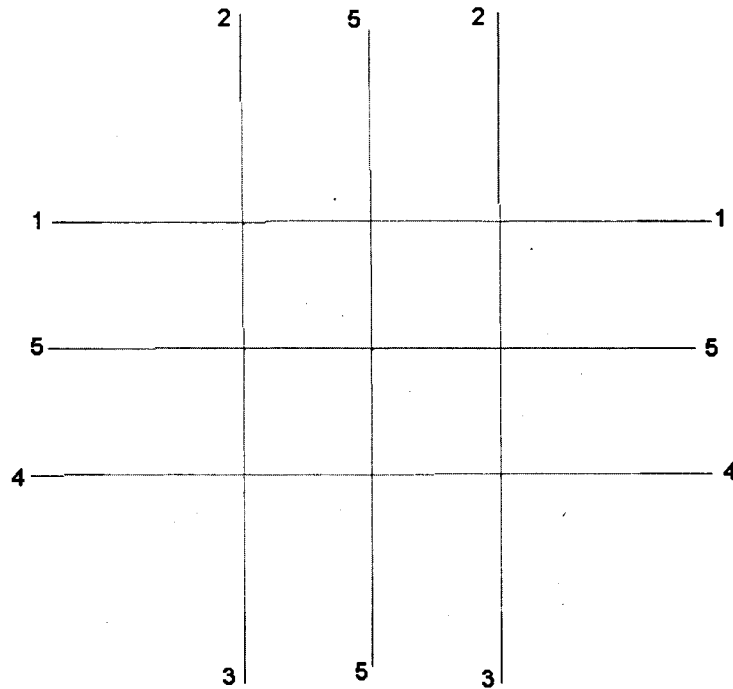
**Figure II-2** The load cell pendant arrangement for later deployment of the load cells to a grid line.



These lines were attached on the grid line approximately three meters from where the float connected the grid and anchor lines. These load cells were shackled to the grid corner and attached to the shackle on the load cell pendants, which would then shift the tension to the load cell. The load cell, now “in-line”, would measure the load in all lines connected to the northeast corner of the grid.

Deployment plan. A procedure for deployment, including the best order for tensioning the anchors for the grid system, was established in advance based on a scale model which was built pre-deployment at UNH. The scale model was built to a physical scale of approximately 1:25 to fit the dimensions of the engineering tank at the Jere Chase Ocean Engineering Laboratory. No attempt was made to match the scaled Young’s modulus, buoyancy, or mass of the grid components. Indicator floats were used to gauge how level the model grid was during trial deployments.

In all scenarios the grid itself was spread out loosely on the surface and supported by corner buoyancy balls (also at the surface). The anchors were lowered to ‘relaxed’ positions closer to the grid center than their final design locations, and anchor lines were attached to their respective grid points. From repeated tests it was determined that the best deployment method to gain proper final geometry and even tension throughout the grid was as follows (see Figure II-3):



**Figure II-3 The order in which the anchors were planned to be tensioned. Each number corresponds to the closest anchor and the steps outlined for deployment.**

- 1) Tension two opposing corner anchors (labeled 1) by pulling outwards on crown lines to the surface. This would set the depth of the grid between these anchors at the approximate correct depth.
- 2) Place the two anchors (labeled 2) attached at the same corners as the already tensioned anchors (labeled 1) in the correct predetermined Global Positioning System (GPS) locations. This would effectively set the entire side of the grid.
- 3) The anchors (labeled 3) across from those placed in step 2 would be tensioned, setting the two opposing sides of the grid.
- 4) The final side of the grid would be tensioned by pulling out anchors labeled 4.
- 5) The anchors, labeled 5, running across the middle of the grid are tensioned.

This method used both predetermined anchor locations and indicator floats for proper grid deployment. While the above method was adequate for getting the grid close to the correct level with even tension, final adjustments were necessary based on the location of the indicator floats to the surface.

## Deployment

On August 6<sup>th</sup>, 2003 the F/V Nobska dismantled the single-bay grid systems which had been at the site since 1999, and began deploying the four-bay grid. The first step in deploying the four-bay grid was placing all anchors in predetermined “relaxed” positions. The anchors were lowered into position with the anchor chain, line, and crown line assembly attached. With the anchors in these ‘relaxed’ locations, the grid corner flotation was at the surface attached to the other end of each then slack line. The lines and corners were pulled on board the vessel via a winch, and were connected together with the corner shackles then welded closed.

The grid segments were next attached to the grid corner flotation. Starting in the northwest corner, the anchor lines were connected by grid line segments in a clockwise fashion. The grid segment connecting the northwest corner joint to the western side joint was initially left disconnected. The northern side joint was then connected to the center joint, which was kept on board the vessel. The eastern side joint was then connected to the center joint. At this point there was not enough line slack in the grid to allow the remaining lines to be pulled on board and welded. The southern side joint was connected to the center joint with the connection at the center being welded, but the south side joint was connected using a small inflatable and only moused. The same method was used to connect the grid segment between the center joint and west side

joint, and finally the northwest corner to west side joint. Once completed, the grid was tensioned.

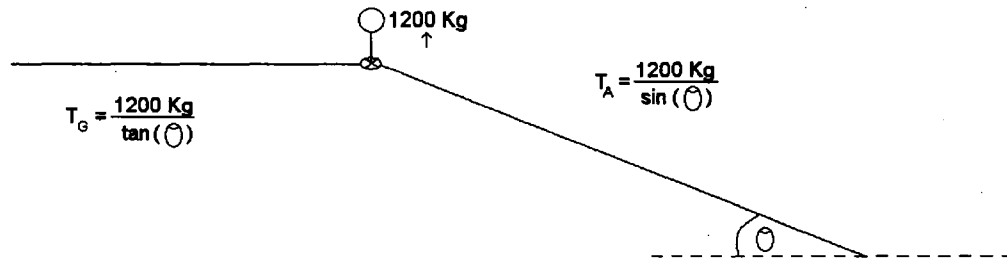
Since the center joint was held laterally by the grid lines, and held at depth by a weight below it, the center joint needed to be in the grid during deployment but not positioned independently. To this end, the weight was tied directly under the center joint, and the center joint was suspended at the correct depth by a temporary surface float. In that way, the center could be in place during tensioning without interfering with horizontal movements as the anchors were pulled out. Once the anchors were in place the weight could be dropped from the center and the surface float cut free.

In order to accurately place the anchors, a Trimble differential GPS was placed on the A-frame of the F/V Nobska. This was connected to a computer running HYPAC software to graphically show the real-time position of the stern of the vessel graphically relative to the desired position of the anchors. Indicator floats were added to all grid joint flotation except the center joint. These lines were set with trawl floats (having 2N buoyancy) at 12m (40ft), 15m (50ft), and 18m (60ft) from the top of the corner and side joint floats. By bracketing the desired depth to the submerged floats, a visual assessment of the grid depth was gained onboard the deployment vessel.

Following the planned tensioning algorithm (see Deployment plan), initial anchor placement was simple since the anchor lines had very little tension. But as the anchors were placed it became apparent from observing the indicator floats that the grid was not at the desired depth. As the grid was tensioned, more crown line scope was needed to pull out on the anchors while keeping them close to the bottom. This scope meant the anchors were an unknown distance behind the boat during tensioning, making

it difficult to accurately place them. If less crown line was used, then the anchor would have lifted well off the bottom and the vessel would have been pulled back significantly before the anchor touched down and dug in. Instead, anchors were placed with consideration to both the desired location for the anchors and the desired depth of the grid using the indicator floats for grid depth. After setting each anchor the position was checked by making the crown line as vertical as possible (without re-lifting the anchors) and using the GPS. The indicator floats were the easiest way to check the success of the grid deployment. Through their use, the grid was made level, though the anchors were pulled further apart than their designed position in order to achieve the desired depth.

Although the grid was level, the grid shape was not square. While attempting to put cages into the grid some months later, the grid quadrants themselves were discovered to have become more diamond shaped, and the grid lines were found to have been stretched in deployment to be longer than designed. Segment lengths were measured (by surveyor's tape) to be approximately 69m. This was greater than their design length of 65m and was likely due to the loose construction of the lines. The grid lines which appeared to be short pre-deployment were now found to be long. While this had repercussions in attaching cage bridle lines, similar stretching of anchor lines also had an effect on the grid tensions. Longer anchor lines with the same grid depth results in higher tensions in all lines as shown in Figure II-4.



**Figure II-4 The dependency of anchor and grid line tensions on the corner ball buoyancy and the angle of anchor line.**

The implications of these higher line tensions were not understood until initial attempts were made in 2005 to install load cells into the north east corner of the grid system.

### Initial Deployment Assessment

After deployment the anchor positions were plotted relative to their designed locations, as shown in Figure II-5. While the accuracy of these positions was not quantified, it was clear that the anchors had been deployed in positions further from the grid than designed.



**Figure II-5** The designed anchor locations (black diamonds) relative to the deployed positions (pink diamonds). Numbers indicate the distance between these positions. Grid corner positions are shown as pink triangles.

In 2005 first attempts were made to install in-line load cells into the grid. The process was anticipated to be simple, since designed tensions were only 2,500 lbs. The plan was to use only a two-ton come-a-long over two work days to pull the load cell auxiliary line close enough to the north east grid corner to attach a load cell. This expectation proved overly optimistic. After employing a combination of techniques and 7-8 days of diving, only three load cells were in place. After preliminary measurements from the 3 load cells gave wildly varying tension readings, the load cells were deemed to be working improperly, and this approach for getting grid tension measurements was abandoned. At the same time, difficulty getting the load cells in-line indicated that the actual line tensions were likely to be above the designed line tensions. Concerns were raised that if the grid tensions were too high, then the holding power of the grid itself

could be compromised. Since future plans for the site included pushing the mooring to its designed limit, further attempts to measure deployed grid tensions were prudent.



## CHAPTER III

### GRID TENSION SENSITIVITY MODELING

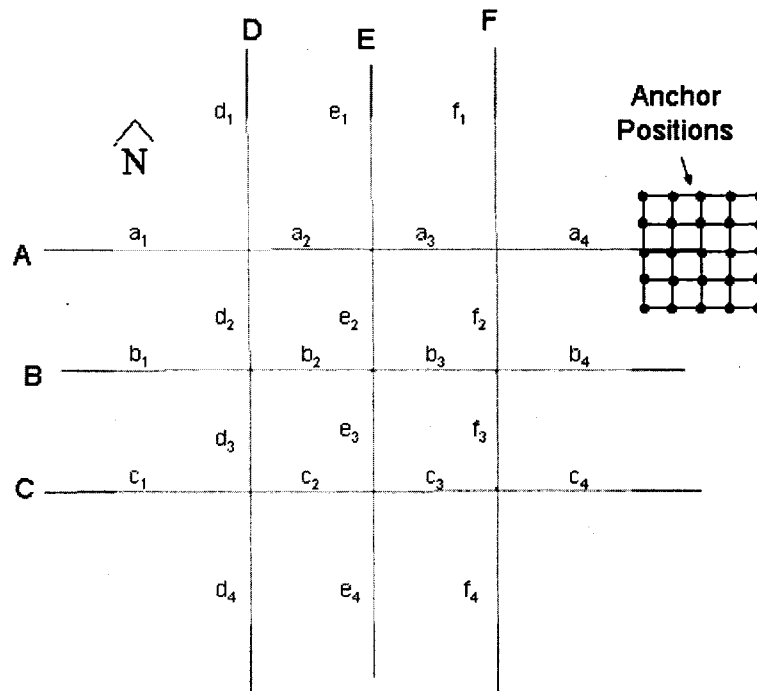
#### Background

Since anchor placement on the deployed submerged four-bay grid system was not exact and line lengths were variable, equilibrium line tensions were expected to vary, possibly compromising reserve anchor capability to cope with storm conditions. To quantify tension changes and assess the sensitivity of line tensions to anchor placement, the finite element program *AquaFE* was applied to the grid/anchor system under modeled equilibrium conditions.

*AquaFE* is a finite element modeling program that uses a modified Morison's equation to estimate the drag on cylindrical truss elements which simulate nets and structures in a dynamic fluid environment (Tsukrov, 2003). *MSC.Mentat*, from MSC Software Corporation, is used as a graphic user interface for constructing three-dimensional arrangements of these elements, and for viewing their dynamic displacement as determined by *AquaFE*. Output files from *AquaFE* also provide the stress and displacement for user defined nodes and elements. By manipulating the submerged four-bay grid system geometry with *AquaFE*, the variability of grid and anchor line tensions could be predicted.

## Modeling Approach

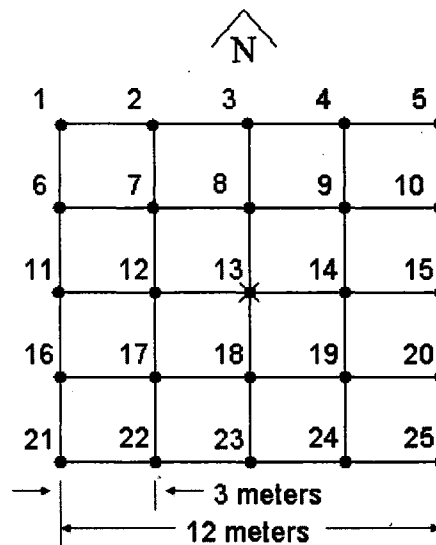
To gauge the sensitivity of the submerged four-bay grid system to changes in geometry, several models were built in *AquaFE*. Each model varied only the placement of the same anchor, and the predicted corresponding changes in grid depth and line tensions were monitored. Initially 25 models were built with a single corner anchor assigned to different locations, as shown in Figure III-1.



**Figure III-1. The grid system with the modified anchor locations. Mooring system lines are labeled for reference. The  $a_4$  anchor line led to an anchor located at one of the 25 position mesh intersection points shown.**

Only one anchor was assigned to various locations in order to minimize variables. A corner anchor was chosen to be relocated because corner anchors comprise the majority of all anchors and symmetry allows the effect of moving this one anchor to be applied to seven of the other locations. Therefore, corner anchors are more likely to have an

impact throughout the grid system. By monitoring the relative change in grid system tensions and depths as a function of one anchor's location, a working understanding of the relationship between anchor placement and line tensions was developed. Individual lines and cross sections are labeled in Figure III-1 for later reference. The single anchor modified was moved in a 12m by 12m pattern in 3m increments, as illustrated in Figure III-2.



**Figure III-2 The pattern for anchor placement modification. Position thirteen is the designed location of the anchor.**

The size of this anchor position grid was based on an estimate of error in the positioning of an anchor, which had not previously been quantified. In addition to the error in deployment positioning, the actual deployed anchors were thought to be even further from designed locations in part due to stretching of the grid and anchor lines.

After the initial 25 models had been studied, eight additional models were built to more closely examine the effect of moving the anchor only toward or away from the grid, as is discussed further in the discussion of the model results. Figure III-3 shows the mesh as built in *AquaFE*, although there were some variations in the mesh to

accommodate small changes in geometry between different models. In all cases the grid was built with the characteristics as shown in Table III-1.

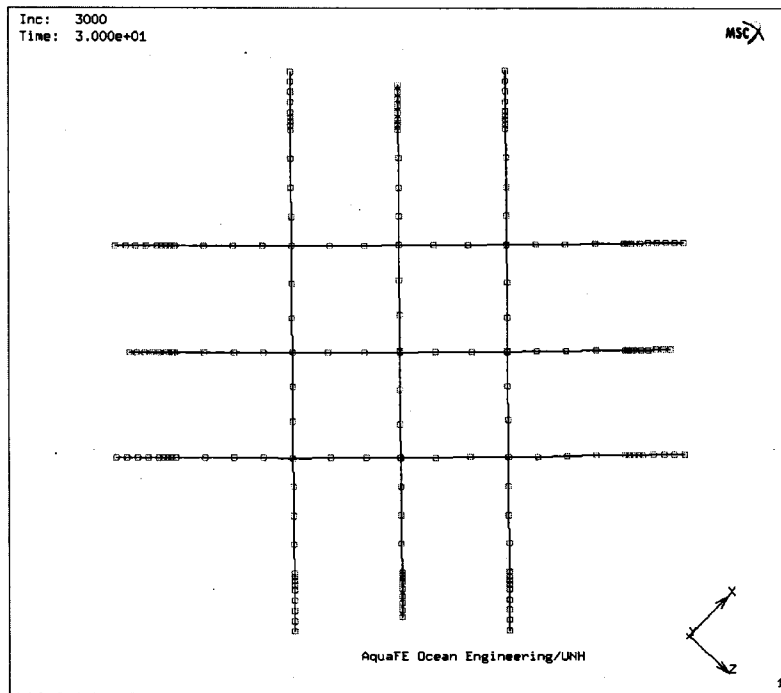


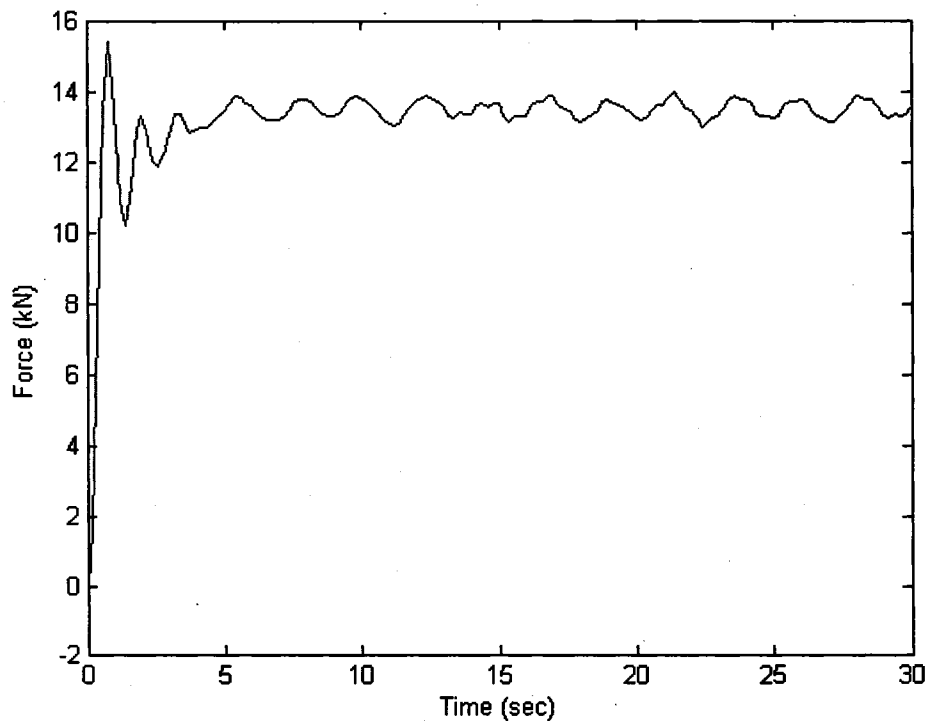
Figure III-3 The mesh used in AquaFE simulations of the grid system.

Table III-1 The properties used for the grid model

	Element length (m)	Cross section (m <sup>2</sup> )	Young's Modulus (N/m <sup>2</sup> )	Density (kg/m <sup>3</sup> )
Mooring line				
Grid line	65	2.026*10 <sup>-3</sup>	1.830*10 <sup>9</sup>	1.026*10 <sup>3</sup>
Anchor line	78			
Anchor Chain				
Corner	37.5	7.024*10 <sup>-3</sup>	2.000*10 <sup>11</sup>	6.610*10 <sup>3</sup>
Side	27.5			
Buoy Chain	2	2.027*10 <sup>-3</sup>	2.000*10 <sup>11</sup>	6.314*10 <sup>3</sup>
Buoy (small)	1	1.301*10 <sup>0</sup>	2.000*10 <sup>11</sup>	1.537*10 <sup>2</sup>
Buoy (large)	1	4.672*10 <sup>-1</sup>	2.000*10 <sup>11</sup>	3.210*10 <sup>2</sup>
Grid corner	.25	7.290*10 <sup>-2</sup>	2.000*10 <sup>11</sup>	1.243*10 <sup>3</sup>

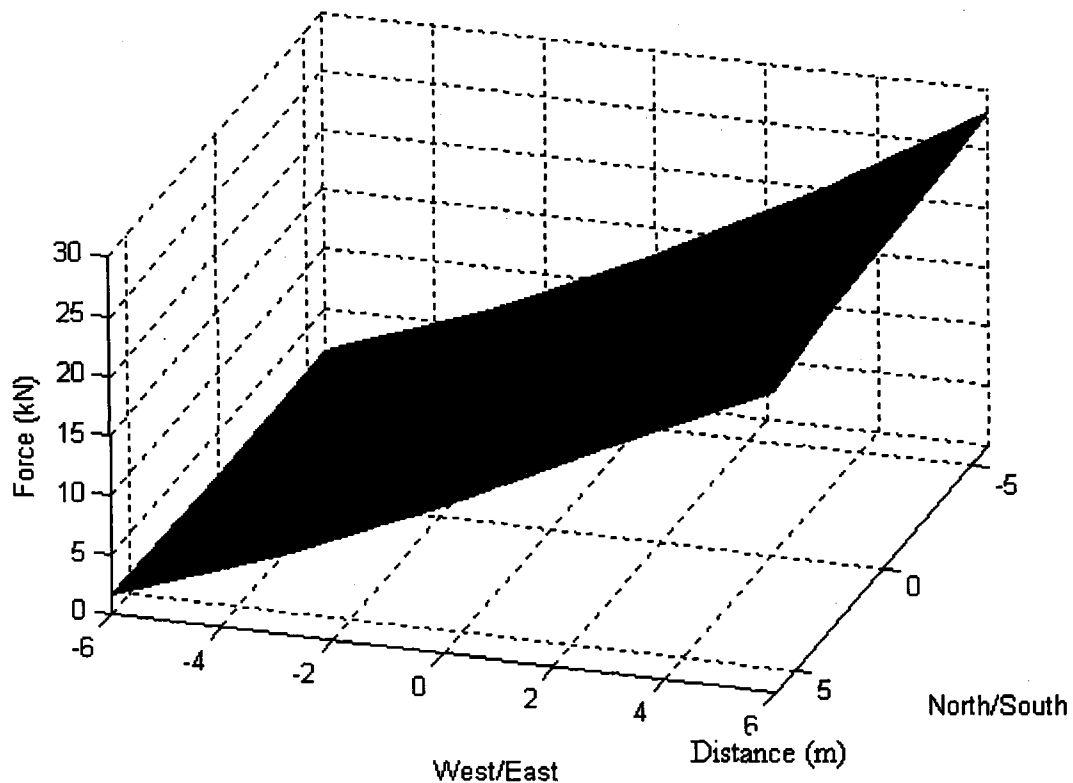
## Model Results

Since *AquaFe* is a dynamic model, the equilibrium state was not calculated directly. Instead, each run began with the grid below design level and the anchor lines slack. The grid then rose due to the flotation's buoyancy and the system tensioned until an equilibrium state was achieved. Thus placed, the grid system could be built without any pre-tensioning. In cases where the anchor was further away than the designed position (column locations 4 through 24 and 5 through 25 in Figure III-2) the grid was built 16m from the bottom. In all other cases the grid was built 34m from the bottom for ease of construction. As the model was run, the grid rose closer to the surface over time and the lines came under tension. Each of the models produced a time series for line tension and grid depth. A typical sequence of line tension is illustrated in Figure III-4.



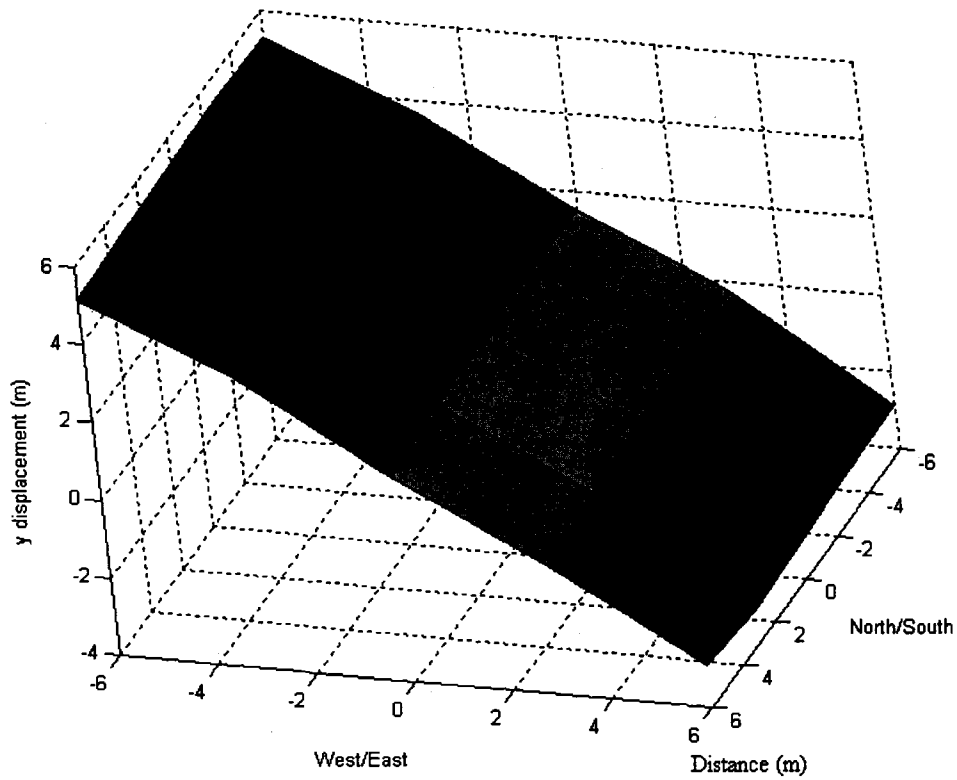
**Figure III-4 The tension in line  $f_1$  as the grid settles to equilibrium.**

Tension and depth data for each line and grid corner, similar to that in Figure III-4, was averaged over the interval between 25 and 30 seconds after the start of the simulation to remove small instabilities in the results. The resulting equilibrium tensions for anchor line  $a_4$  as a function of anchor displacement are plotted in Figure III-5. The complete series of plots for all grid segments and anchor lines identified in Figure III-1 are provided in Appendix A.



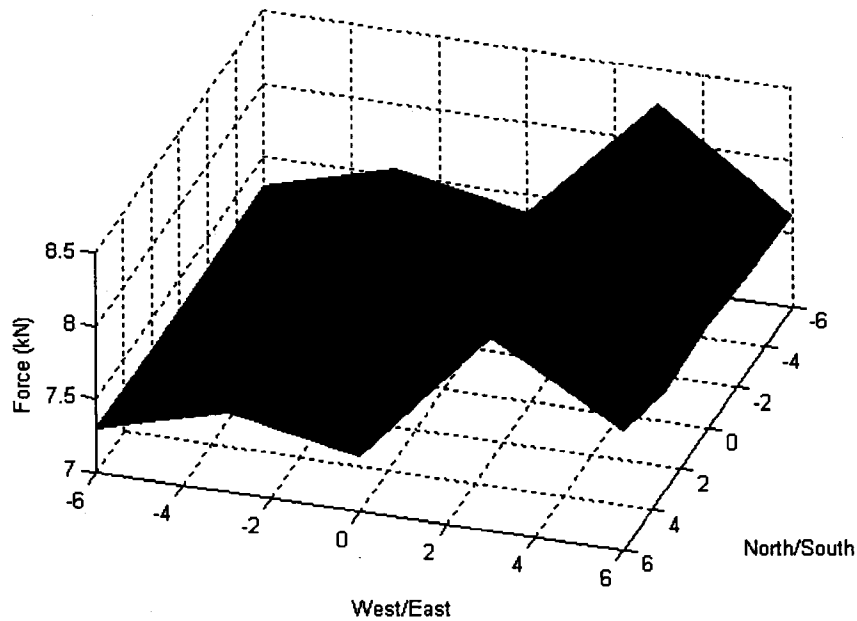
**Figure III-5 The tensions in line  $a_4$  as a function of anchor displacement.**

The tension in anchor line  $a_4$  is representative of tensions along cross-section A. Cross-sections C, D and F also show similar trends in lines within each cross-section. Depth results for the intersection of cross-sections A and F are shown in Figure III-6.



**Figure III-6 Northeast grid corner vertical displacement as a function of the horizontal displacement of the northeast anchor.**

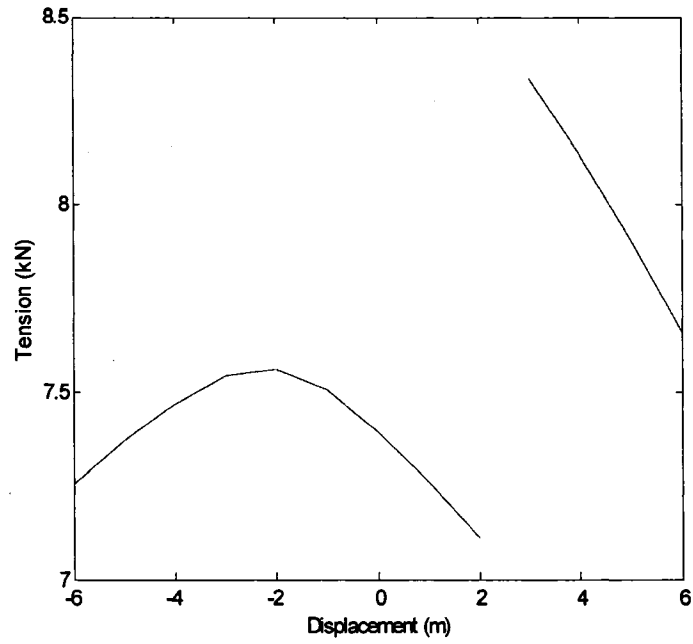
These cross sections have a very pronounced pattern of changing tension and depth as a result of an anchor being placed relatively closer to or further from the grid, in the east/west direction. Moving the anchor north or south produced very little change in tensions as the resulting change in angle of pull is only  $\pm 3$  degrees. The tensions in cross sections B and E did not show a monotonic pattern, as demonstrated, for example, in Figure III-7.



**Figure III-7 The tension in line  $e_1$  as a function of anchor displacement.**

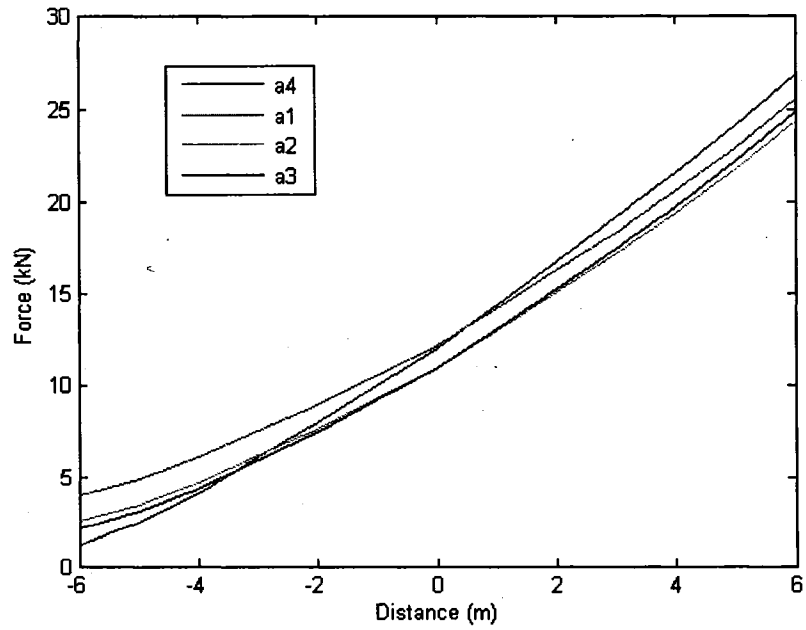
Grid depths as a function of anchor displacement, typified in Figure III-6, largely showed a monotonic pattern. Plots for all grid corners are in Appendix A. The non-linear behavior of cross-sections B and E (the two perpendicular central cross-sections) in Figure III-7 prompted an additional eight models to be built with the displaced anchor in between positions 11 to 15 in 1m increments (toward/away in an east/west direction). This allowed for closer examination of unexpected results. Figure III-8 shows the results for line  $e_4$  with the smaller 1m distances between anchor movements.





**Figure III-8  $e_1$  line tension as a function of the  $a_4$  anchor movement from positions 11 to 15. The discontinuous section is where the grid was built at a different depth.**

Figure III-9 shows the tensions of the individual lines in cross section A.



**Figure III-9 Tensions of the individual lines in cross section A as anchor is moved east/west.**

A plot with the tensions of all the anchor lines from position 11 through 15 in 1m increments is shown in Figure III-10.

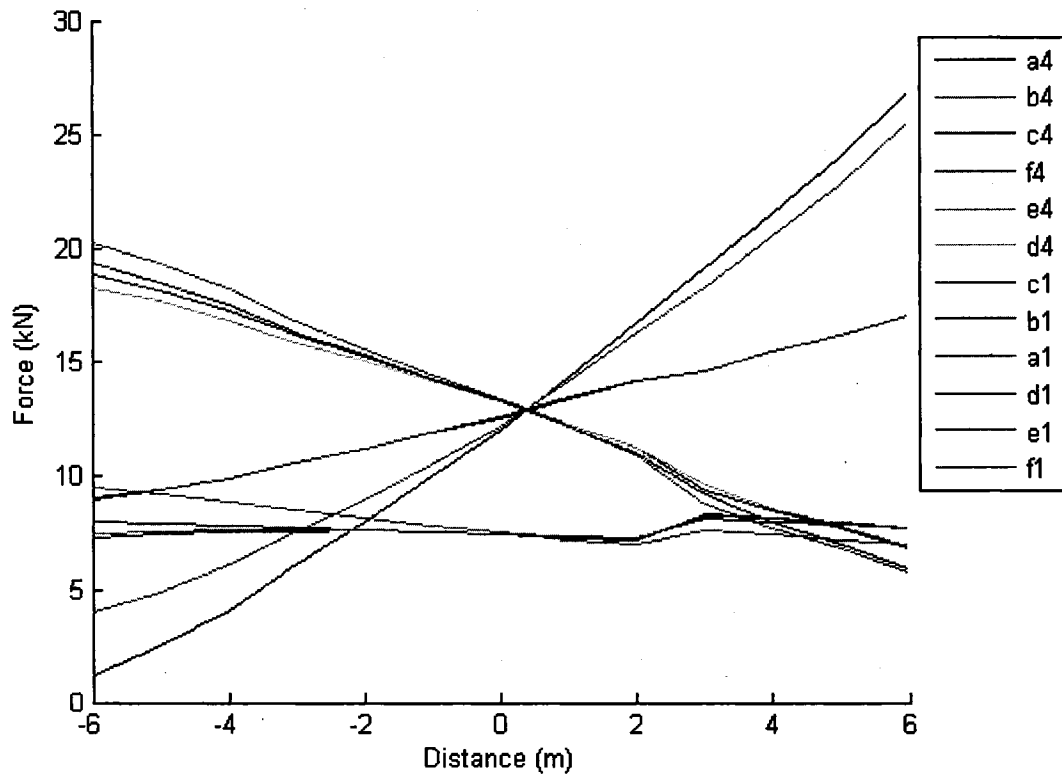


Figure III-10 Anchor line tensions as a function of anchor displacement east/west.

### Discussion of Model Results

While this study was conducted by re-locating a particular anchor, it is important to keep in mind that the results are symmetric. Although one anchor was moved, all the grid and anchor lines exhibited changes in tensions. Cross-section A in Figure III-9 increased in tension relatively linearly between approximately 1.3 kN /meter and 2.2 kN /meter. Since cross-section A is pulled downward as the anchor is

displaced further away, it relieves tension in the perpendicular lines, in this case cross-section D and F. Because cross-sections D and F have less tension, cross-section C takes up tension from the buoyancy of submerged flotation on the southern side. In this way cross-sections that run parallel and along the side of the grid have correlating tensions. The cross-sections that run through the center of the grid, lines B and E, did not change substantially as a corner anchor was moved within this range. The described patterns are most clearly illustrated by the anchor line tensions graphed in Figure III-10.

The first set of models produced a higher order pattern for the tensions of lines B and E. For this reason the second set of 8 models was built to resolve any more complex effect. The results, shown between 2m and 3m in Figure III-8 for the anchor line  $e_4$ , show that the evident higher order effect is a consequence of the different model initial conditions. In initial models the grid was released 34 meters from the bottom. Models that had the anchor moved further away from the grid than the designed location required the grid to be released at a depth of 16 meters. The effect of the grid starting deeper resulted in a small shift in the data for all lines, but is most evident in the lines that run through the middle since they have such a small change in tension. While this artifact is not useful in itself, the result that changes in initial conditions can affect the equilibrium tensions is interesting. Since the disparity between the two data sets is likely due to very small difference in model properties, such as line lengths or number of elements, this provides a context for the sensitivity of the system when modeled.

The depth of the grid also changes symmetrically with anchor movement. Generally, the corner connected to the shifted anchor gets deeper as the anchor moves away from the grid, as shown in Figure III-7. The opposing (southwest) corner rises as

the anchor is placed further away from the grid. This is because cross-section D has less tension and allows the corner to rise until cross-section C holds it. The overall effect is a general sloping of the grid platform toward the corner with the anchor being moved outward.

Overall, discrepancies in positioning an anchor by  $\pm 3\text{m}$  result in tension changes on the order of  $\pm 7\text{kN}$  (see Figure III-4). Such tension changes could easily arise if the anchors were simply placed using a surface GPS. However, this sort of error also leads to depth changes of  $\pm 3\text{m}$  (see Figure III-5) which can easily be detected by indication floats (in the absence of strong current). Thus the expected range of grid tension variability should be less than  $\pm 7\text{kN}$  using the grid deployment method described in Chapter 2.

## CHAPTER IV

### MOBILE TENSION METER

#### Impetus

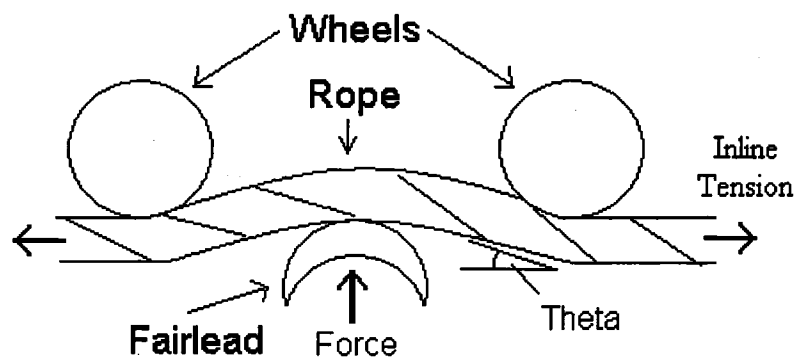
Although the sensitivity analysis suggests that variation in actual tension from the design value should be no more than  $\pm 7\text{kN}$ , the divers' experience while installing the load cells provided some evidence that as-deployed tensions exceeded the design by an amount that was much greater than  $7\text{kN}$ . Unfortunately, the in-line load cells were not functioning properly, and the data was inconclusive. Thus there was a pressing need to measure tensions in the grid system and anchor line directly.

One measurement approach would have been to re-deploy the four in-line load cells in the Northeast corner of the grid after refurbishing the instruments. Arguments against this approach include difficulties in the first deployment and lack of reliability. Furthermore, placing a load cell in-line always decreases segment length to some extent. The sensitivity analysis (interpreted symmetrically) revealed that moving any one of the twelve anchors could significantly alter the grid tensions such that there could be large variations in the grid system tensions that could not be measured from just the northeast corner. In order to measure tensions without altering the system and to measure the tensions (sequentially) in multiple places, a mobile tension meter that could be used on all of the lines in the grid mooring was designed.

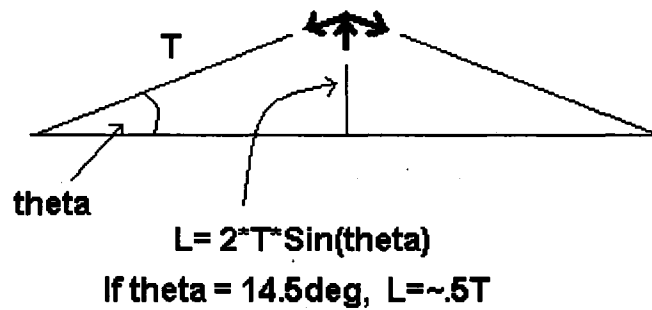
## Concept Development

The main criterion for the mobile tension meter design was ease of deployment on the submerged grid. Therefore, the instrument needed to be deployable by diver, ideally with the ability to move the instrument from point to point to obtain multiple measurements during a single dive. Multiple same-day measurements could provide near-synoptic grid tension measurements. Criteria for being diver deployable also meant the mobile tension meter should be simple to use and neutrally buoyant. The target maximum measurable load was 89kN, half the holding power of the anchors, with an accuracy of 1.5 kN.

The design approach to measure line tension consisted of deflecting the line a small amount and measuring the load required to deflect it (see Figure IV-1). If the line was deflected with a known geometry, then the load required to deflect the line could be related to the in-line tension.



**Figure IV-1 A conceptual drawing of rope deflection. Theta is the angle of deflection.** As a target, the line would be deflected 14.5 degrees from straight ( $\theta$  in Figure IV-1). The resulting force needed to deflect the line would then be approximately half the load in the line as demonstrated in Figure IV-2.



**Figure IV-2 The relationship between line tension(T) and the force to displace it orthogonally(L).** This ratio provides a reasonable compromise between measurement resolution and the force and distance needed to deflect the line. Having theta as a small angle minimizes the stress differential in the cross-section of the line without requiring large fairleads to handle the bending radius of the rope. Unfortunately, a small angle also means that small errors in displacement may result in unacceptably large errors in measurement.

A crucial part of the tension meter was the selection of a mechanical apparatus to deflect the line. The component needed to be able to provide the force to deflect the line several centimeters while providing up to 44.5kN (5 tons) of force. The apparatus also needed to work underwater and be easy to operate. A hydraulic bottle jack was chosen for its compact size and availability. In addition, a bottle jack will work on its side, enabling the tension meter to operate on vertical lines such as buoy moorings. Finally, the jack has a pressure valve such that were the jack to be jacked on a line with tensions higher than 89kN, there would be no risk of apparatus failure or danger to divers. The only modifications that needed to be made to the bottle jack were to seal the hydraulic fluid fill to keep water out.

Another crucial component that effected the size and geometry of the tension meter was the mechanism for measuring the force of deflection. Load cells are commonly used for these types of tasks. A pancake style load cell from Sensing Systems Corporation in New Bedford, MA was used at UNH for the in-line load cells, and was readily available. This sensor also takes up minimal vertical space in the tension meter design, minimizing the size of the frame required. Another benefit was the availability of recorders used for interfacing with these load cells.

### Preliminary Testing

Since a diver-deployable tension meter was untested for this application, an approximate half-scale test was devised. The wheels, fairlead and rope were all set up at half the size of the expected full size components as shown in Figure IV-3.



**Figure IV-3 The half-scale tension meter trail setup.**

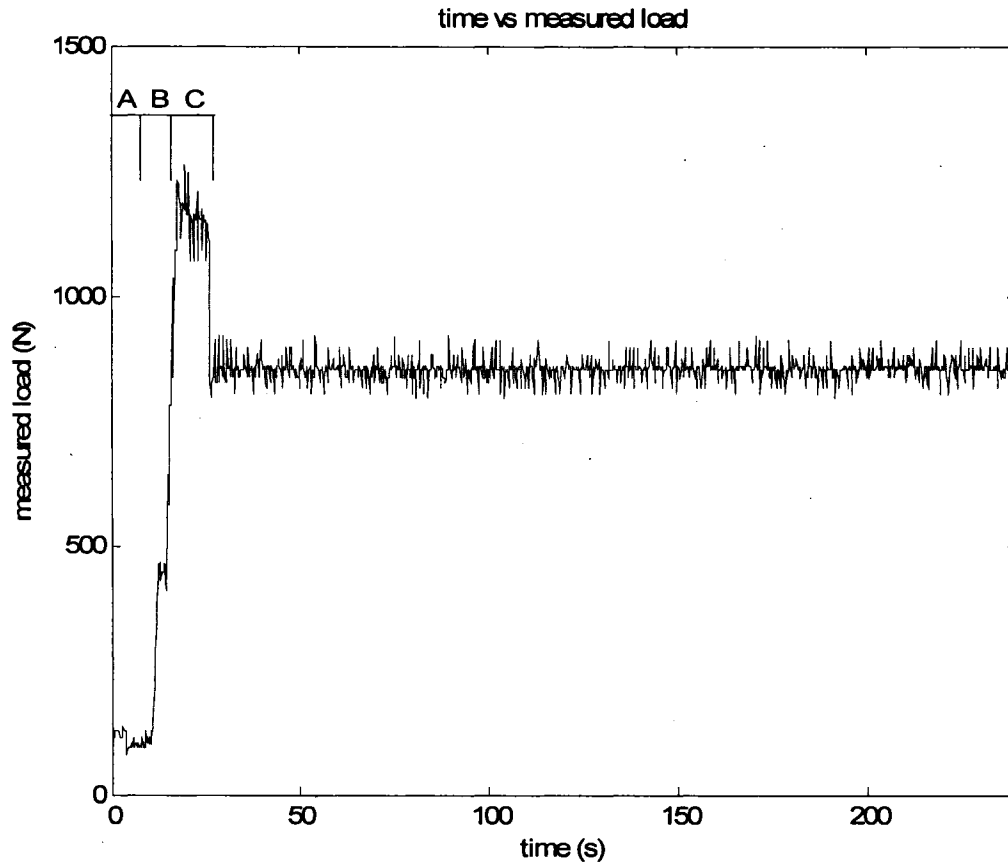
The half-scale test consisted of measuring the tension in a line that was suspending various known weights. The fairlead/loadcell assembly was jacked against the rope to a measured displacement, and load measurements were taken from the load cell. Initial



trials showed a downward trend in the tension data with time. Initially the 25mm (1in) rope of three strand construction was thought to be getting longer as a result of reorientation and compaction of the rope fibers. After being replaced with a 19mm ( $\frac{3}{4}$ in) twelve plaited rope, it became apparent that the aged hydraulic ram was leaking and slowly retracting. This slow retracting resulted in a decrease in load cell force with time. To get consistent measurements, a pipe, halved along its axis, was placed around the ram, and the jack was relaxed so the pipe supported the load cell. Chocked in this way, the line was displaced the same amount in every trial.

### Preliminary Trial Data

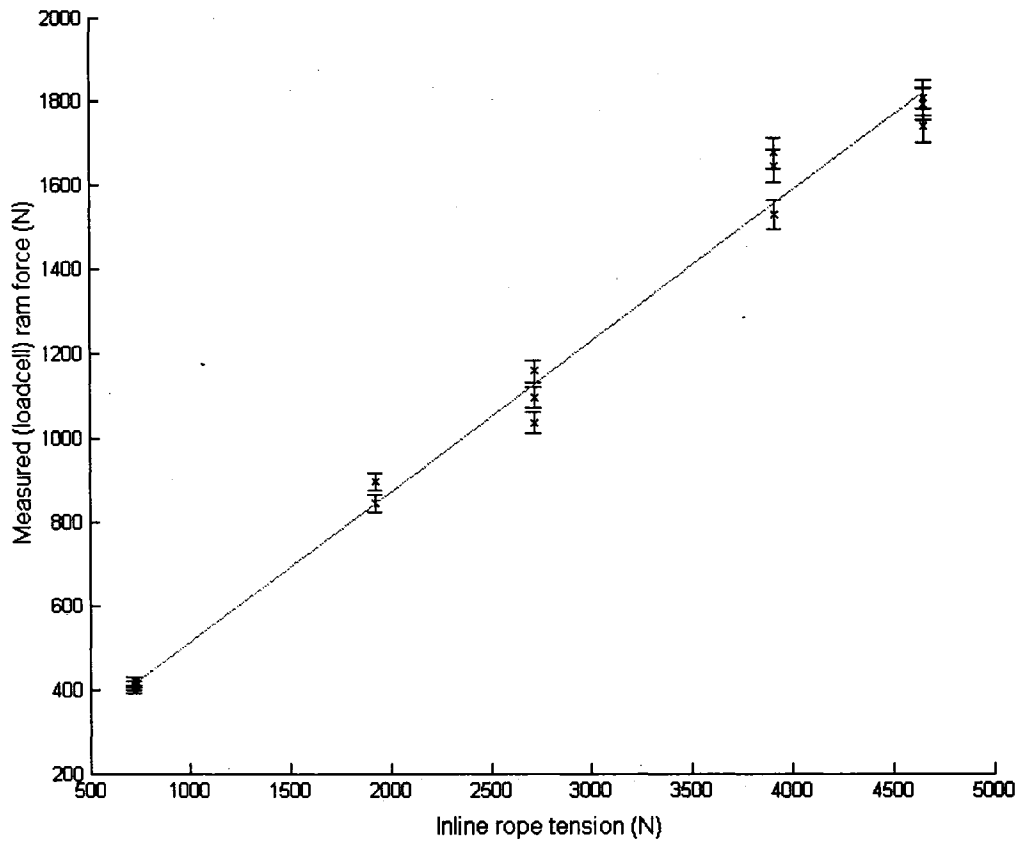
Five different weights were used to tension the line during half-scale tests. The line tension with each weight was measured three times, for four minutes each time. Each trial included starting with the load cell under no load, and then jacking it into position and subsequently relaxing the jack so the load cell was supported by the pipe chock. A sample data file is shown in Figure IV-4.



**Figure IV-4 Measured ram load cell force during a half-scale trial.**

In Figure IV-4, each stage of the trial is apparent. Section A in Figure IV-4 shows the load cell under no load (zero offset of 93 N); then in section B the jack pushes the load cell to deflect the line, and in section C the jack is relaxed onto the pipe chock and the measured load drops to the equilibrium value. The noise in the load values had a standard deviation of less than 40N, and was partly due to unavoidable swinging of the weight as the ram was jacked into position.

The measured load for the last 167 seconds of each test was time averaged to represent that trial. Figure IV-5 shows each test with a linear regression.



**Figure IV-5** The results of the averaged half-scale data. Black 'x' is the average from each test with the error bars representing the one standard deviation for each trial. The green line is a linear regression.

Figure IV-5 represents the results of testing with the half-scale mobile load cell. The equation for the linear regression was:

$$\text{Measured (loadcell) ram force} = 0.3568 * \text{In-line rope tension} + 159 \text{ (N)} \quad (1)$$

The slope of the line in Equation 1 is related to the amount of displacement of the line as shown in the geometry of Figure IV-2. Since the trial rope diameter (19mm) was smaller than initially planned (25mm) and the displacement of the line was not increased, the geometry of line in the apparatus was changed. As a result, the ratio of measured (load cell) force to rope tension was smaller than desired due to a smaller

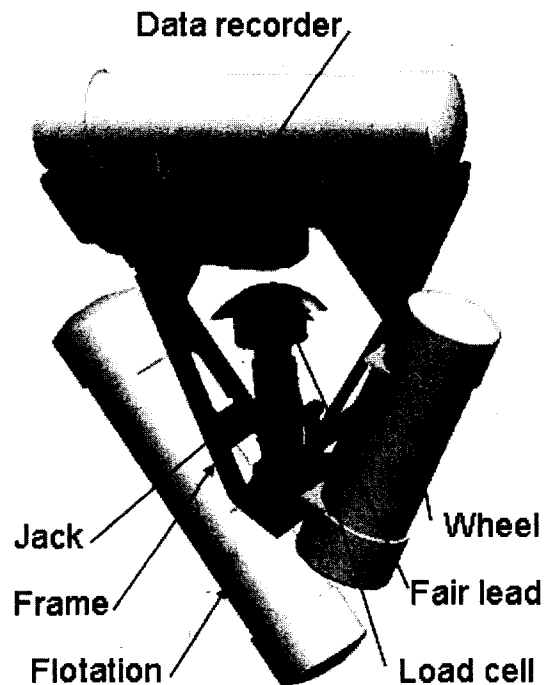
displacement angle. The regressed line slope was 0.3568, while the intended slope was closer to 0.5.

Assuming the ratio of measured (load cell) load to rope tension accurately reflects the geometry of deflection, then the angle that the rope was deflected was only 10.28 degrees. At this angle, and for the small geometry used, an additional 0.25mm of displacement would increase the measured (load cell) force by 27 N corresponding to a 76 N increase in rope tension for the largest weight used. A small misplacement of the pipe chock could account for this error. For the full-scale setup these errors would be small compared to the larger displacement needed at full-scale.

### Full-scale Design

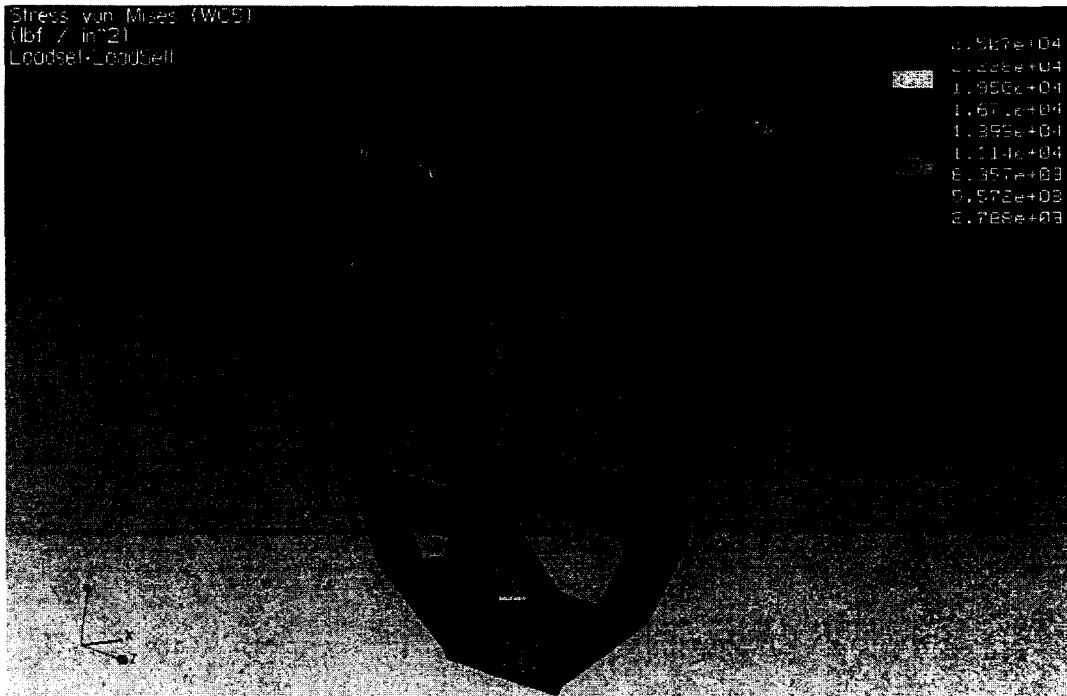
With the proof of concept in the half-scale trial completed, the final design for the tension meter was initiated, including the design of the frame and selection of the final components. The tension meter needed to be built in a cost-effective manner since no budget existed for its construction. This meant using as many off-the-shelf parts as possible, together with easy-to-fabricate pieces. Marthane wheels, commonly used as fairleads for anchor rode on small vessels, were employed as fairleads for the tension meter. An off-the-shelf 5-ton bottle jack was selected, and was slightly modified by welding a threaded coupling over the hole in order to prevent water from entering the fluid fill cap. An adaptor was fabricated to clamp to the end of the jack and allow the load cell to be threaded onto the jack (see Figure IV-6). A 50mm (2in) thimble was welded to a plate which would distribute the load to the outside of load cell. A pipe chock, similar to the one used in preliminary tests, was made using 32mm (1.25in) pipe

to go around the hydraulic ram to prevent any variation in the length of displacement. The frame itself was fabricated from A36 ¼-inch steel. The complete assembly is shown in Figure IV-6, with the individual parts shown in Appendix B.



**Figure IV-6 A Pro/Engineer solid model of the assembled tension meter.**

Design of the tension meter frame for holding all the parts together in the correct orientation was primarily completed using Pro/Engineer from PTC. The major parts were drawn and assembled in the program to ensure fit. Drawings for the frame parts are in Appendix C. The framing was modeled in Pro/Mechanica, also from PTC, to optimize proper structural integrity (Figure IV-7). The maximum von Mises stress was 192MPa (27,850 psi) while the minimum yield strength is 248MPa (36000 psi), so that the factor of safety with respect to yielding is 1.3 .



**Figure IV-7 The Results from Pro/Mechanica for stress on the frame for the maximum designed load.**

Once final dimensions were determined, PRO/Engineer was used to calculate the mass and center of gravity for the assembly. This helped in establishing the amount and location of flotation that was required for the instrument to float properly. The flotation was made primarily from 15cm (6in) PVC pipe, with an additional 10cm (4in) PVC section. Buoyancy was tested in the Chase Ocean Engineering Laboratory engineering tank. The final design erred on buoyancy and added a small amount of extra flotation in case of miscalculation, since it is easier to compensate for by simply adding weight to the frame in the form of lead dive weights.

The load cell used was a Sensing Systems pancake-style load cell. Details can be found in the Irish et al. (2001). The load cell recorder was modified in the UNH Monitoring and Control Laboratory from an existing load cell recorder based on a Persistor computer, from Persistor Instruments Inc in Bourne, MA. The Persistor was

placed inside an Iklite underwater housing and powered by a 7Ah, 12v battery. Magnetic switches were used to turn the computer on and off underwater, while a second switch was used to set an amplifier depending on which of the UNH load cells was in use. In this way the recorder could be used to get data from any UNH load cell, not just the mobile tension meter. Upon activation the computer would run a program written at Woods Hole Oceanographic Institution (WHOI) to measure the load cell force. The program was preset to sample at two hertz for one minute, although this could be adjusted. A parts list for the entire assembly is shown in Table IV-1.

**Table IV-1 The parts and their weights as measured as well as predicted by Pro/E.**

<b>Part</b>	<b>Dry Weight (N)</b>	<b>Pro/E Dry Weight (N) (predicted or defined)</b>
Frame	279	258
Bottle Jack	67	76
Load cell adaptor + Load cell + Fair Lead	56	56
Wheels	18	18
Axel assembly	4	4
Recorder	44	44
6" x 23" PVC	48	48
6" x 32.25" PVC	56	56
6" x 32.5" PVC	58	60
4"x 25.75" PVC	25	25
<b>Total</b>	<b>654</b>	<b>641</b>

## Calibration

In order to best calibrate the mobile tension meter, calibration conditions, including tensions and rope properties, should be similar to those in the field. The calibration scheme was similar to that in the scale trials. An in-line load cell was used for comparison while the mobile tension meter took measurements. The in-line load cell was calibrated to  $\pm 50\text{N}$ . Because the desired range of tensions for calibration was up to  $80\text{kN}$ , a weight could not simply be hung from a crane as in the scale model trials.

To provide tensions in the range the instrument was designed for, an arrangement of blocks and tackle was stretched between trees. A schematic of the calibration setup is shown in Figure IV-8.

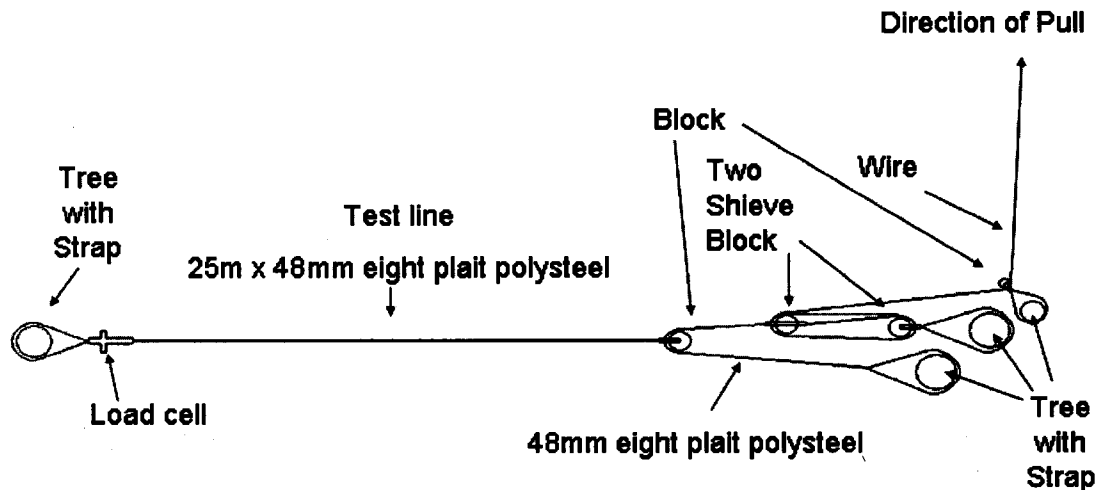


Figure IV-8 The calibration setup.

The arrangement of blocks provided 10:1 ratio of line tension to pulling force. A combination of a single part tackle with 48mm eight plait polysteel was attached to the end of the calibration line, providing a 2:1 ratio for tension. On one end of the rope through the first block another two part tackle was utilized with 9.5mm (3/8 inch) wire



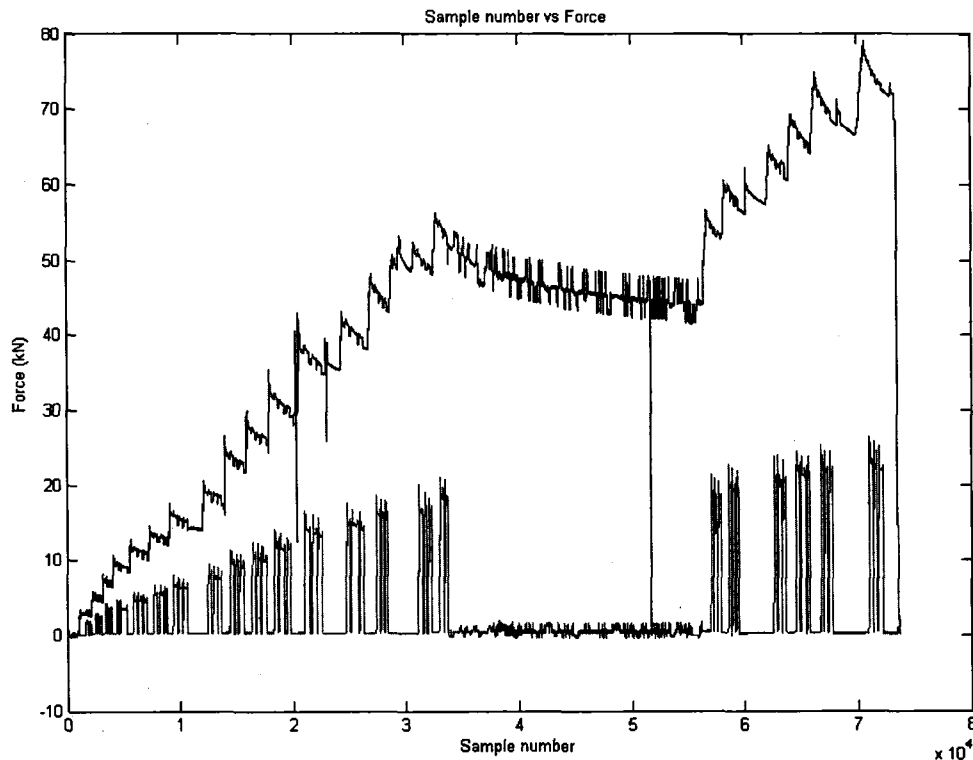
rope, providing a 5:1 ratio. Pulling power was provided by a combination of a 2.5-ton capacity come-a-long and a small tractor.

Since the mobile tension meter shortens the rope by 9.5mm (3/8 inch), the calibration rope should be relatively long to minimize the effect, preferably similar to the length of the deployed lines. An old cage bridle line, 25m in length, that had been in use at the open ocean site for two and a half years was used for calibration. This line was ordered at the same time and was of the same material and construction as the anchor and grid lines that were then currently in the grid at the OOA site. Other than immersion in salt water during testing, it was expected that this rope was a good approximation of the rope that would be measured in the field using the mobile tension meter.

The process during each calibration test included increasing line tension incrementally by ~2.5kN, installing the mobile tension meter, taking measurements, and then removing the tension meter. Also, after the tension meter was removed, the amount of elongation over a 3.65m (12ft) section of the line was measured, as was the maximum diameter of the line in the area of the line next to the tension meter. The tension was then stepped up another ~2.5kN and the process repeated.

The in-line load cell, on the opposite end of the calibration line from the block and tackle, sampled the tension at 5 hertz. During the first calibration, the tension meter data was recorded in minute-long increments on its custom recorder at 1 hertz. During the second test the ram load measurements were recorded on a laptop at 5 hertz for consistency in the data acquisition process. During the first calibration, at each increase a single tension measurement was taken with the mobile tension meter. During the

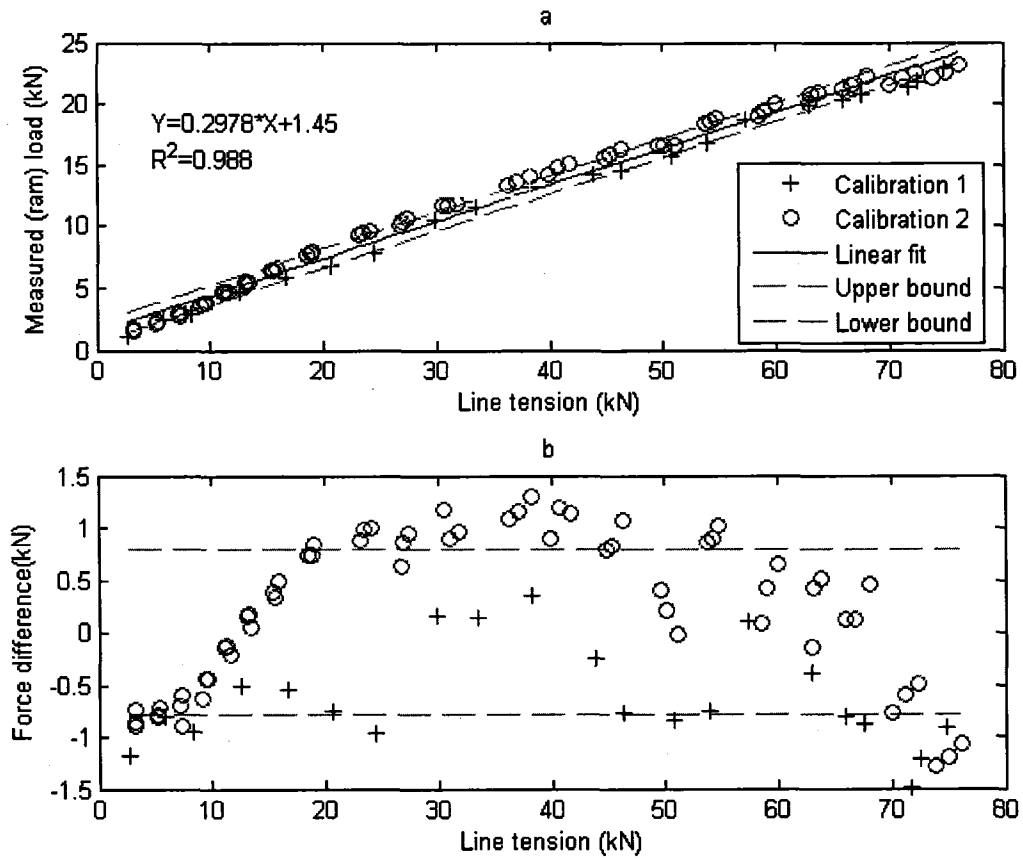
second calibration, three measurements were taken at each tension to provide more data points and reduce uncertainty. Figure IV-9 shows the data from the second calibration.



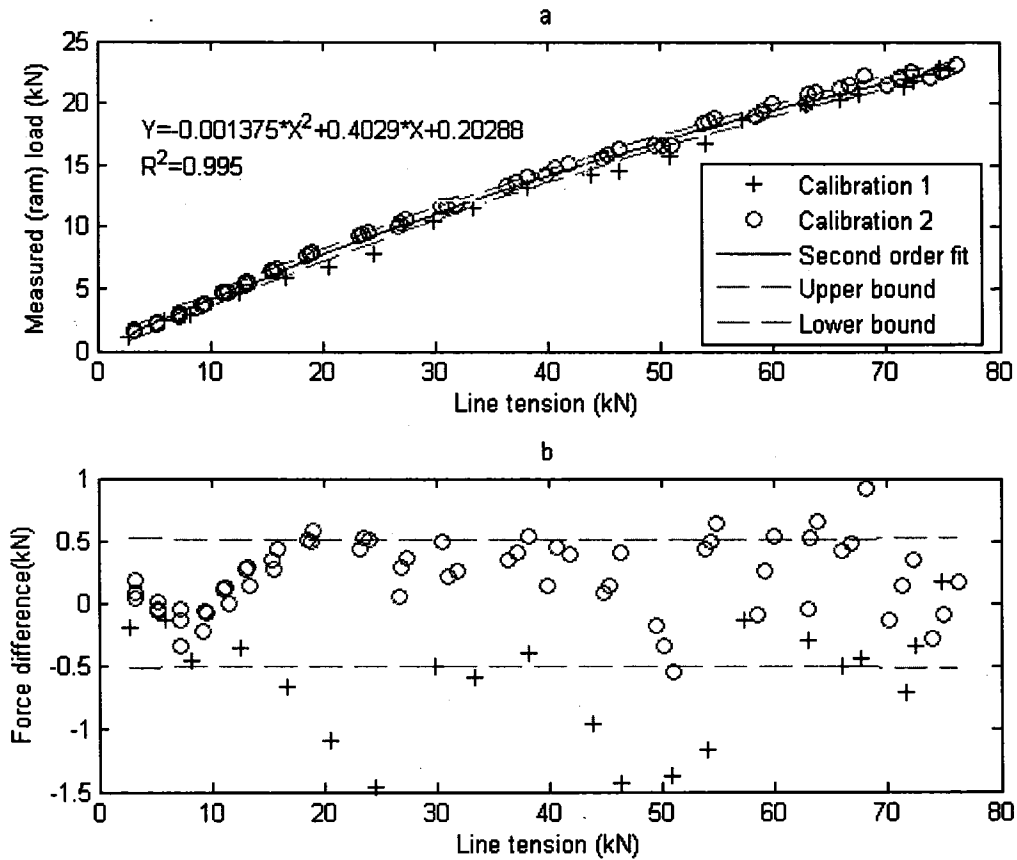
**Figure IV-9** The calibration time series from the second test. Blue is the load measured in the in-line load cell, while red is the load measured in tension meter (ram) load cell.

Spikes in the red line shows when measurements were taken. In post processing, the data was sectioned manually using time stamps to synchronize in-line load cell and mobile load cell (ram) data. The data for each of the two load cells was averaged within the chosen range and plotted against each other. Figure IV-10 shows the results for a linear fit, and Figure IV-11 for a second order fit. Although the data sections chosen are stable over time, the tension in the calibration line had a constant downward trend overall. This trend is assumed to be stretching of the line and of the other components

used for maintaining the tension, for example compression of the wheels, flexing of steel.



**Figure IV-10 The (a) calibration with a linear fit and (b) the difference between measured force and the linear fit. Data from the separate calibration tests are displayed with different symbols. The “best fit” formula is given on graph (a). Bounds denote one standard deviation of  $\pm 0.8$  kN.**



**Figure IV-11** The (a) calibration with a second order fit, and (b) the difference between measured force and the linear fit. Data from the separate calibration tests are displayed with different symbols. The “best fit” formula is given on graph (a). Bounds denote one standard deviation of  $\pm 0.5\text{kN}$ .

The linear regression data was used to process mobile load cell data during field measurements. Standard deviation of the difference between the linear regression and measured force at the ram was  $0.8\text{kN}$ . This is considered the uncertainty in measurement.

### Field Measurements

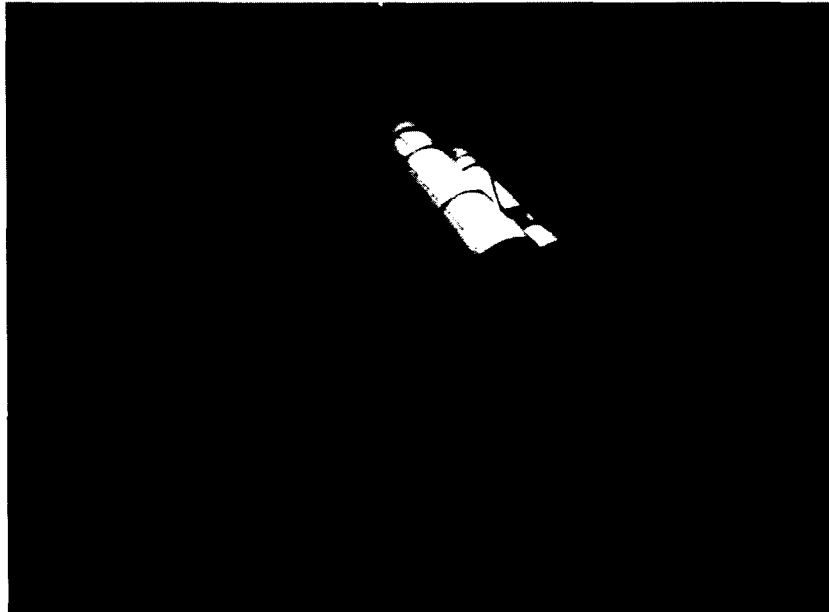
On the sixth of April, 2006, the tension meter was taken out to the UNH OOA site to take measurements. A pre-deployment picture is shown in Figure IV-12.



**Figure IV-12 The mobile tension meter fully assembled pre-deployment.**

Because of its 654N dry weight, the tension meter was lowered into the water using the crane on the R/V Meriel B. Once in the water, the instrument with an additional 22N (5 lbs) of dive weight proved to be slightly buoyant. A 27m line with flotation was also attached to the instrument frame in case of flotation failure. Divers descended down a line to the northeast corner for the first measurement. Both the grid and anchor lines had been cleaned of biofouling in the area 4 meters from the grid corner to insure that biofouling would not interfere with the instrument. Tension measurements for each of these lines were taken by installing the instrument, switching on the computer and allowing it to record for 1 minute at 1 hertz sampling rate. Once the program stopped and the computer was shut off, the tension meter was removed and reinstalled on the next line. Installation was not difficult even for a single operator. An additional handle on the frame was used to hold the frame in the correct location while the jack was operated. Once the jack began to pinch on the line the instrument held itself in place. Removal was equally as simple, and even faster than anticipated, as both the vacuum

inside the jack and the increased external pressure caused the ram to retract quickly. The dive time for measuring these four lines totaled 25 min at a depth of 24m (80ft) feet. Figure IV-13 shows the tension meter during deployment.

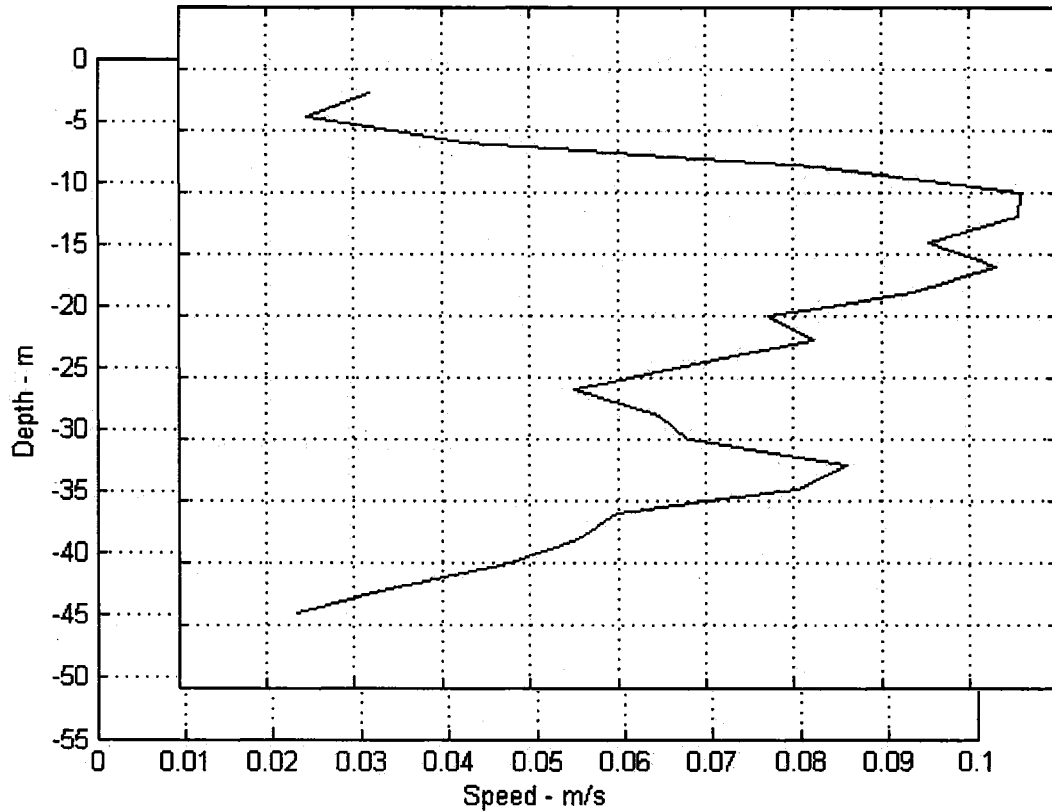


**Figure IV-13 The mobile tension meter during deployment.**

For the second set of measurements also taken on April 6, 2006, divers were dropped at the surface marker at the southern side grid joint, closest to the southwestern grid joint where measurements were to be taken. Divers swam with the tension meter to the southwest joint, and the measurement process was repeated. In addition to the four measurements taken at this corner, a measurement was taken at the same depth while not connected to the line. This measurement provided the zero offset for the load cell. The dive for the measurement of four lines and swimming the grid line (twice) took 28 minutes at a depth of 17m (57ft).

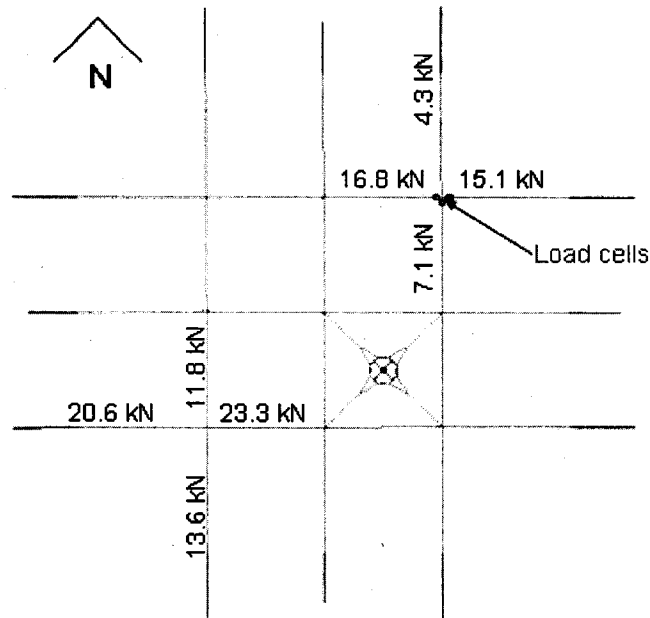
Conditions at the site during the field measurements were considered comparable to those for the modeled static grid. In one of the mooring bays was a submerged 600 m<sup>3</sup> Sea Station with no net. Only small surface buoys were present to

possibly couple the sea surface with the mooring. Environmental conditions were calm, with the UNH environment monitoring buoy at the UNH OOA site, measuring a significant wave height of 0.8m and a current profile as shown in Figure IV-14.



**Figure IV-14** The current profile as measured from a bottom mounted ADCP at the UNH OOA site.

Post-processing of the data was performed using the linear regression from calibration. The final field measurement for zero offset was averaged and applied. The grid tension measurements taken on April 6, 2006 are shown in Figure IV-15.



**Figure IV-15** A schematic of the grid with the measured tensions next to the lines where they were measured. For reference, grid segment design tensions were 11kN while design anchor line tensions were 14kN. Error is considered to be  $\pm 0.8\text{kN}$ .

These measurements were lower than expected given the difficulty experienced in deploying the in-line load cells in the northeast grid joint. These tensions suggest the grid is tensioned more in an east-west direction, particularly in the southern-most cross section.

The direct measurements of tension provided an opportunity to evaluate an *AquaFE* application to the as-deployed equilibrium configuration based on field estimates of anchor geometry. An overview of the methods and results are presented here, while details are provided in Appendix C. Anchor positions were inferred using two methods, shipboard GPS over vertical crown lines at the time of deployment, and an acoustic survey which was conducted later. Replicate measurements using both approaches exhibited standard deviations ranging from 1.6m to 3.5m. Grid segment and anchor line lengths (under no-load conditions) were estimated using measured final



lengths and tensions, as well as rope elastic properties obtained during the tension meter calibration process.

Predicted equilibrium grid tensions, shown in Figure IV-16, are extreme compared to both designed and measured tensions. Given the uncertainties in actual anchor position and rope parameters, the observed lack of agreement is probably to be expected. This exercise, however, is another confirmation of how sensitive tensions are to as-deployed geometry.

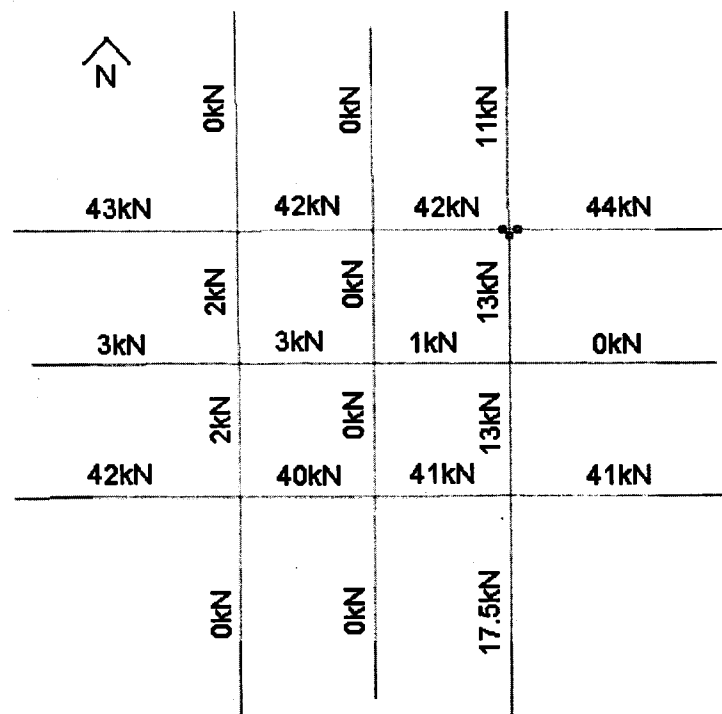


Figure IV-16 The tensions in the deployed grid as model in *AquaFE*.

## CHAPTER V

### CONCLUSIONS

#### Deployment Success

Evaluation: In evaluating the success of the deployment of the UNH OOA submerged four-bay grid, several deployment outcomes were taken into account. Field measurements indicate that the grid was not over tensioned during deployment. The standard deviation of measured tensions from the designed tensions is 6.5kN. Grid tensions are not compromising the holding power of the anchors, although some anchors, namely those on the east and west sides, are providing most of the pre-tension. While there are some variations in tensions throughout the grid, the grid is relatively level due to the use of indicator floats during deployment. Stretch in the rope created some irregularities in the shape of the system and position of the anchors. The standard deviation in measured radial anchor placement from the designed location is 11m, although the error in these measurements is  $\pm 3.5\text{m}$ . Stretch in the rope also made the pre-designated anchor positions inadequate for deploying the grid at the correct depth. Standard deviation of the observed grid depths compared to the designed depth is 2.7m. While the grid, as deployed, has functioned well for three years, below are detailed improvements that could be made for the future deployment of a similar system.

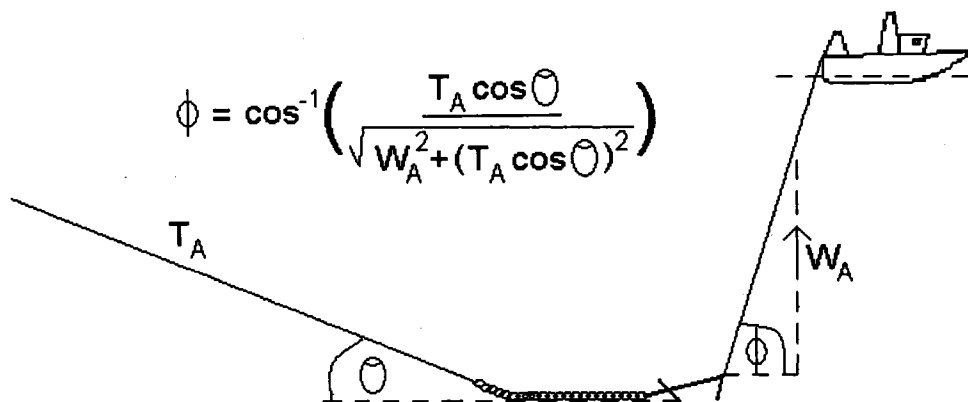
Recommendations: Tensions throughout the grid system should be symmetrical; an outcome achievable in large part by controlling anchor positions during deployment. In order to place the anchors more precisely, acoustic transponders could be placed on the anchors themselves. Transponder gathered knowledge of the anchor position could help ensure that anchors are not placed significantly further away from the grid than other anchors, and, secondarily, that anchors are placed in-line with their corresponding cross-section. Transponders could be attached to the anchors before deployment and released acoustically after the anchors are placed. In addition, multibeam sonar could be used during deployment to obtain anchor locations; however, the need for data processing from such a system could prove logistically unrealistic for providing feedback into an active deployment process.

To establish useful target deployment positions, line lengths and rope properties should be well known. Correct line lengths and rope properties allow target anchor positions to be computed more accurately and take some uncertainty out of deployment. This would be particularly important in areas where anchors need to be placed so as to avoid particular bathymetric obstacles (such as a rock outcropping). One way to establish rope lengths is to pre-stretch the rope to remove the constructional stretch, a process outlined in the Cordage Institute's *Test Methods For Fiber Rope* (CI 1500-02). Pre-stretching rope could be a time consuming process, however, as the line would need to be cycled to 20% percentage of its breaking load ten times as outlined in the referenced manual. For systems that do not have a large pre-tension, but expect large peak tensions, a benefit of pre-stretching the line is the stability of the system after

deployment. Once the constructional stretch is removed, large tensions are less likely to permanently deform the system into a different geometry.

Pre-stretching the rope and using transponders on the anchors can help insure a successful deployment. In addition, while indicator floats should still be used as a visual reference for grid depth and levelness, reliable modeling of the static system would assist planning of deployment positions. Also, the ability to measure tensions anywhere in the system, through use of the mobile load cell, significantly benefits future operations as changes in tensions over time, or after a large storm event, can indicate anchor movement, which is particularly significant as the anchor location itself cannot be tracked without transponders or a multibeam system.

Another approach to gaining the approximate target tensions in the grid during deployment would be to specify a crown line length during deployment using the scheme shown in Figure V-1.



**Figure V-1** The relationship between the anchor line tension and the crown line angle needed to pick up the anchor.  $T_A$  is the anchor line tension, and  $W_A$  is the weight of the anchor.

If the anchors are dragged out and placed slowly, then the horizontal component of the designed tension in the anchor line can be calculated as if static. When dragging out the anchor, the horizontal component of tension in the crown line is equal to that in the

tensioned anchor line. As an anchor is dragged out and the tension in the anchor line increases, so does the crown line tension. Since the crown line length does not change during towing, the vertical force crown line picks the anchor off the bottom. To make use of this and the correlation of the anchor and crown lines, the crown line length can be set to such that the anchor is picked off the bottom by the crown line when the anchor line tension is too high. To do this, the vertical component of the crown line tension is assumed to be equal to the weight of the anchor when the tension in the anchor line is correct. The relationship in Figure V-1 defines an angle that the crown line would pull on the anchor at the design anchor line tension. For a given depth only a particular crown line length can achieve this angle. The deploying vessel could then pull the anchor out slowly with the specified crown line length and then drift backward until the anchor set in the correct position. While this method does not take into account the friction of the chain on the bottom, with some experience this method could prove useful.

### Future Work

Present information on the UNH OOA submerged four-bay grid mooring is insufficient to accurately specify input parameters needed to predict equilibrium tensions. While line lengths and properties can be estimated, the sensitivity of the grid system results in discrepancies between field measured line tensions and *AquaFE* predictions. Further work identifying the root cause that is specifically creating this difference would enhance *AquaFE's* usefulness. Despite this disparity, *AquaFE* is still useful for understanding how equilibrium tensions are achieved. A basic understanding of how the grid reacts to a misplaced anchor or a shortened line has been outlined. This

information applies to operations regarding both line replacement and repositioning a dragged anchor. With further work quantifying input parameters, *AquaFE* could more accurately reflect the field measurements and become a more useful tool for enhancing the understanding of changes in line tension as a function of anchor placement.

It is likely that mooring platforms in an open ocean grid, similar to the UNH submerged four bay grid, will be designed to increase site efficiency and availability by maximizing fish cage volume and by moving to deeper water. Given the complexity of a large system with multiple bays and the difficulty of deploying anchors accurately in deeper water while under tension, it would be operationally sound to utilize more complex technology in order to place anchors with precision. In addition, line tensions and grid depth should also be monitored during deployment to ensure the proper geometry of the system.

## LIST OF REFERENCES

Cordage Institute. 2002. "CI 1500-02."

Fredriksson, D.W., Muller, E., Swift, M.R., Tsukrov, I., Celikkol, B., 1999. Offshore grid mooring/net pen system: design and physical model testing. In: Proceedings of the 18<sup>th</sup> International Conference on Offshore Mechanics and Arctic Engineering. ASME, St. John's, Canada.

Fredriksson, D.W. 2001. "Open Ocean Fish Cage and Mooring System Dynamics." Ph.D. Dissertation, University of New Hampshire, Durham, NH.

Fredriksson, D.W., Swift, M.R., Irish, J.D., Tsukrov, I., and Celikkol, B. 2003. "Fish Cage and Mooring System Dynamics Using Physical and Numerical Models with Field Measurements." *Aquacultural Engineering*, v. 27, No. 2, pp. 117-146.

Fredriksson, D.W., DeCew, J., Swift, M.R., Tsukrov, I., Chambers, M.D. and Celikkol, B. 2004. "The Design and Analysis of a Four-Cage Mooring for Open Ocean Aquaculture." *Aquaculture Engineering*, v. 32, No. 1, pp. 77-94.

Irish, J., Carroll, M., Singer, R., Newhall A., Paul, W., Johnson, C., Witzell, N., Rice, G., 2001. "Instrumentation for Open Ocean Aquaculture Monitoring." Woods Hole Oceanographic Institution Technical Report.

Ling, S. 1977. "Aquaculture In Southeast Asia." University of Washington Press, Seattle.

Tsukrov, I., Ozbay, M., Fredriksson, D.W., Muller, E., Swift, M.R., and Celikkol, B. 1999. "Offshore Grid Mooring/Net Pen System: Finite Element Analysis." Proceedings of the 18<sup>th</sup> International Conference on Offshore Mechanics and Arctic Engineering, St. John's, Canada:ASME.

Tsukrov, I., Ozbay, M., Fredriksson, D.W., Swift, M.R., Baldwin, K. and Celikkol, B. 2000. "Open Ocean Aquaculture Engineering: Numerical Modeling." Marine Technology Society Journal, Vol.34, No. 1, pp. 29-40.

Tsukrov, I., Eroshkin, O., Fredriksson, D.W., and Celikkol, B. 2003. "Finite Element Simulation to Predict the Dynamic Performance of the Tension Leg Fish Cage." Open Ocean Aquaculture: From Research to Commercial Reality. The World Aquaculture Society, Baton Rouge, LA, PP. 169-175.

Tsukrov, I., Eroshikin, O., Fredriksson, D.W., Swift, M.R., and Celikkol, B. 2003. "Finite Element Modeling of Net Panels Using a Consistent Net Element." Ocean Engineering, Vol. 30, pp 251-270.



## **APPENDICES**

## APPENDIX A

Appendix A consists of the data from Chapter 3. This is broken down into three sections; 1) the grid tensions by line as a function of the position of the anchor in a boxed area, 2) the grid depth by corner as a function of the position of the anchor in the in a boxed area, 3) the grid tensions by as a function of the position of the anchor along a straight line parallel to the anchor line.

### Section 1

This section contains the tensions for each line in the grid as a function of the placement of a single corner anchor. They are grouped by cross section and labeled as in figure III-1.

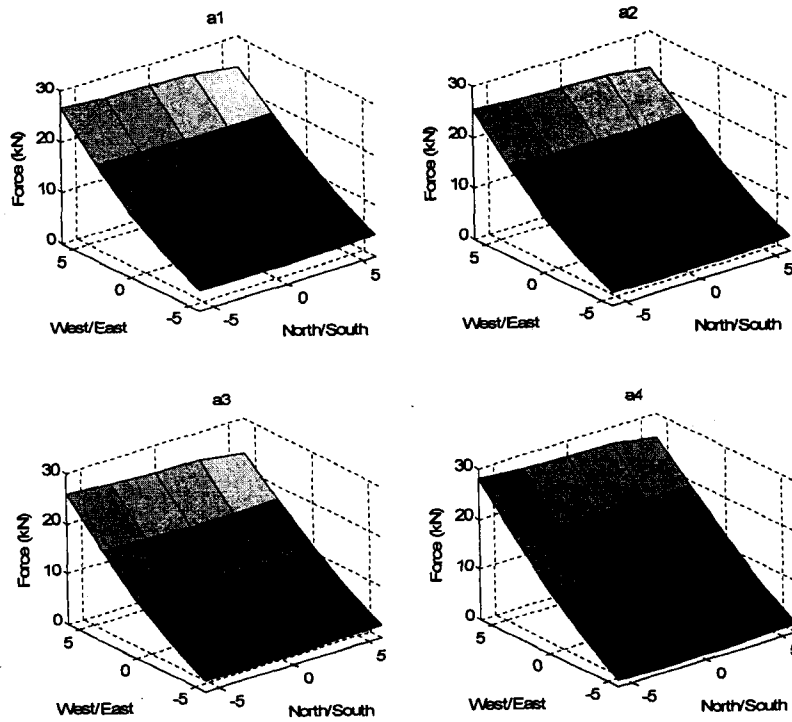


Figure A-1 Cross-section A tensions by line as a function of the northern east anchor displacement.

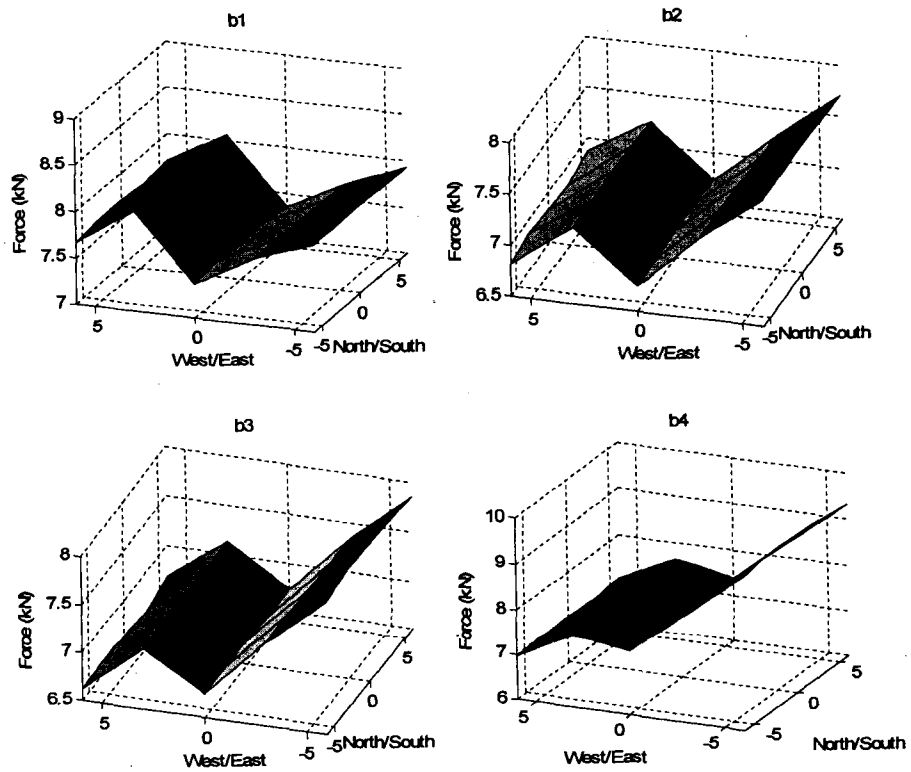


Figure A-2 Cross-section B tensions by line as a function of the northern east anchor displacement.

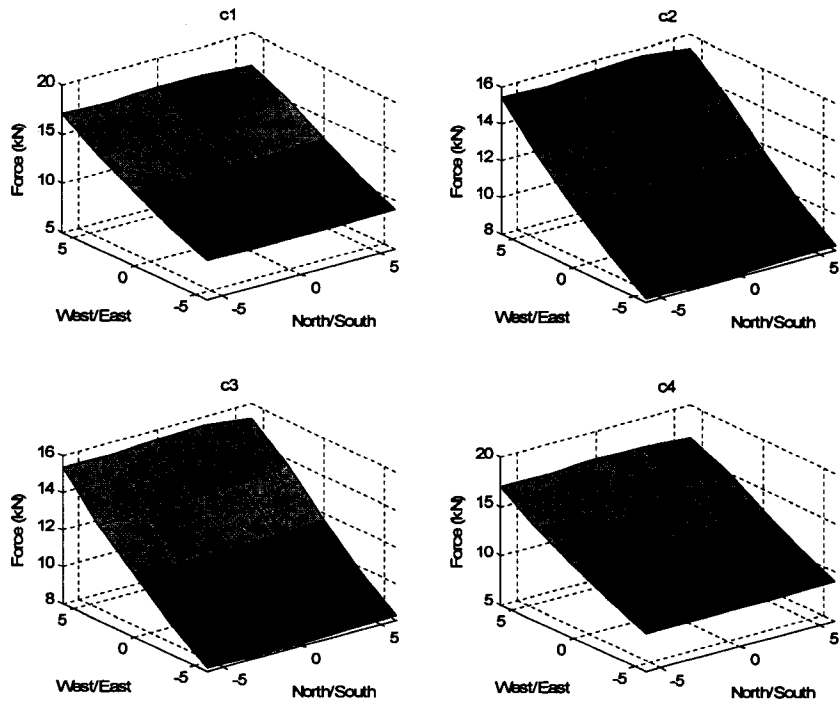


Figure A-3 Cross-section C tensions by line as a function of the northern east anchor displacement.

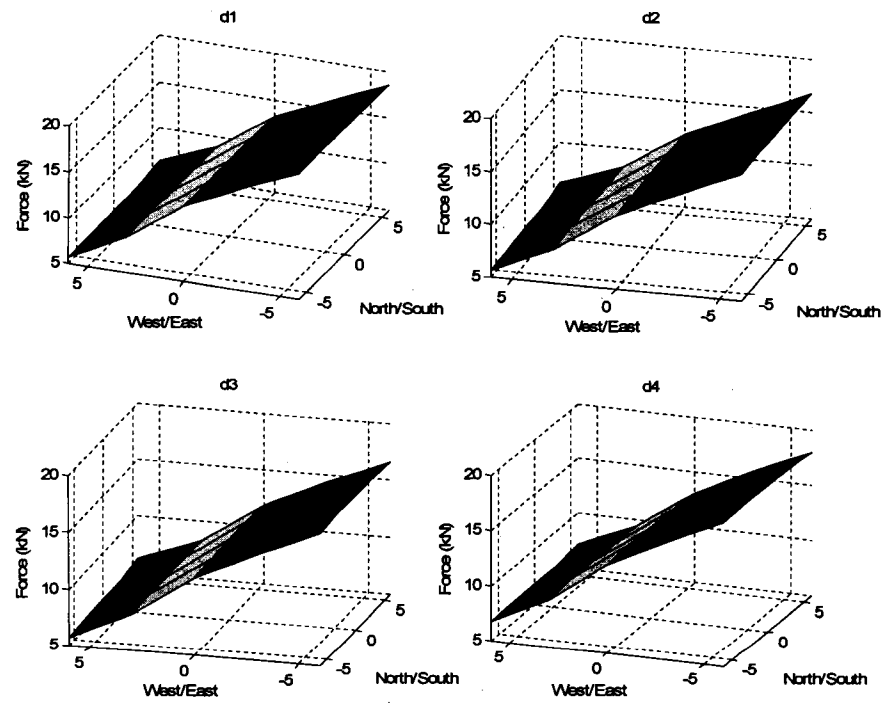


Figure A-4 Cross-section D tensions by line as a function of the northern east anchor displacement.

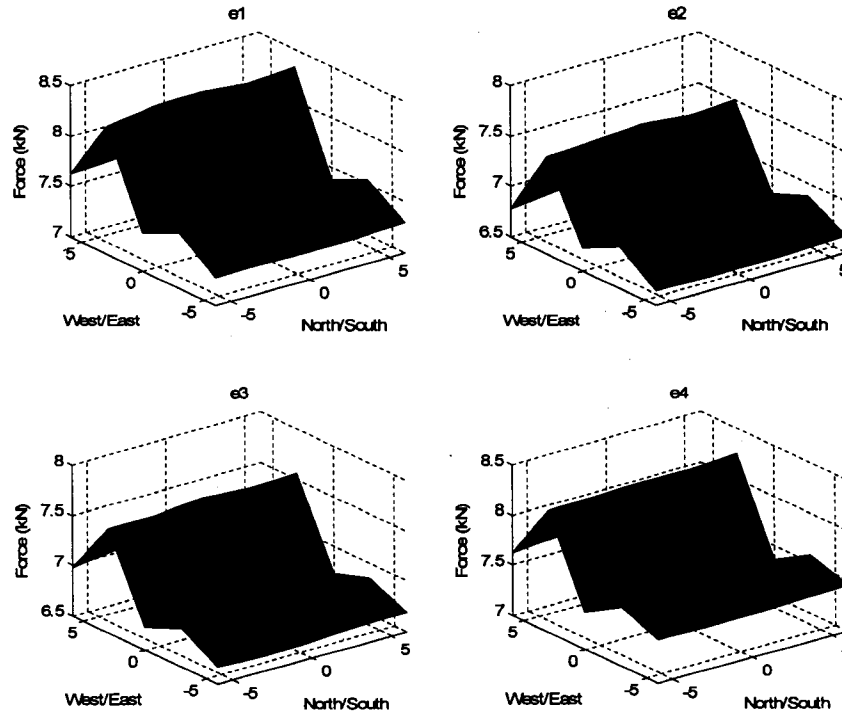


Figure A-5 Cross-section E tensions by line as a function of the northern east anchor displacement.

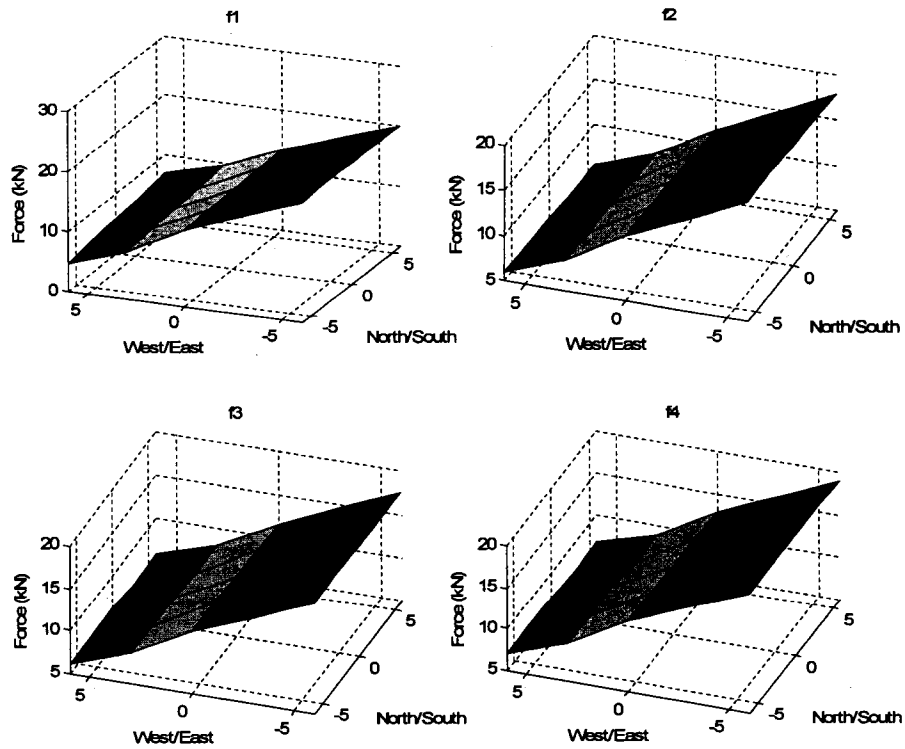


Figure A-6 Cross-section F tensions by line as a function of the northern east anchor displacement.

## Section 2

The grid corner and side joint displacement from the designed position as a function of the northern east anchor displacement are shown in this section.

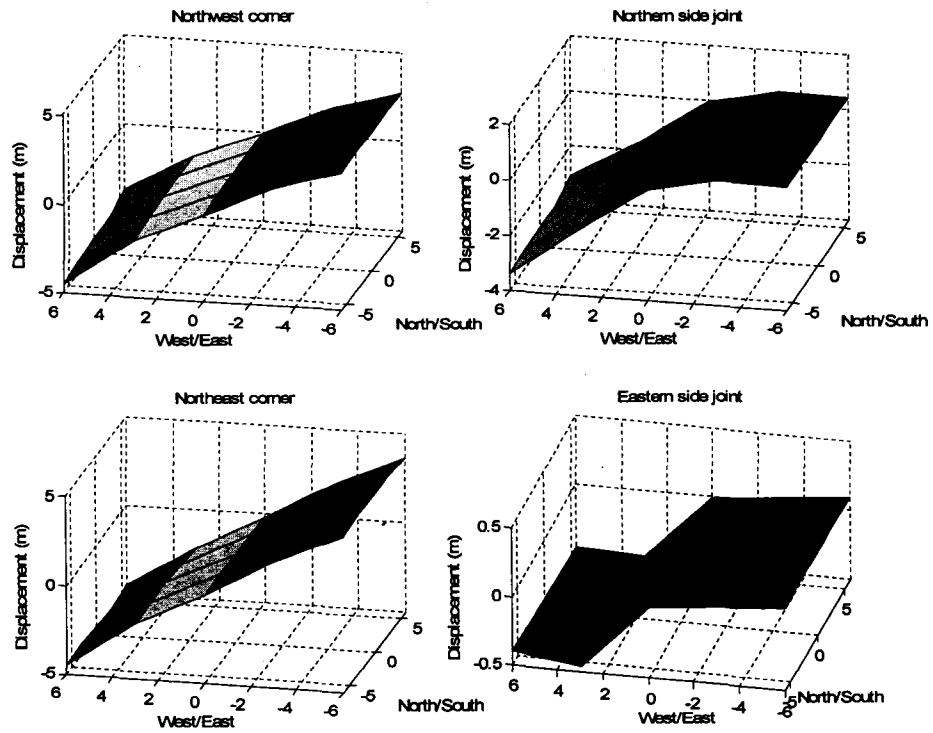
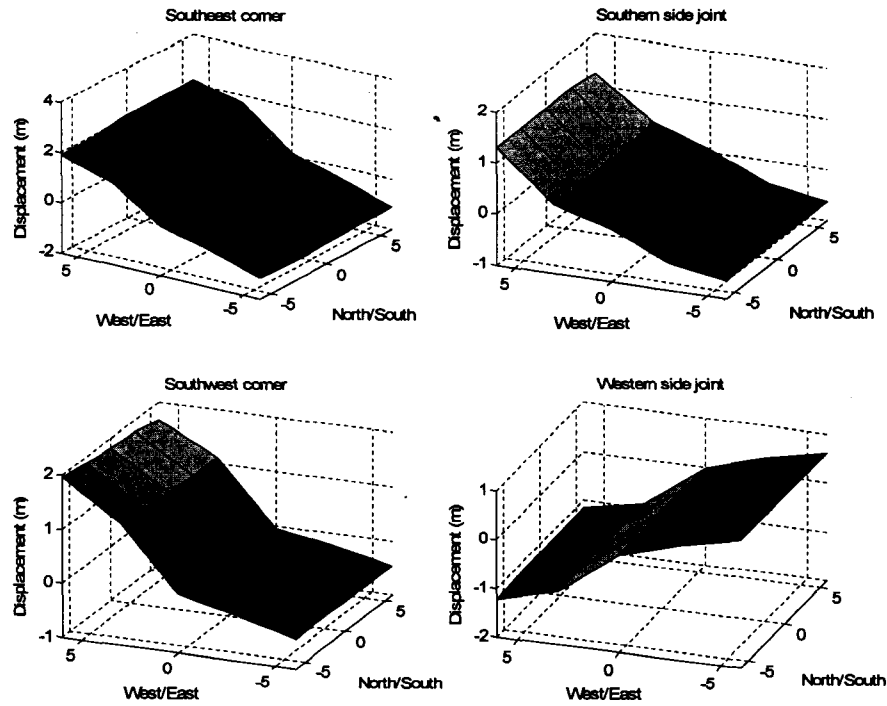


Figure A-7 Grid corner displacement as a function of the northern east anchor displacement.

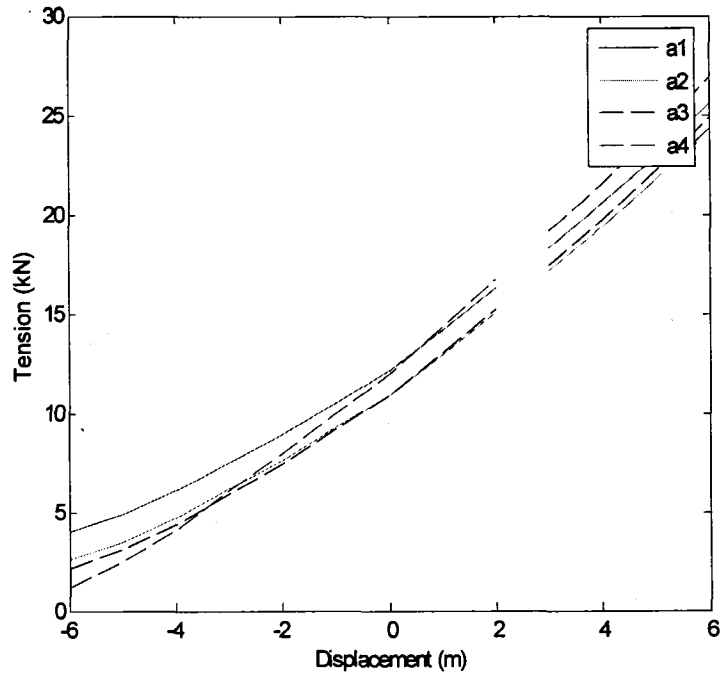


**Figure A-8 Grid corner displacement as a function of the northern east anchor displacement.**

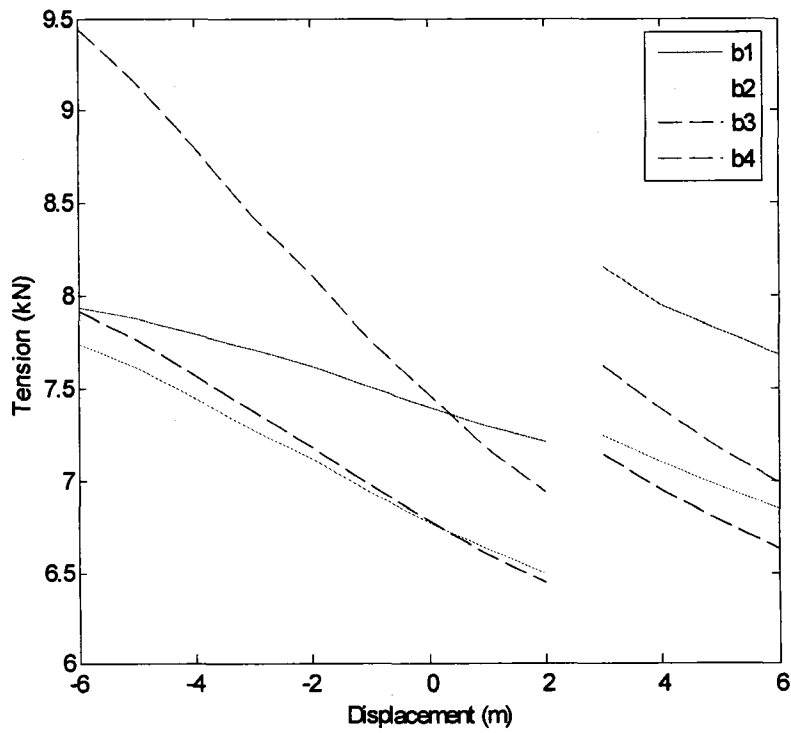
### Section 3

Included in this section are the plots for the second set of *AquaFE* models.

These graphs are for anchor positions from position 11 to 15 as shown Figure III-2. The graph is discontinuous in the area between the models built at different depths.



**Figure A-9 The tensions for cross-section A.**



**Figure A-10 The tensions for cross-section B.**



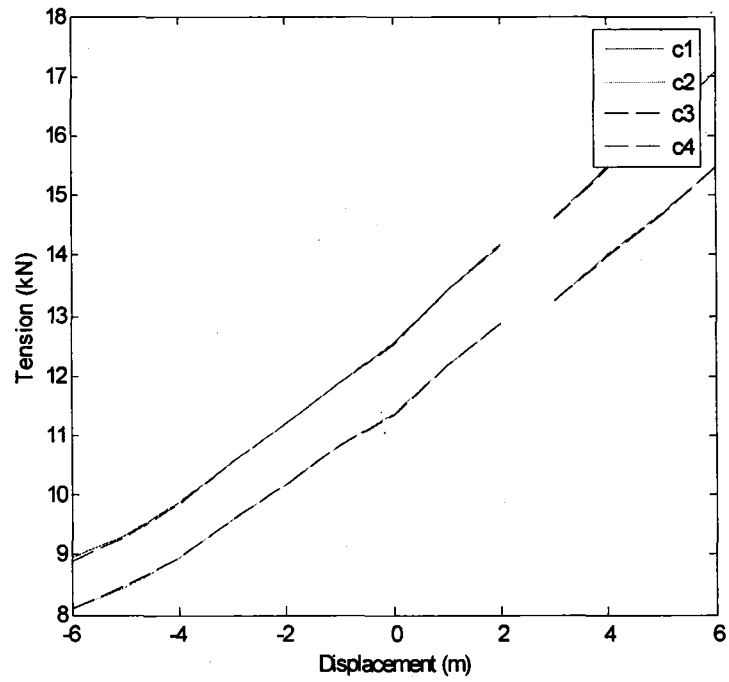


Figure A-11 The tensions for cross-section C.

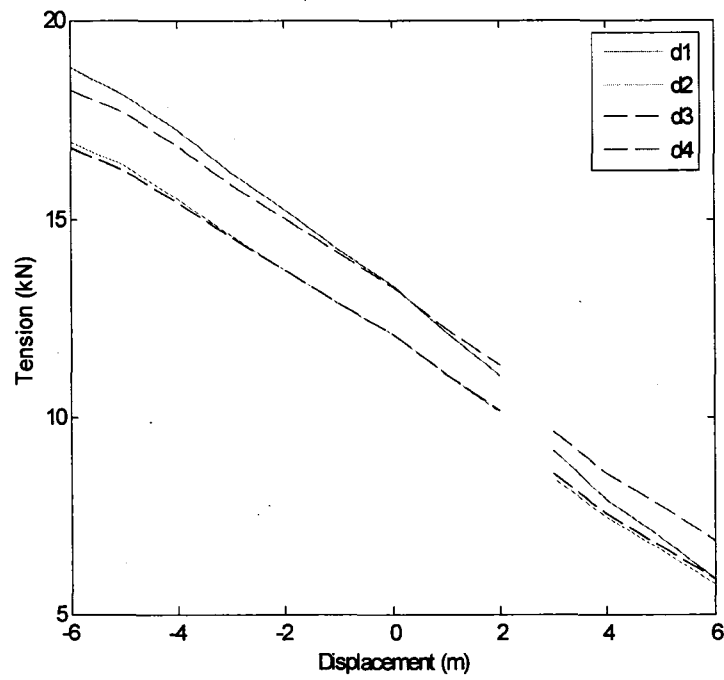


Figure A-12 The tensions for cross-section D.

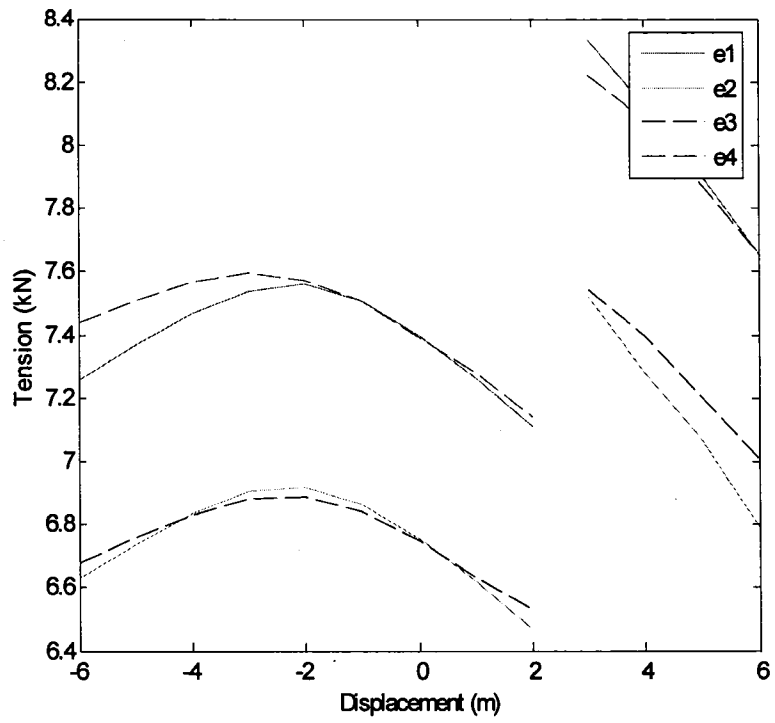


Figure A-13 The tensions for cross-section E.

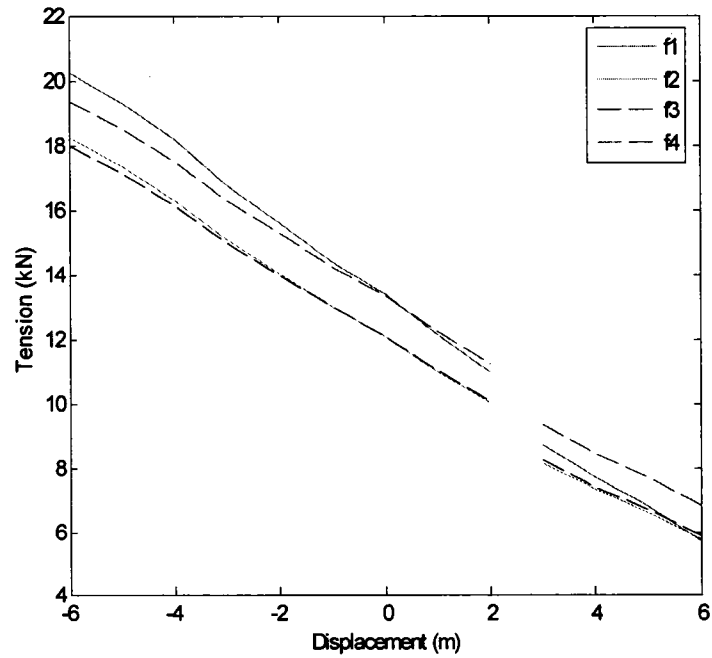
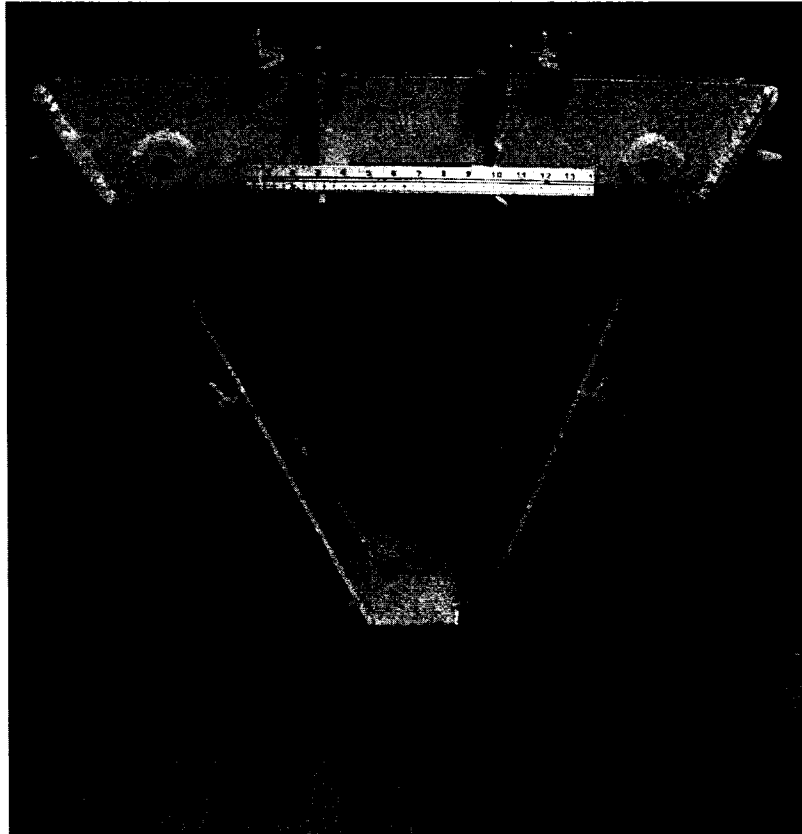


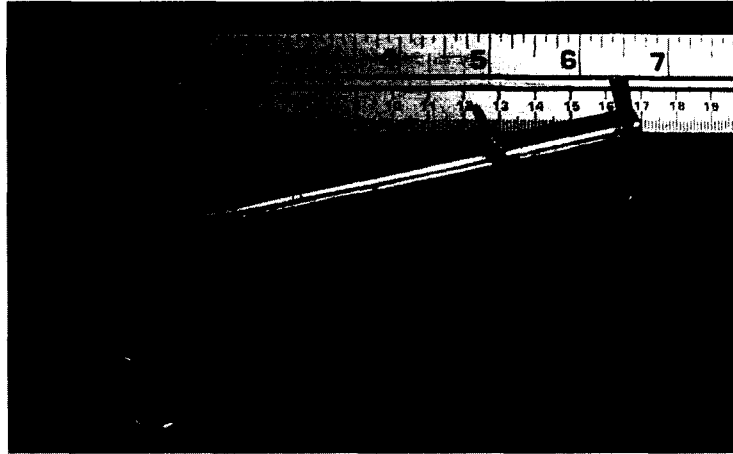
Figure A-14 The tensions for cross-section F.

## APPENDIX B

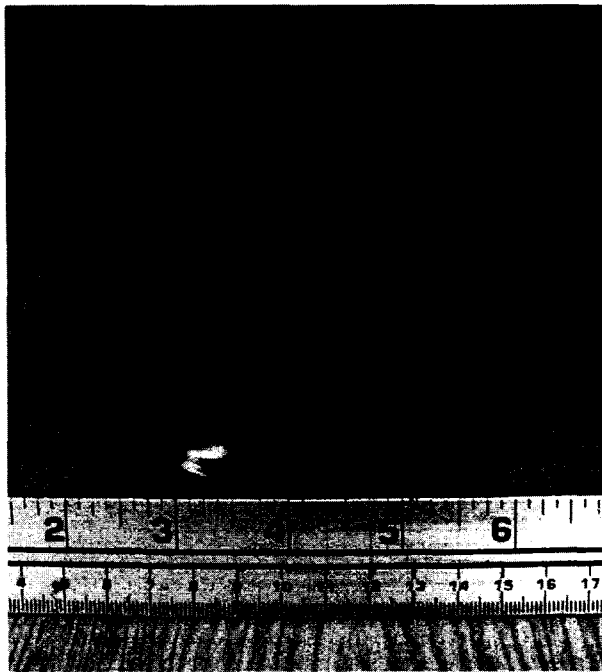
Appendix B consists of pictures of the major parts for the tensions meter.



**Figure B-1 The tension meter frame.**



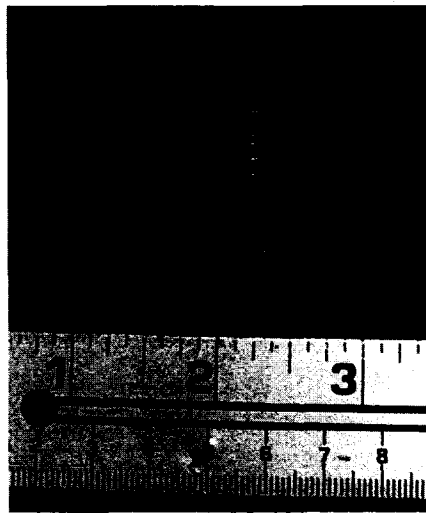
**Figure B-2 The axel assembly for the wheels.**



**Figure B-3 The marithane wheels.**



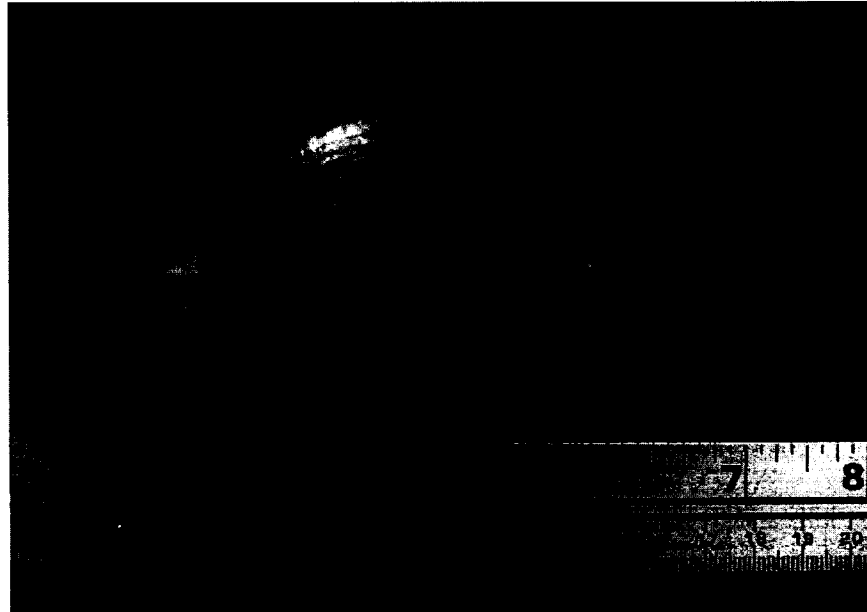
**Figure B-4 The bottle jack.**



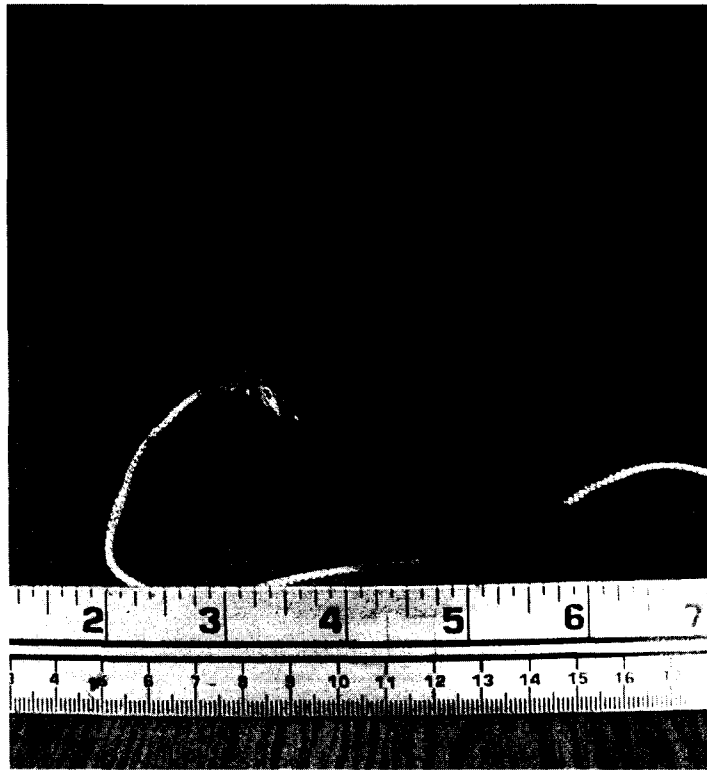
**Figure B-5 The bottle jack to load cell adaptor.**



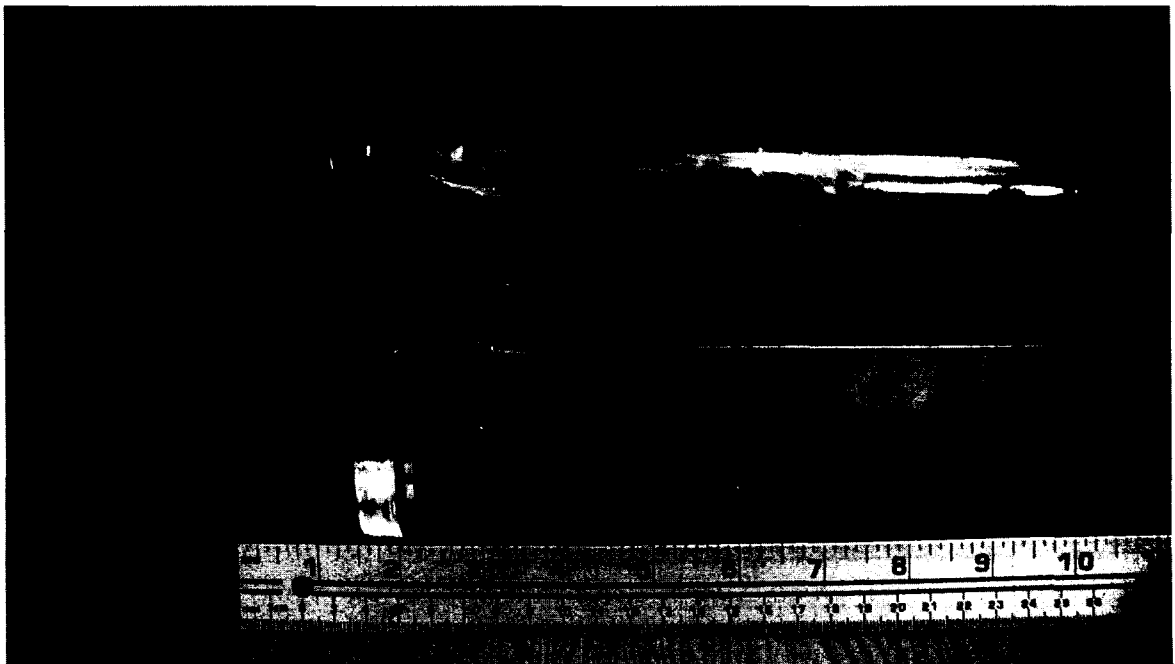
**Figure B-6 The pancake style load cell.**



**Figure B-7 The fairlead for the rope over the load cell.**



**Figure B-8 The pipe chock used for holding the load cell at the correct displacement.**

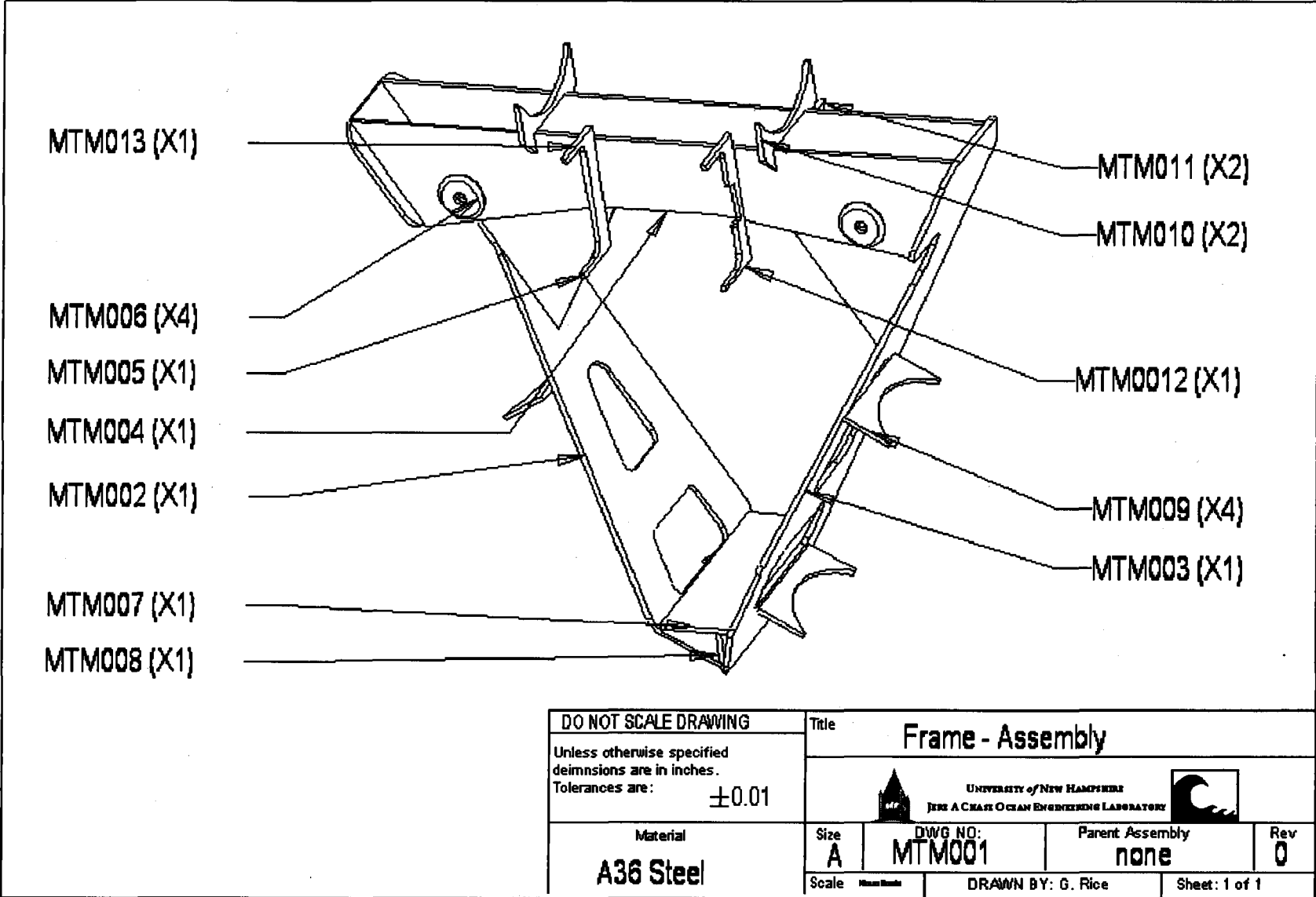


**Figure B-9 The load cell recorder.**


## **APPENDIX C**

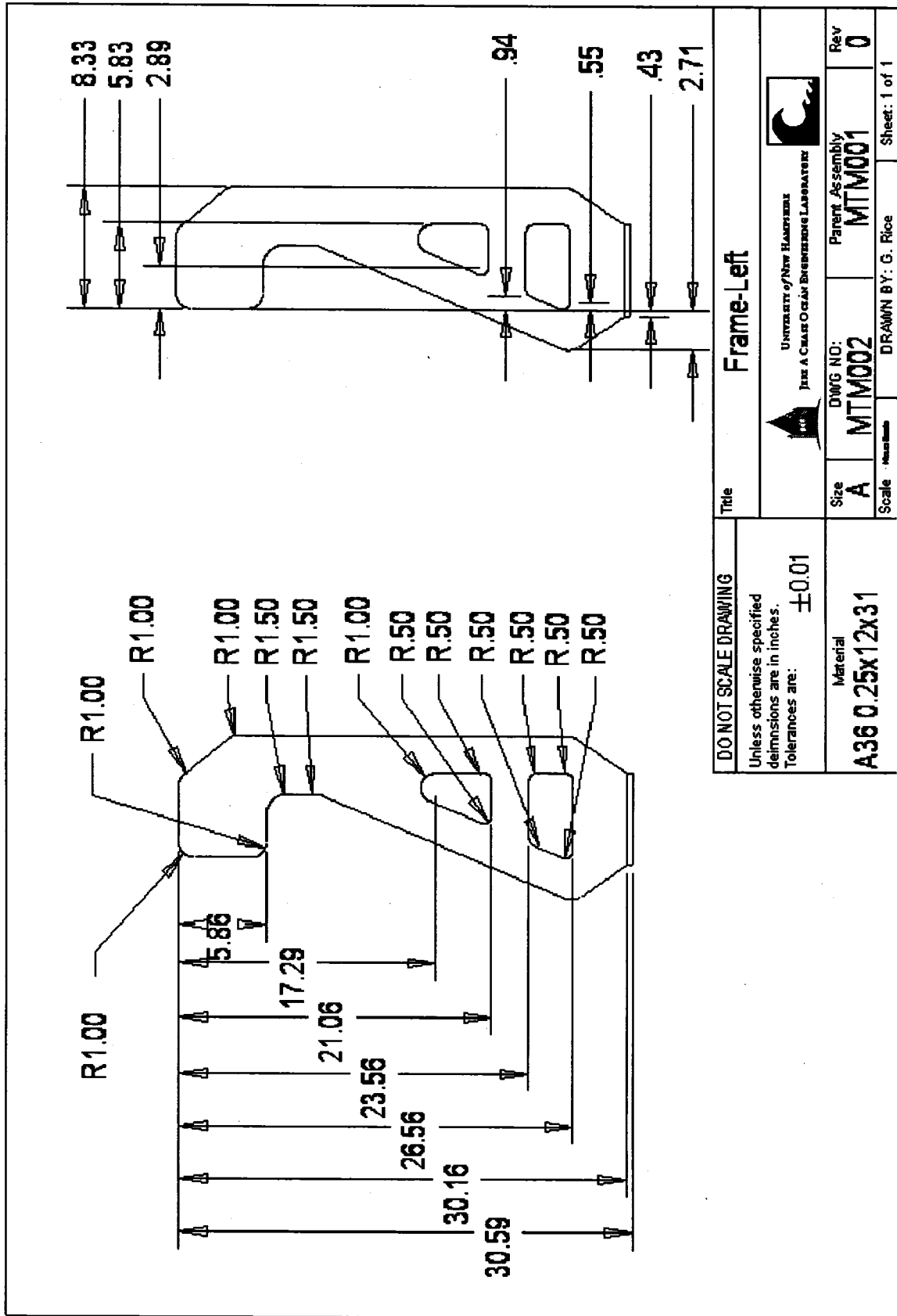
Appendix C consists of drawing for the parts of the frame that was constructed for the tension meter.



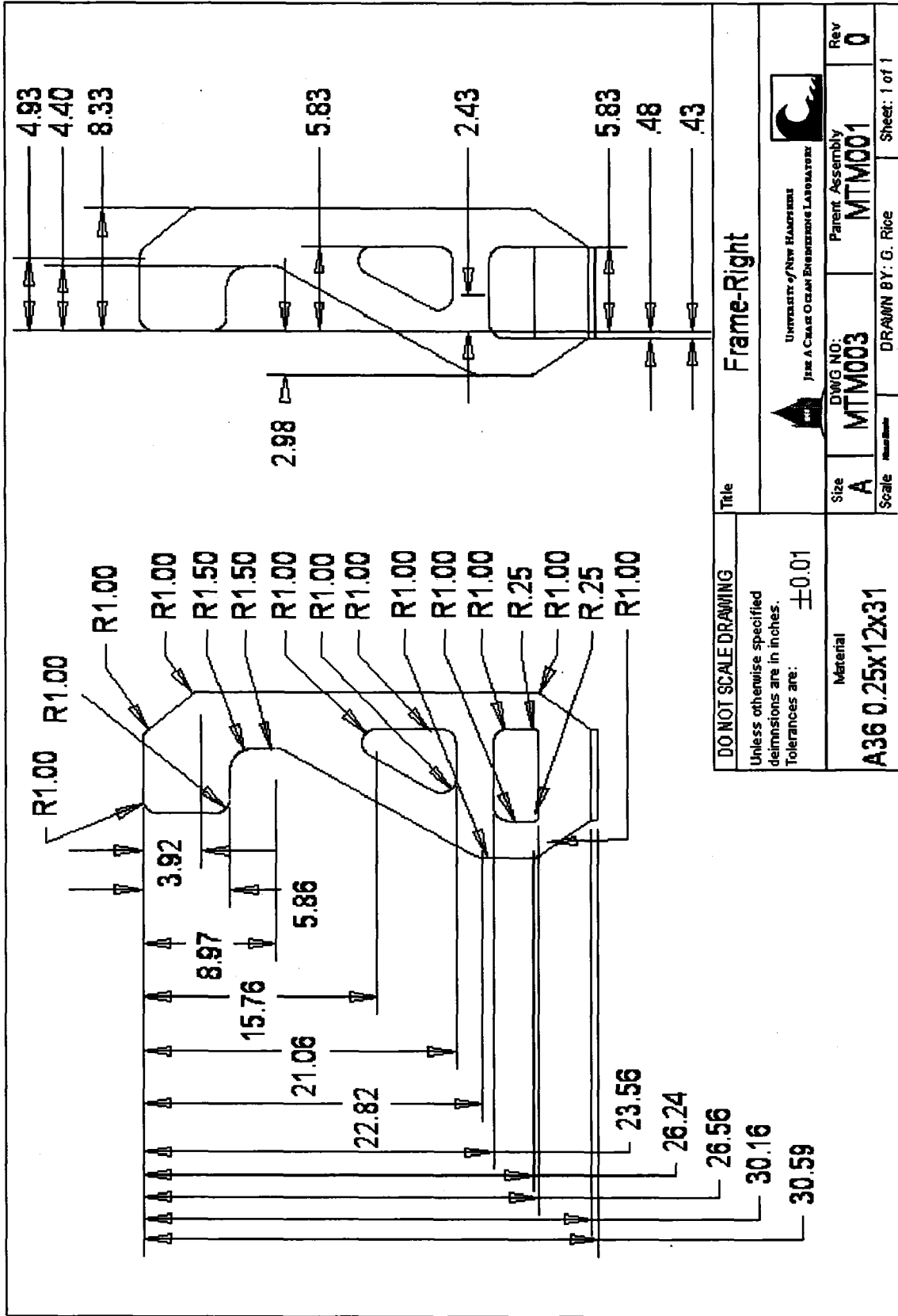


74

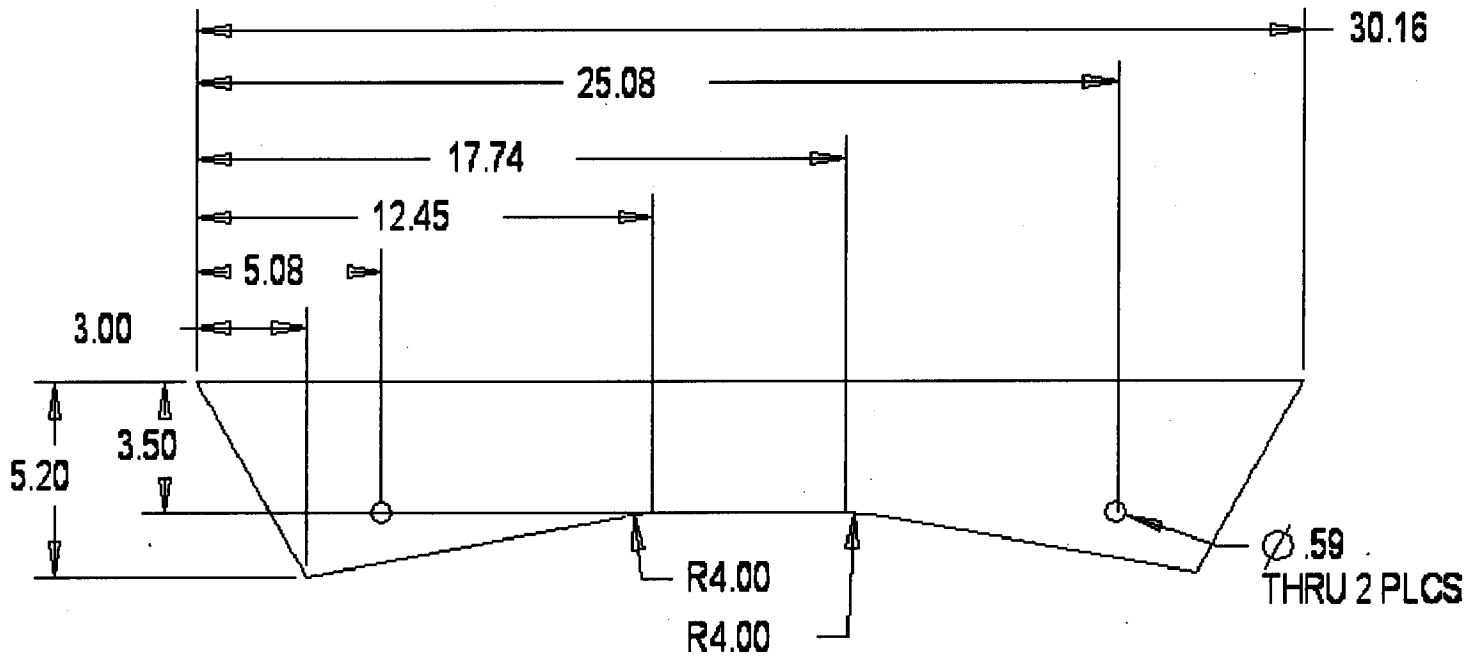
<b>DO NOT SCALE DRAWING</b>		Title <b>Frame - Assembly</b>		
Unless otherwise specified dimensions are in inches. Tolerances are: $\pm 0.01$		 UNIVERSITY of NEW HAMPSHIRE JEROME A. CHASE OCEAN ENGINEERING LABORATORY		
Material <b>A36 Steel</b>	Size <b>A</b>	DWG NO: <b>MTM001</b>	Parent Assembly <b>none</b>	Rev <b>0</b>
Scale <small>None Made</small>		DRAWN BY: G. Rice		Sheet: 1 of 1



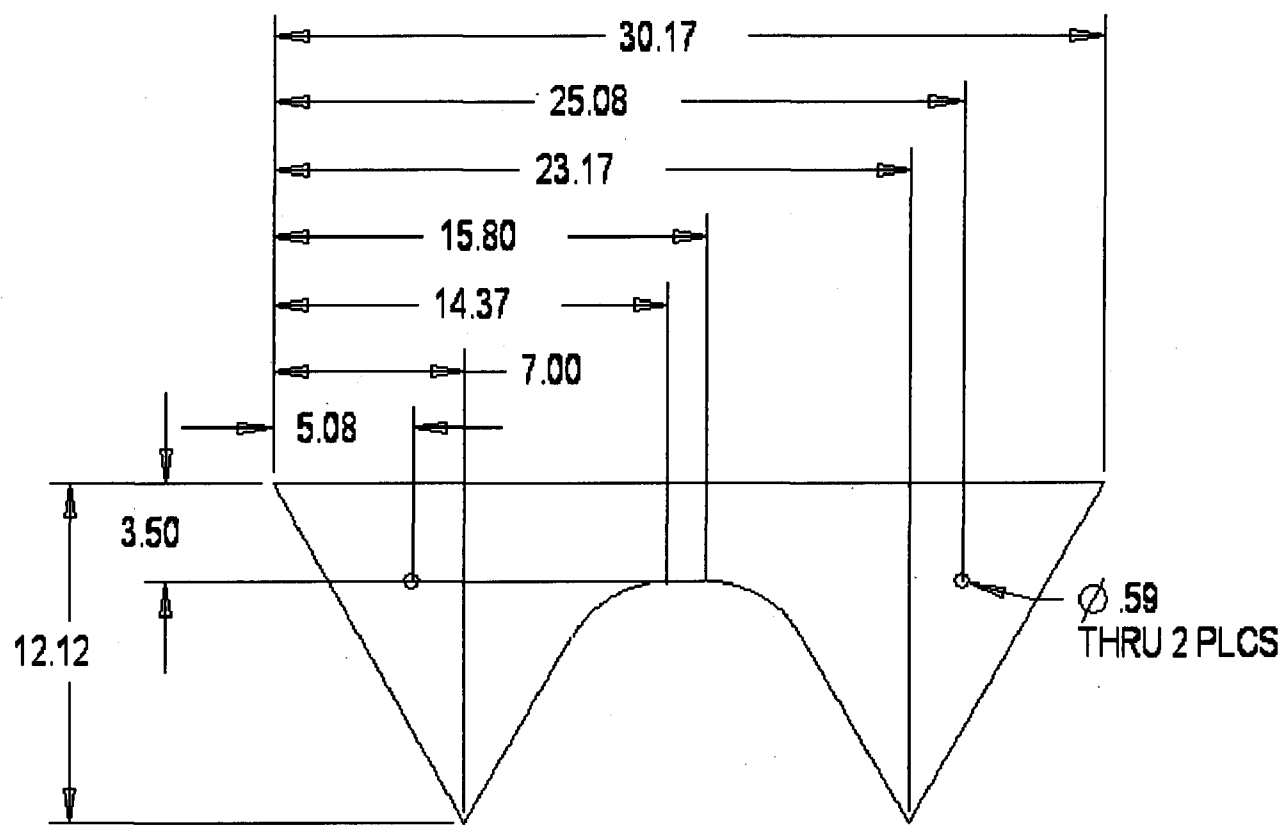
DO NOT SCALE DRAWING		Title	
Unless otherwise specified dimensions are in inches.		Frame-Left	
Tolerances are: ±0.01		UNIVERSITY OF NEW HAMPSHIRE JESSIE A. CRENSHAW OCEAN ENGINEERING LABORATORY	
Material	Size	DWG NO:	Parent Assembly
A36 0.25x12x31	A	MTM002	MTM001
		Scale	Sheet: 1 of 1
		DRAWN BY: G. Rice	Rev 0



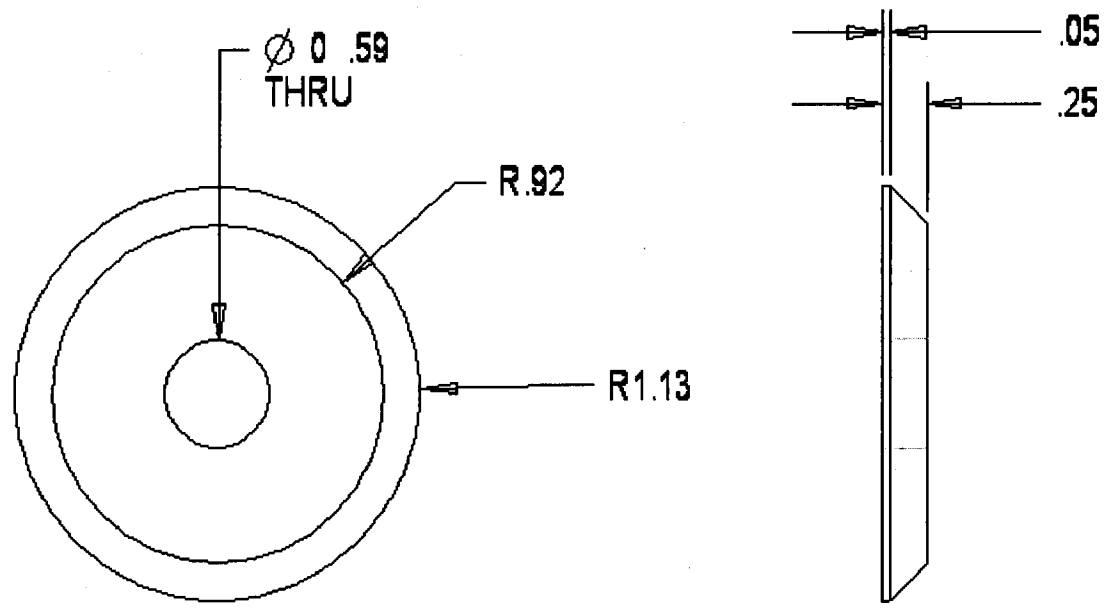
77





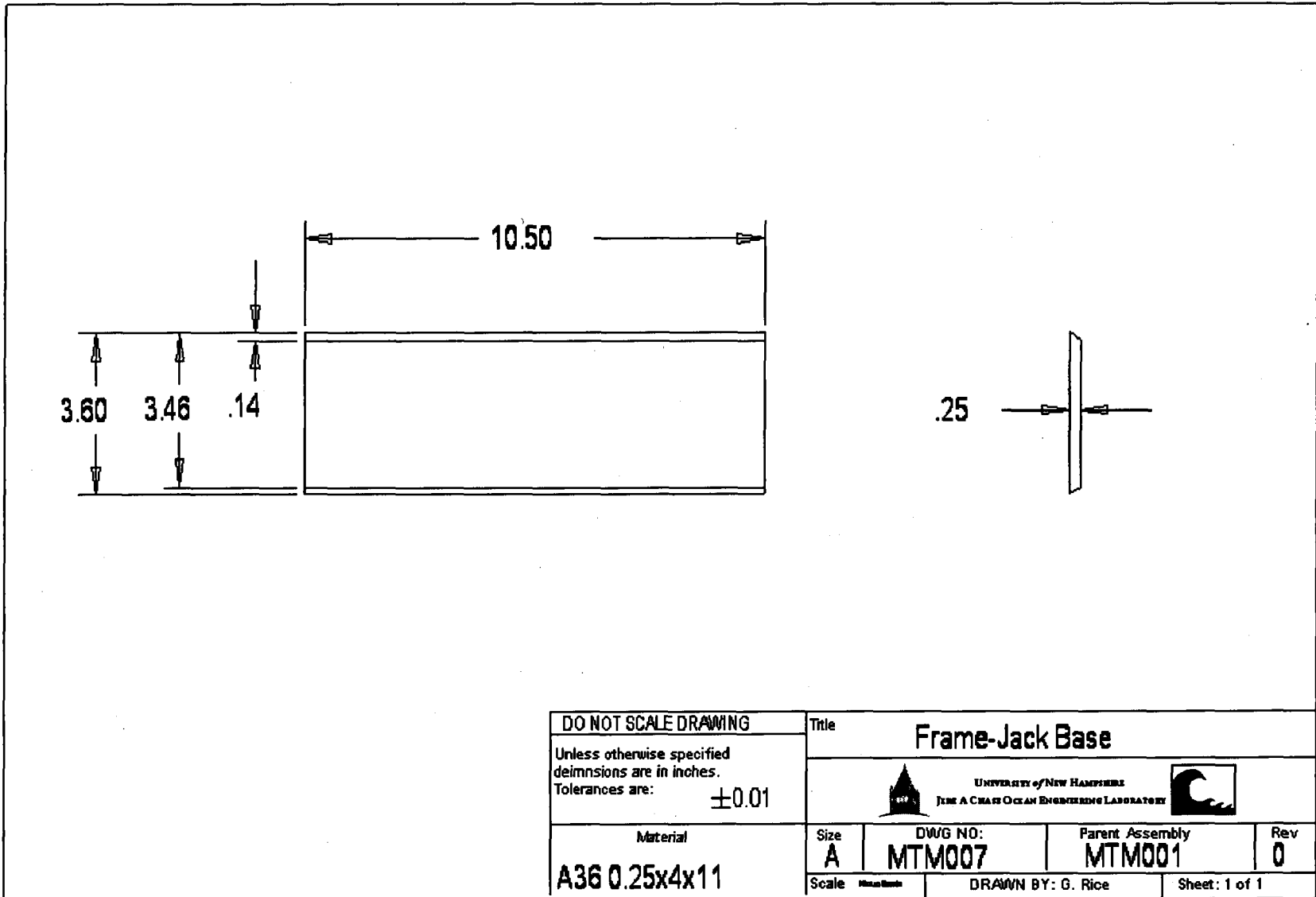
DO NOT SCALE DRAWING		Title		
Unless otherwise specified dimensions are in inches. Tolerances are: ±0.01		Frame-Front		
Material		UNIVERSITY of NEW HAMPSHIRE JEROME A. CRANE OCEAN ENGINEERING LABORATORY		
A36 0.25x6x31		Size	DWG NO:	Parent Assembly
		A	MTM004	MTM001
		Scale	DRAWN BY: G. Rice	Rev
				0
				Sheet: 1 of 1



<b>DO NOT SCALE DRAWING</b>		Title		
Unless otherwise specified dimensions are in inches. Tolerances are: $\pm 0.01$		<b>Frame - Back</b>		
Material		UNIVERSITY OF NEW HAMPSHIRE JEROME A. CRANE OCEAN ENGINEERING LABORATORY		
<b>A36 0.25x13x31</b>		Size	DWG NO:	Parent Assembly
		<b>A</b>	<b>MTM005</b>	<b>MTM001</b>
		Scale	DRAWN BY: G. Rice	Rev
		<b>AS SHOWN</b>		<b>0</b>
				Sheet: 1 of 1

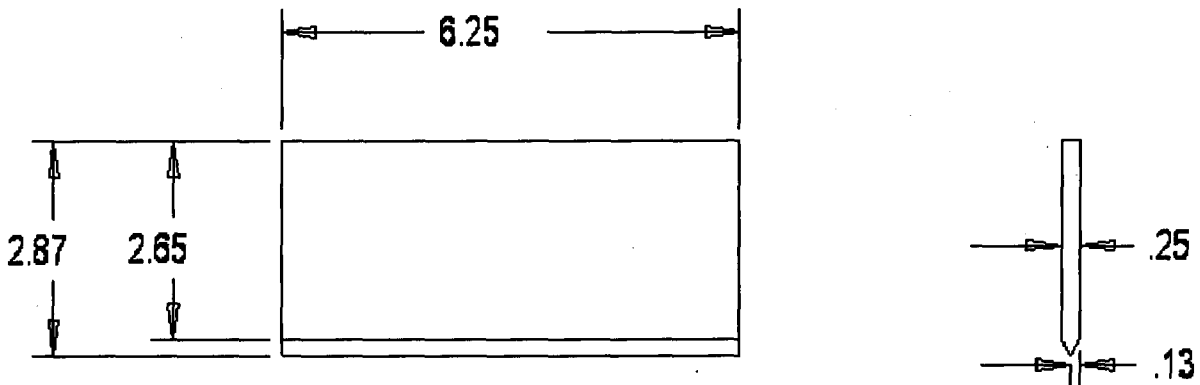



DO NOT SCALE DRAWING		Title		
Unless otherwise specified dimensions are in inches. Tolerances are: ±0.01		Frame-Axel Doubler		
Material <b>A36 0.25x3x3</b>		 UNIVERSITY of NEW HAMPSHIRE JEROME A. CHASE OCEAN ENGINEERING LABORATORY		
		Size <b>A</b>	DWG NO: <b>MTM006</b>	
		Scale	DRAWN BY: G. Rice	Rev <b>0</b>
				Sheet: 1 of 1



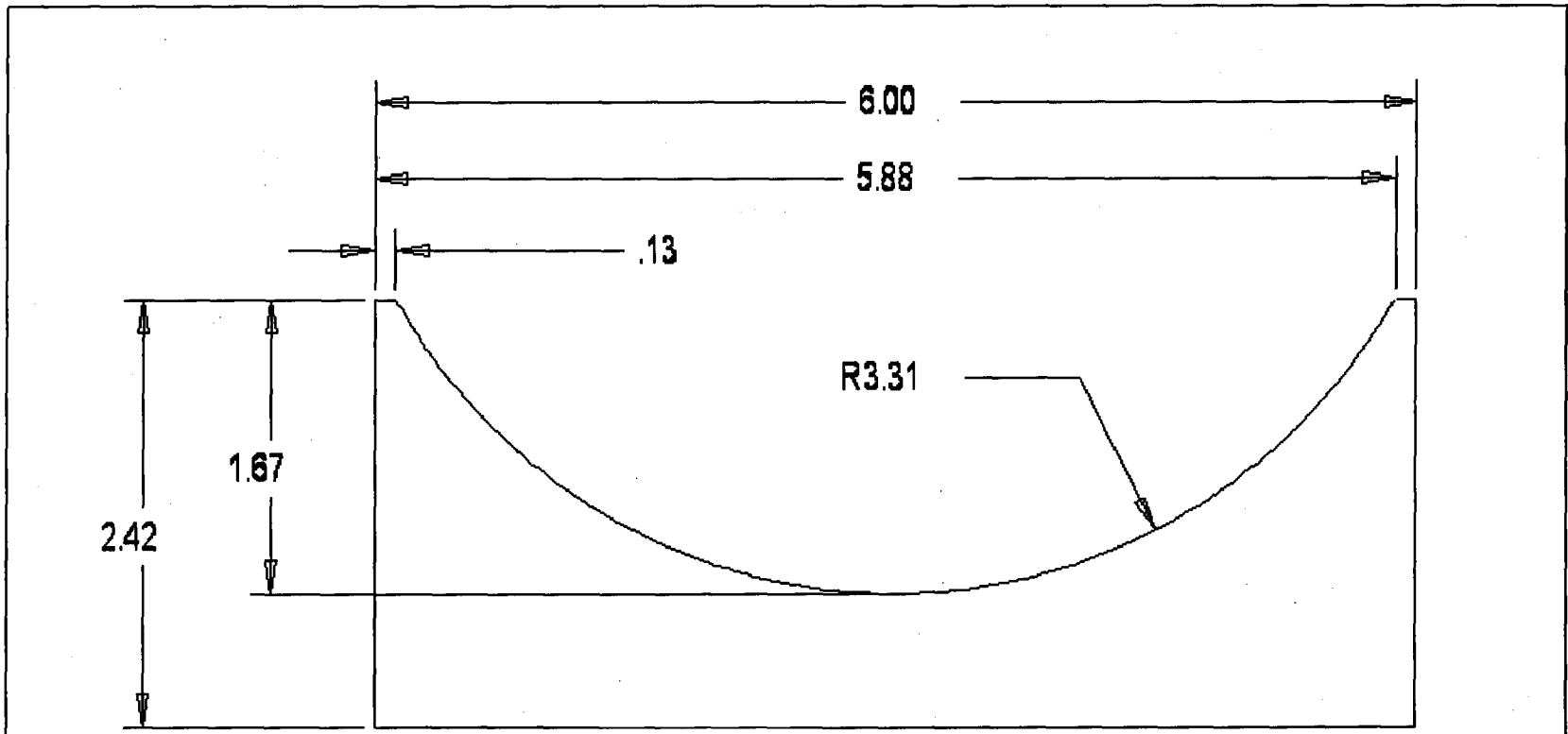
80

<b>DO NOT SCALE DRAWING</b>		Title		
Unless otherwise specified dimensions are in inches. Tolerances are: $\pm 0.01$		<b>Frame-Jack Base</b>		
Material		UNIVERSITY of NEW HAMPSHIRE JIM A. CHASE OCEAN ENGINEERING LABORATORY		
<b>A36 0.25x4x11</b>		Size	DWG NO:	Parent Assembly
		<b>A</b>	<b>MTM007</b>	<b>MTM001</b>
		Scale	DRAWN BY: G. Rice	Rev
		<small>1/4" = 1"</small>		<b>0</b>
				Sheet: 1 of 1




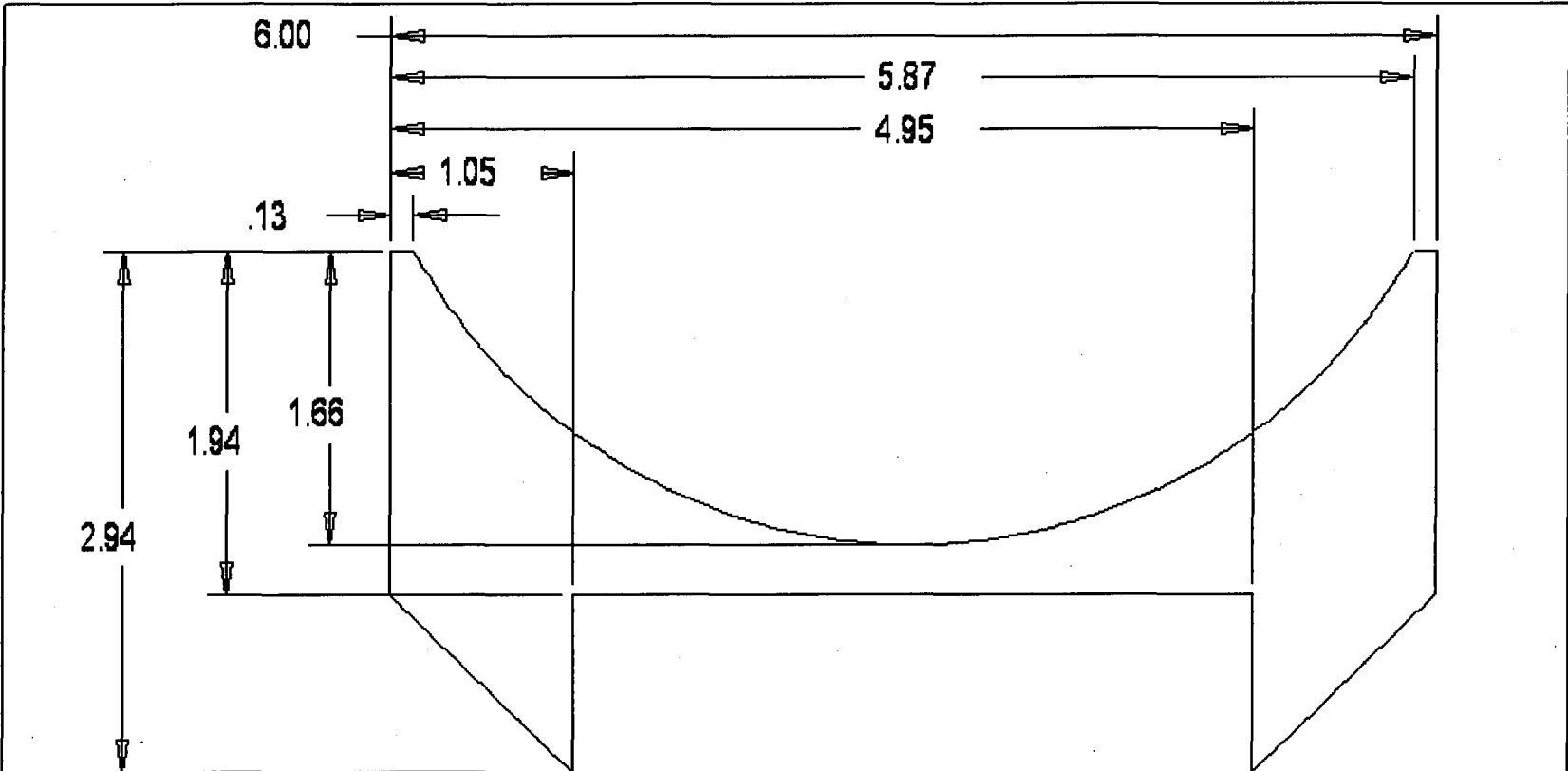
DO NOT SCALE DRAWING		Title		
Unless otherwise specified dimensions are in inches. Tolerances are: $\pm 0.01$		Frame-Jack Support		
		 UNIVERSITY of NEW HAMPSHIRE JIM A CHASE OCEAN ENGINEERING LABORATORY		
Material	Size	DWG NO:	Parent Assembly	Rev
A36 0.25x3x7	A	MTM008	MTM001	0
Scale		DRAWN BY: G. Rice		Sheet: 1 of 1




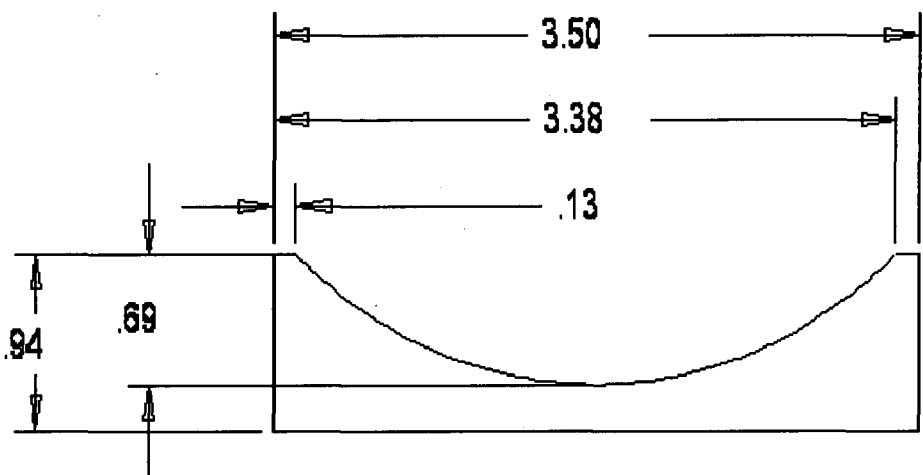


82


<b>DO NOT SCALE DRAWING</b>		Title <b>Frame - Side Float</b>		
Unless otherwise specified dimensions are in inches. Tolerances are: $\pm 0.01$		 UNIVERSITY OF NEW HAMPSHIRE JIM A CHASE OCEAN ENGINEERING LABORATORY		
Material	Size	DWG NO:	Parent Assembly	Rev
<b>A36 0.25x3x6</b>	<b>A</b>	<b>MTM009</b>	<b>MTM001</b>	<b>0</b>
Scale	DRAWN BY: G. Rice		Sheet: 1 of 1	

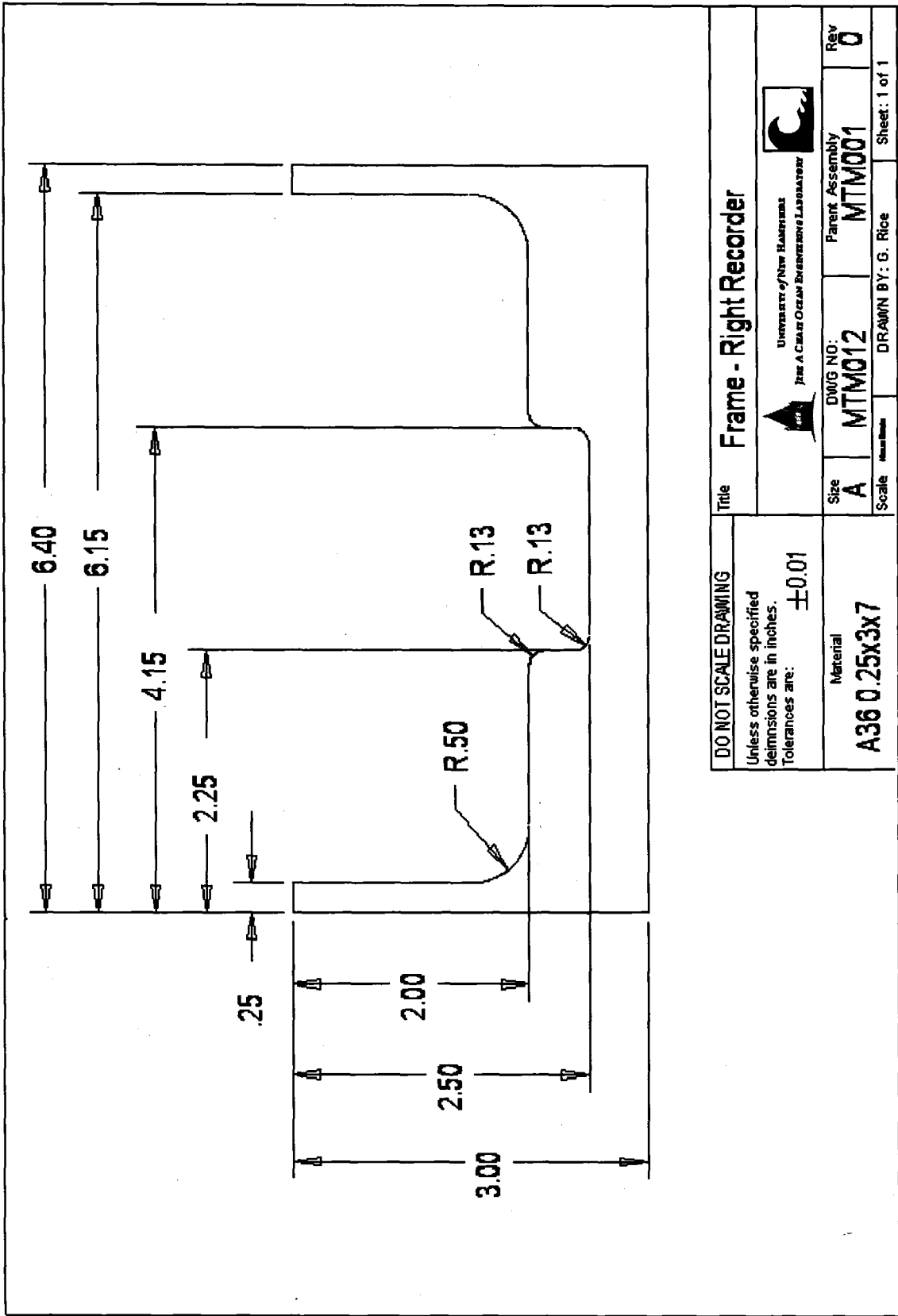


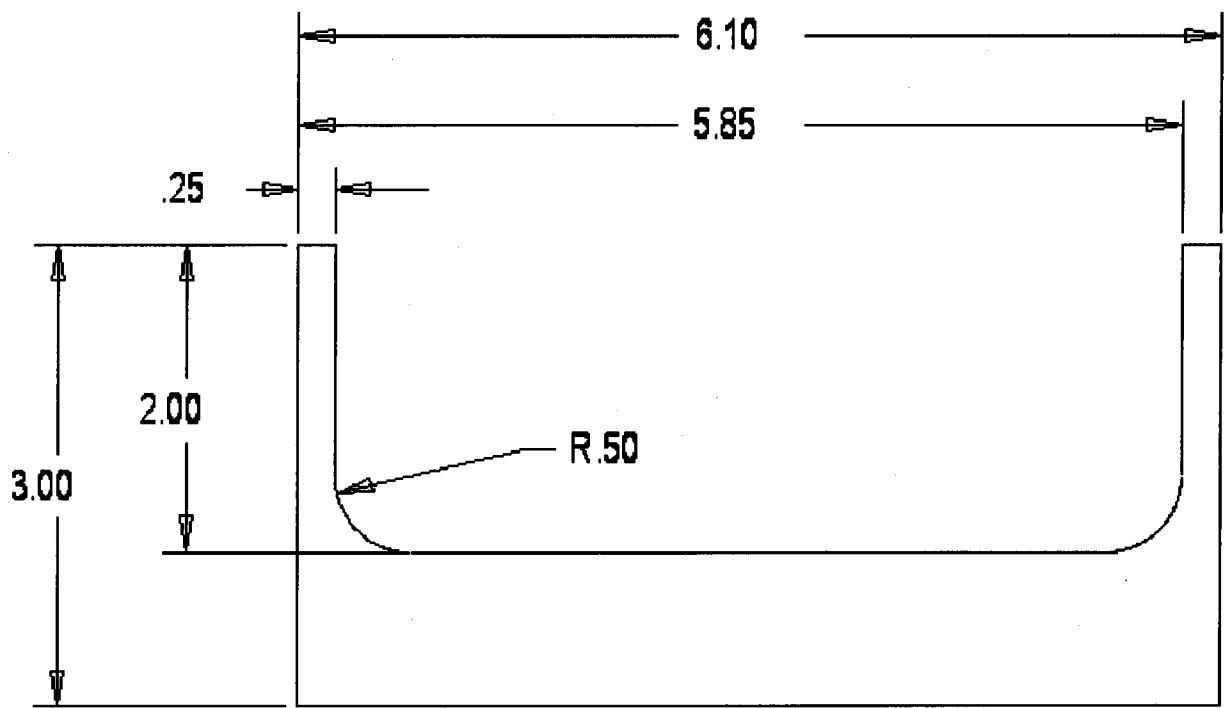
<b>DO NOT SCALE DRAWING</b>		Title <b>Frame - Top Float</b>		
Unless otherwise specified dimensions are in inches. Tolerances are: $\pm 0.01$		 UNIVERSITY of NEW HAMPSHIRE JEROME A. CHASE OCEAN ENGINEERING LABORATORY		
Material <b>A36 0.25x3x6</b>	Size <b>A</b>	DWG NO: <b>MTM010</b>	Parent Assembly <b>MTM001</b>	Rev <b>0</b>
Scale <small>None</small>	DRAWN BY: G. Rice		Sheet: 1 of 1	




84

DO NOT SCALE DRAWING		Title		
Unless otherwise specified dimensions are in inches.		Frame - Back Float		
Tolerances are: ±0.01		 UNIVERSITY OF NEW HAMPSHIRE JEROME A. CRANE OCEAN ENGINEERING LABORATORY		
Material		Size	DWG NO:	Parent Assembly
A36 0.25x1x4		A	MTM011	MTM001
		Scale	DRAWN BY: G. Rice	Rev
				0
				Sheet: 1 of 1





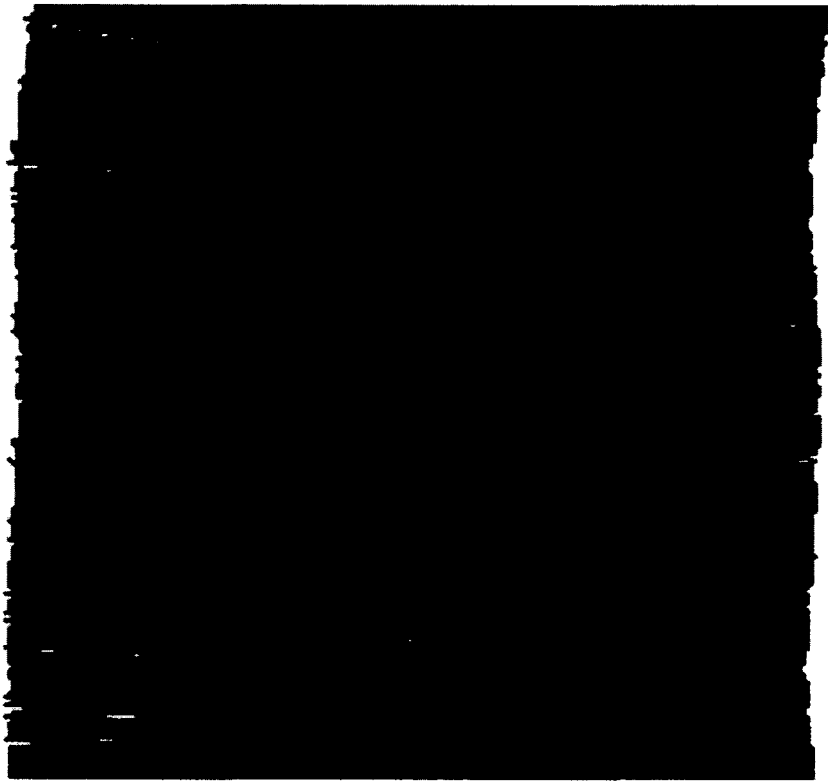
DO NOT SCALE DRAWING		Title <b>Frame - Recorder Left</b>		
Unless otherwise specified dimensions are in inches. Tolerances are: $\pm 0.01$		 UNIVERSITY OF NEW HAMPSHIRE JEROME A. CHASE OCEAN ENGINEERING LABORATORY		
Material	Size	DWG NO:	Parent Assembly	Rev
<b>A36 0.25x3x7</b>	<b>A</b>	<b>MTM013</b>	<b>MTM001</b>	<b>0</b>
Scale	DRAWN BY: G. Rice		Sheet: 1 of 1	

## APPENDIX D

### AN AQUAFE MODEL OF THE AS-DEPLOYED CONDITION

#### Numerical Model Parameters

The actual anchor locations were deduced based on data collected in 2004 when the Joint Hydrographic Center Summer Hydrographic class surveyed the UNH OOA site using a Simrad EM 3000 multibeam sonar. The presence of anchors was inferred by analysis of the backscatter data, an example of which is illustrated in Figure D-1.



**Figure D-1 The backscatter data from the 2004 survey of the OOA site. The dark lines are thought to reflect anchor chain and anchor positions. The labeled locations are deployed anchor locations as measured from the surface. WNA is the western north anchor. NNA is the northern center anchor. ENA is the eastern north anchor.**

While the anchors themselves cannot be distinguished, the anchor chain is evident. The deployed anchor locations are shown as black squares. Nine of the eleven anchors in the grid system can be located from this data. Locations of the same anchor in multiple transects indicates a standard deviation in the detected anchor locations of 1.6m. For the remaining anchor locations the deployed position (from GPS) was used. The standard deviation for the deployed position relative to the backscatter positions for the nine detected anchors was 3.5m. This is assumed to represent the uncertainty in the actual anchor positions compared the presumed deployed positions of the anchors. Table D-1 lists the anchor positions used in the modeling of the deployed grid.

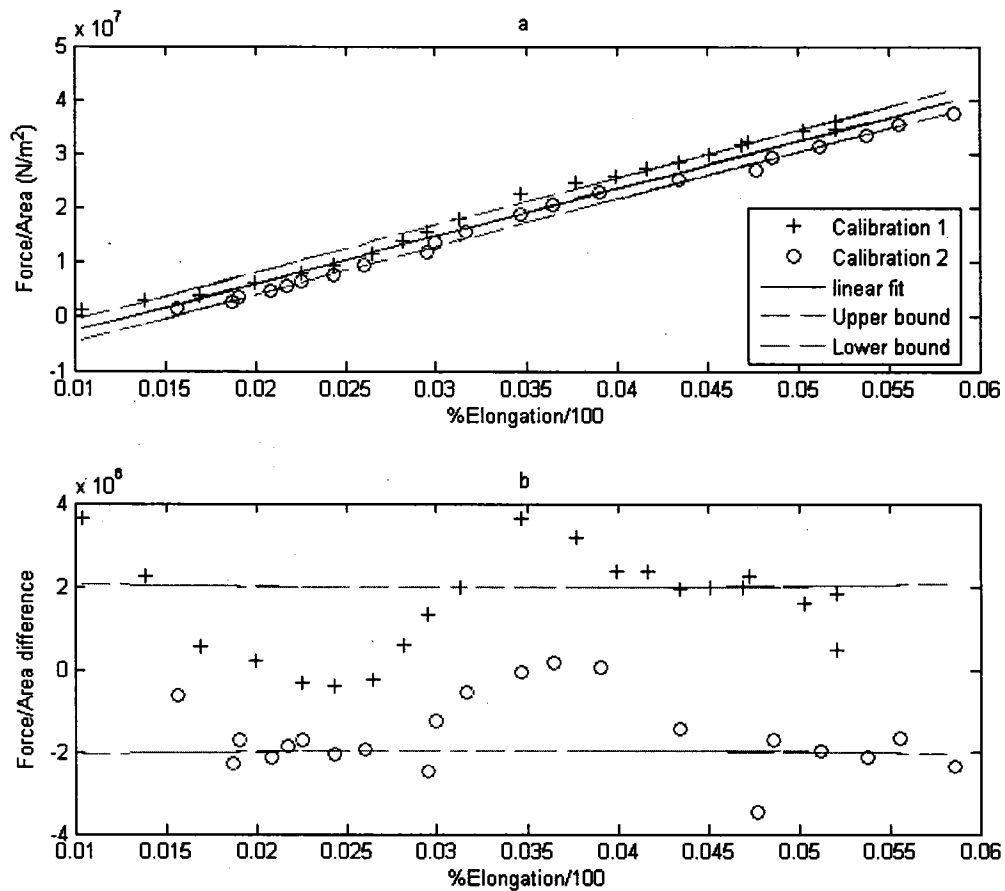
**Table D-1 The anchor positions used to model the deployed grid. Easting and Northing positions are for the UTM Northern Hemisphere zone 19, (WGS84) convention.**

Anchor	Line	Latitude(N)	Longitude(W)	Easting (m)	Northing (m)
Northern East	a <sub>4</sub>	42°56.610'	70°37.821'	366989	4755830
Center East	b <sub>4</sub>	42°56.567'	70°37.850'	366948	4755750
Southern East	c <sub>4</sub>	42°56.536'	70°37.825'	366981	4755694
Eastern South	f <sub>4</sub>	42°56.463'	70°37.907'	366867	4755561
Center South	e <sub>4</sub>	42°56.475'	70°37.949'	366810	4755582
Western South	d <sub>4</sub>	42°56.469'	70°37.997'	366745	4755574
Southern West	c <sub>1</sub>	42°56.522'	70°37.110'	366593	4755674
Center West	b <sub>1</sub>	42°56.559'	70°37.094'	366617	4755744
Northern West	a <sub>1</sub>	42°56.603'	70°37.106'	366602	4755824
Western North	d <sub>1</sub>	42°56.665'	70°37.017'	366725	4755937
Center North	e <sub>1</sub>	42°56.660'	70°37.956'	366808	4755927
Eastern North	f <sub>1</sub>	42°56.670'	70°37.910'	366871	4755944

Two rope properties, the rope diameter and the Young's modulus, are important in *AquaFE*. The specified rope diameter for the rope in use at the site was 48mm (2in). For previous models in *AquaFE* the Young's modulus is approximated using published information for this type of line as  $1.83 \times 10^9 \text{N/m}^2$ . Different line from different manufacturers can have different properties. The Young's modulus was not available from the particular manufacturer of the rope purchased for use in the grid system. Given the amount of constructional and elastic stretch in the line during deployment, it is more



accurate to use a Young's modulus calculated from the elongation data gathered during the tension meter calibration. Figure D-2 shows the calibration curve.



**Figure D-2 (a) The linear regression to find the value for the Young's Modulus from tension meter calibration data. (b) Data to linear fit difference. Bounds denote one standard deviation.**

The in situ measurement indicated that the Young's modulus of the rope in the deployed grid model was  $9 \cdot 10^8 \text{ N/m}$ . Over the range of tensions this estimate used a constant rope diameter of 48mm (2in), which was deemed appropriate as *AquaFE* does not account for changes in the rope diameter. As a result, the model actually reflects the ratio of measured stretch to force.

Since the numerical model is built in a relaxed state and then released to come to equilibrium, the line length with zero tension after constructional stretch needs to be known. Constructional stretch, also known as permanent elongation, is the change in length of a line after it has been under tension due to the settling and compaction of rope fibers. To account for the constructional stretch already in the grid, the deployed line lengths were measured, and using the relationship in equation 2 with the measured Young's modulus and line tension, the zero tension length is derived. From the relationship of stress versus strain it can be shown that:

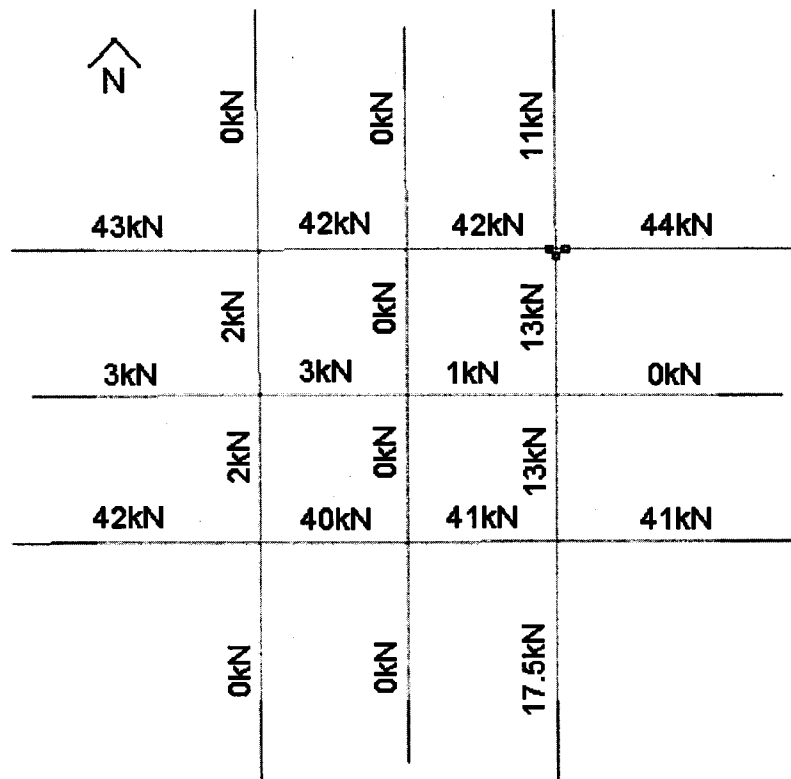
$$L_o = L_m YA / (T + YA) \quad 2$$

where  $L_o$  is the zero tension length,  $L_m$  is the measured length,  $Y$  is the Young's modulus,  $A$  is the cross-sectional area of the rope, and  $T$  is the measured tension on the line.

The grid lines have been measured by diver to be between 68m and 69m. These measurements were taken using a surveyor's tape. Using the calculated Young's modulus, the line lengths without tension (but with construction stretch) can be estimated from the field measurements. Using a line length of 69m with a known measured tension of 12kN, the grid line with zero tension should be 68.5m long. Line lengths used for the grid lines were 70m to account for shackles and rope rings as part of the grid lengths. The anchor lines were modeled at 84m, keeping the ratio of rope length to construction stretch the same as for grid lines. The lines that included an in-line load cell were shortened by 1m to account for the change in length of these lines.

## Modeling the Deployed Geometry

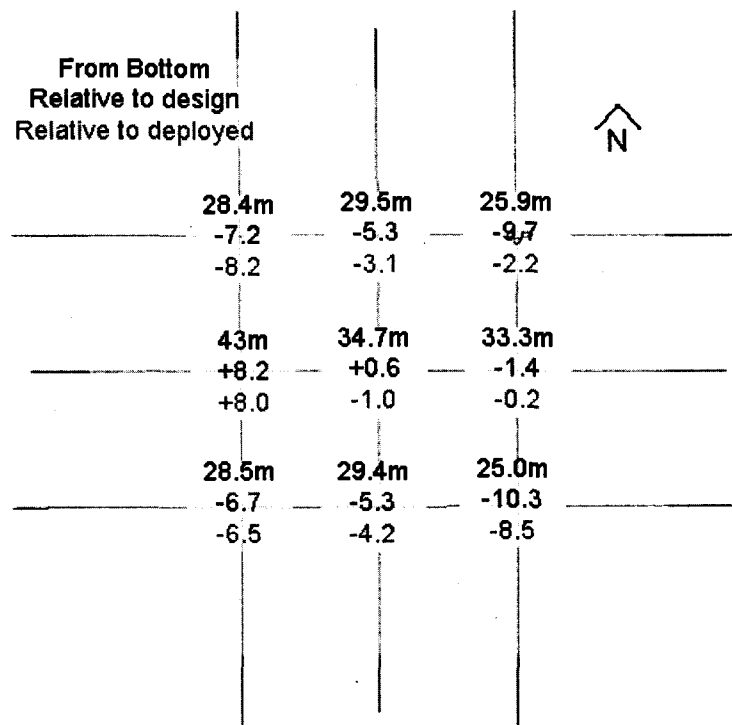
To model the grid in its deployed geometry the grid system had to be constructed at a depth much closer to the bottom than the depth used during the sensitivity study. To allow sufficient proximity between the grid corners and their respective anchor points such that the anchor lines would reach, the grid was built 1m from the bottom. Even with rearranging the grid itself to a non-symmetric starting position, the anchor on line  $c_1$ , in Figure III-1, (southern east anchor) needed to be moved 7m closer to allow all anchor lines to reach. The resulting tensions are shown in Figure D-3.



**Figure D-3 The tensions in the deployed grid as model in *AquaFE*.**

It is apparent from the tensions shown in Figure D-3 that the range of tensions (0kN to 43kN) is much higher than the range measured in the field, as shown in Figure IV-14

(4kN to 23kN). The modeled tensions in the side cross-sections running east/west are more than double the tensions that were measured in situ. These lines are holding the grid flotation down so the lines running north/south are not under much tension. All the modeled grid depths are presented in Figure D-4. The lack of tension in the modeled north/south lines is reflected in the depth of the western grid joint where the north/south grid tensions is very low.



**Figure D-4 The deployed grid depths as modeled by *AquaFE*. The depth relative to the designed locations and the measured depths at the site are also given.**

Discrepancies between the modeled deployed grid and in situ field measurements stem from errors in the information provided to the model, an unaccounted for variable, or by the time between the multibeam survey and the tension measurements. The uncertainties in the buoyancy of the grid flotation, line lengths and properties, and anchor positions could be too large to allow accurate modeling of such a sensitive system. There are also parameters that have not been accounted for, such as

the weight and distribution of biofouling or of the in-line load cells. This extra weight reduces the buoyancy in the grid, effectively reducing the tensions as the grid sinks. While this might be a contributor to error, it seems unlikely that this would be a cause for the higher than measured tensions in the model since the effect is opposite to those expected. In the time between the multibeam survey and field measurements anchors could have changed position. This seems to be an unlikely source of error since the grid depth has remained stationary.

That the modeled results do not correspond with field measurements possibly reflects shortcomings in the modeler's ability to input sufficiently accurate parameters. The numerical model shows patterns useful for studying grid reaction to different deployment configurations; however, actual numbers generated from modeling may not accurately represent reality for such a sensitive system. Small errors in many variables may result in large differences between model and physical results. Although *AquaFE* has been validated for large storm events (Fredriksson, 2001) and provides a relative scale with which to consider field measurements, this study reveals the usefulness of revising models to incorporate real as-built geometries.